

UC Santa Barbara

UC Santa Barbara Electronic Theses and Dissertations

Title

Hydrosilylation of Carbonyl Compounds with High-Valent Pincer Oxo-Rhenium Complex

Permalink

<https://escholarship.org/uc/item/7d4853vc>

Author

xiong, manxi

Publication Date

2021

Peer reviewed|Thesis/dissertation

UNIVERSITY OF CALIFORNIA

SANTA BARBARA

Hydrosilylation of Carbonyl Compounds with High-Valent Pincer Oxo-Rhenium
Complex

A dissertation submitted in partial satisfaction of the
requirements for the degree Doctor of Philosophy
in Chemistry

by

Manxi Xiong

Committee in charge:

Professor Mahdi M. Abu-Omar, Chair

Professor Steven K. Buratto

Professor Trevor W. Hayton

Professor Gabriel Ménard

March 2021

The dissertation of Manxi Xiong is approved.

Prof. Steven K. Buratto

Prof. Trevor W. Hayton

Prof. Gabriel Ménard

Prof. Mahdi M. Abu-Omar, Committee Chair

January 2021

© Copyright by MANXI XIONG 2020
All Rights Reserved

parents,

To my

ACKNOWLEDGEMENTS

First of all, I would like to express my appreciation to my research advisor Prof. Mahdi Abu-Omar for the opportunity he gave me to work for him, from Purdue to UC Santa Barbara, and also for his guidance and persistent help throughout both my graduate study and life, especially during this difficult year. His excellent mentorship and dedication towards excellence in chemistry has made a tremendous impact on my life and will continue exert a strong influence in the future. I would also like to acknowledge my committee members for their support and time, Dr. Hayton, Dr. Buratto and Dr. Ménard.

In addition, I would like to thank all of the current and past group members of the Abu-Omar research group. Your help was one of the most important factors that allowed me to succeed as a researcher.

Leaving my family and my country to study in the United States was not easy, Yueyue and Yinshuan thank you so much for your friendship and support.

Finally I would like to thank my parents for giving me the freedom to study and supporting my choices to their accomplishment.

VITA OF MANXI XIONG

December 2020

EDUCATION

Bachelor of Science in Chemistry, Purdue University, Aug 2010-May 2014

Doctor of Philosophy in Chemistry

Purdue University, Jan 2015-Jun 2016

University of California, Santa Barbara, Jun 2016-Dec 2020

(expected)

PUBLICATIONS

Mazzotta, M. G.; Xiong, M.; Abu-Omar, M. M. “Carbon Dioxide Reduction to Silyl-Protected Methanol Catalyzed by an Oxorhenium Pincer PNN Complex”. *Organometallics*. **2017**, *36* (9), 1688–1691.

FIELDS OF STUDY

Major Field: Inorganic Chemistry

Studies in reduction catalyzed by rhenium complexes with Professor Mahdi M. Abu-Omar

ABSTRACT

Hydrosilylation of Carbonyl Compounds with High-Valent Pincer Oxo-Rhenium Complex

by

Manxi Xiong

Catalytic hydrosilylation is an efficient method for making organosilicon compounds and one of the most widely used reactions in silicon chemistry. Metal-catalyzed hydrosilylation of carbonyl compounds is an atom-economical methodology to access synthetically useful silyl ethers. Considering the heightened interest in hydrosilylation catalyzed by high-valent pincer oxo-rhenium complexes and the current lack of detailed mechanistic understanding, catalytic hydrosilylation of various carbonyl compounds, including biomass-derived carbonyl molecules, using oxo rhenium(V) pincer complex $[\text{Re}(\text{O})_2(\text{PNN})][\text{OTf}]$ ($\text{OTf} = \text{CF}_3\text{SO}_3^-$) with organosilanes is described in this work. Direct reductive deoxygenation can be accomplished at moderate temperature (80 °C). Both the isolation of the potential intermediate metal hydride and stoichiometric deuterium scrambling experiment reveal that the rhenium hydride is not the active catalyst, hydride transfer results from additional silane in the system. An alternative nonhydride Lewis acid catalysis pathway is proposed with the formation of frustrated Lewis pair between metal center and silane. *In-situ* ^1H NMR experiments were conducted to address the kinetics of benzaldehyde hydrosilylation in a rhenium pincer system. The rate of reaction is determined to be independent of substrate concentration but first-order

with respect to silane and catalyst, suggesting silane activation is the rate-determining step.

TABLE OF CONTENTS

Chapter I. Introduction to and Background of High-Valent Pincer Oxo-Rhenium

Complexes

1. Introduction.....	1
2. Pincer Ligand Design	2
3. Efficient Reduction Methodologies Catalyzed by Oxo-Rhenium Complexes	7
4. Small Molecule Activation through Frustrated Lewis Pair	18
5. Conclusions and Future Prospects	21
6. References	2

Chapter II. Synthesis of Pincer Rhenium Complexes

1. Introduction	2
8	
2. Experimental.....	
32	

3. Results and discussion	42
a. Determination of Equilibrium Constant	42
b. Structural Discussion of [(PNN)Re(O) ₂ (ACN)][OTf] (1-ACN)	44
c. Structural Discussion of (ⁱ PrPNP ⁱ Pr)Re(O) ₂ I (4)	46
d. Pincer Hemilabile Effect	47
4. Conclusion.....	49
5. References	49

Chapter III. Carbon Dioxide Reduction to Silyl-Protected Methanol Catalyzed by an Oxorhenium Pincer PNN Complex

1. Introduction	5
2	
2. Experimental.....	54
3. Results and Discussion	59

a. Hydrosilylation of CO ₂ to silyl formate, bis(silyl) formal and silyl methanol ...	59
b. Isolation and identification of oxo-rhenium complexes 1-a and 1-OTf....	60
c. Mechanistic study and proposed catalytic cycle.....	62
4. Conclusion.....	67
5. References	67

Chapter IV. Reactivity of High Valent Pincer Oxo-Rhenium Complexes in Catalytic

Reduction with Organosilanes

1. Introduction	69
2. Experimental	72
3. Results and discussion	74
a. Hydrosilylation of Benzaldehyde Catalyzed by Various Oxo-Rhenium Catalysts	74
b. Effect of Organosilane on Hydrosilylation.....	75

c. Effect of Reaction	
Medium.....	77
d. Substrate	
Scope.....	79
4. Conclusion	
	83
5. References	
	84

Chapter V. Kinetics and Mechanism of Hydrosilylation Catalyzed by Oxo Pincer

Rhenium Complex (PNN)Re(O)₂ Cation

1. Introduction.....	
	86
2. Experimental.....	
	88
3. Results and	
Discussion	91
a. Kinetic Studies of Benzaldehyde Hydrosilylation	91
b. Influence of the Order of Reagents Addition	97
c. Mechanistic Insights into 1 Catalyzed Hydrosilylation	98
d. Proposed Catalytic Cycle	106
e. Comparison and Discussion of the Rate Constant	107
4. Conclusion	11
	0

5. References	112
Chapter VI. Additional Reactions and Studies of Rhenium Pincer Complexes	
1. Kinetic Studies of Imine Hydrosilylation Catalyzed by 1	115
2. Hammett Correlation Study.....	119
3. Dearomatized rhenium complexes catalyzed hydrosilylation	120
4. Discussion on acridine-based rhenium pincer complex 4 and 5	125
5. References.....	125

Chapter I. Introduction to and Background of High-Valent Pincer Oxo-Rhenium Complexes

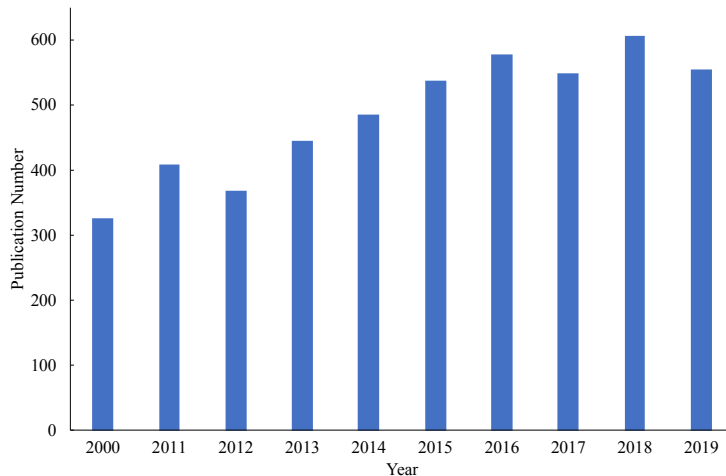
1. Introduction

The choice of appropriate ligand in metal complexes is critical for their catalytic performance especially in the field of homogeneous catalysis. Pincer tridentate ligands stand out because they can be fine-tuned for steric and electronic properties. The balance of both stability and reactivity of pincer-based complexes can be determined by ligand modification and metal center variation; this allows enhancement of metal complex stability, chemoselectivity, and reactivity in catalytic reactions^{1 2}.

Pincer ligands are tridentate ligands that coordinate tightly to three vacant sites of a metal center, usually in a *mer* geometry³. Rigid pincer ligands are extraordinarily efficient ligands in asymmetric catalysis by stabilizing wingtip groups from rotating, thus maintaining a geometry that directs appropriate substituents into active site of the catalyst. The English word “pincer” was first introduced in 1981 by van Koten and derived from Dutch word *tang* which means wrench⁴. This phrase emphasizes the characteristic that pincer ligands bind metal center tightly.

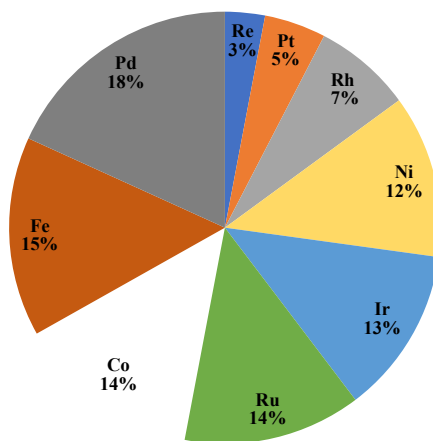
Due to a number of unanticipated properties, an extremely diverse range of pincer complexes have been designed and reported over the past few years (Figure 1.1). However, rhenium pincer complexes have not been researched as much as other metal complexes such as palladium and iron. In 2019, rhenium pincer complexes made up only around 3% of the total publications on pincer complexes (Figure 1.2).

Figure 1.1 Number of publications on pincer complexes since 2000



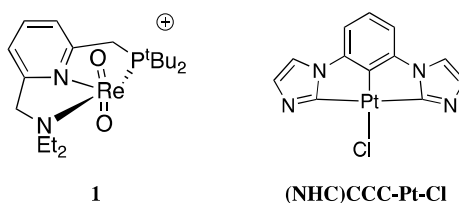
Rhenium pincer complexes have shown broad activity in different catalysis including metal ligand cooperation through aromatization/dearomatization process ⁵, alkane dehydrogenation, Lewis acid catalysis ⁶, and small molecules activation ^{7 8}.

Figure 1.2 The percentages of publications in 2019 on pincer complexes displayed by metal ions



The nomenclature of pincer ligand represents three donor positions in order (**1** contains PNN ((PNN = 6-(di-*tert*-butylphosphinomethylene)-2-(*N,N*-diethylamino-methyl)-1,6-dihydropyridine)) pincer (Figure 1.3) ⁹. Pincer complexes like **1** feature a fixed meridional geometry with approximately 90° inter-ligand angles. If N-heterocyclic carbene exists as one of donor ligand, the representation of pincer ligand would be (NHC)CCC ((NHC)CCC = 2-(1,3-Bis(N-butylimidazol-2-ylidene)phenylene)(chloro)) indicating that donor carbon belongs to N-heterocyclic carbene (Figure 1.3 (NHC)CCC-Pt-Cl)¹⁰.

Figure 1.3 Nomenclature of pincer ligand complexes



Pincer complexes reveal distinct natures by fine tuning steric and electronic factors on ligand design without varying coordination geometry¹¹⁻¹³. The coordination usually favors *mer* tridentate geometry but permit uncommon *fac* coordination ¹⁴.

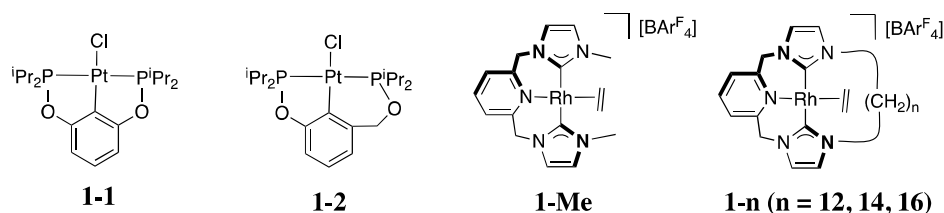
2. Pincer Ligand Design

Ring Size Effects

Researchers usually report results on one specific ring size and rarely involve different ring sizes. Wang and coworkers report unsymmetrical PCP' bis(phosphinito) ligand complex **1-1**, with a flexible 6-membered ring and increased P–M–P angle, is more reactive than related symmetrical PCP bis(phosphinito) complex **1-2** towards allylic alkylation (Figure 1.4)¹⁵.

Analogous ligand ring effect are discussed recently by Gyton et al¹⁶. NHC based pincer complexes $[\text{Rh}(\text{CNC}-n)(\text{C}_2\text{H}_4)][\text{BAr}^{\text{F}}_4]$ (**1-n**; $n=12, 14, 16$; $\text{Ar}^{\text{F}}=3,5-(\text{CF}_3)_2\text{C}_6\text{H}_3$) are more efficient in mediating terminal alkyne homocoupling reactions than $[\text{Rh}(\text{CNC}-\text{Me})(\text{C}_2\text{H}_4)][\text{BAr}^{\text{F}}_4]$ (**1-Me**) as macrocyclic ligand is introduced. Ring size modification in turns expands tunability of pincer ligand chelating effect and leads to unanticipated properties of metal complexes.

Figure 1.4 Ring size effect

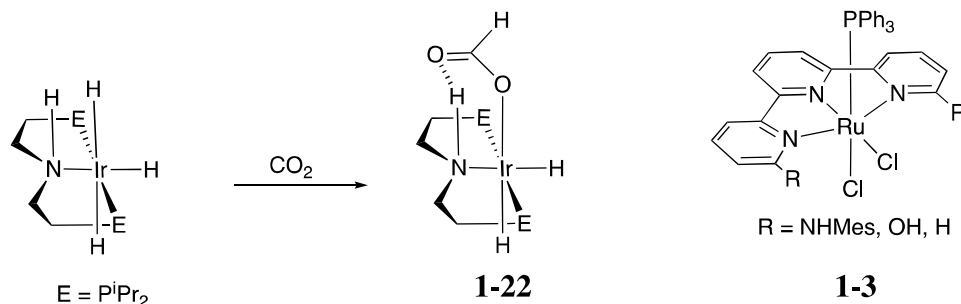


Secondary Coordination Sphere Effects

Pincer geometry allows secondary sphere coordination with a wide variety of functional groups adjacent to the metal center, while also electronically controlling the complexes. Hazari et al. successfully inserted CO₂ into iridium hydride with a H-bond donor in the outer sphere (Figure 1.5)¹⁷, unfavored generally. Thermodynamic study suggests *trans*-effect of ligand opposing to

hydride is the main factor in CO₂ insertion: strong donating *trans*-effect ligand weakens metal hydride bond, decreases electrophilicity of hydride and promotes CO₂ insertion. Iridium complex **1-22** is isolated and reported one of the most active water-soluble catalyst for CO₂ reduction to formate.

Figure 1.5 Outer sphere effect



In a more recent study, dehydrogenation catalyzed by ruthenium terpyridine pincer complexes (**1-3**) is improved through outer sphere ligand substitution, from -H to -OH to -NH(Ar)¹⁸. Catalyst recycling experiments demonstrate steric effect exerted by mesityl amino group on terpyridine ligand stabilizes reactive ruthenium intermediate. Modification of secondary sphere ligand opens the gate for new ligand design. Moreover, precisely understanding these outer sphere interactions and ultimately elucidating the influence on transition metal catalysis are warranted.

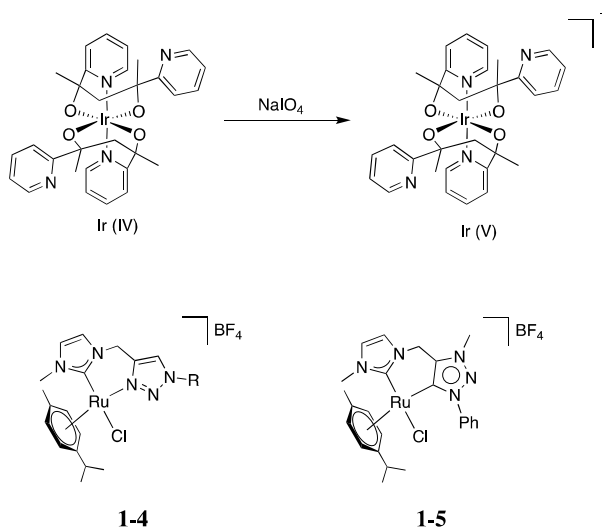
Stereoelectronic Effects

Orientation of pincer ligand permits various oxidation state of metal centers. For example, iridium pincer complexes in Figure 1.6 reveal four coplanar alkoxide groups in *d_{xy}* plane, therefore, allowing oxidation state of Ir(IV) and even Ir(V) through oxidation¹⁹. This unusual phenomenon of mononuclear coordination with N₂O₂ pincer donor ligand breaks the degeneracy of d-orbital and favors high iridium oxidation states +4 and +5.

This example also reveals by introducing more branched linker between donors, the N,O,O ligand can represent unfavored *fac* coordination geometry in pincer complexes.

Another example of stereoelectronic impact is by fine-tuning electronic profile of ancillary chelating carbene donors, catalytic efficiencies on Ru (II) pincer complexes have been significantly enhanced²⁰. Dicarbene species **1-5** showed better reactivity towards hydrogenation of ketone and aldimine compared to **1-4**. This may be due to a relatively electron-rich metal center promoted by superior donating effect of triazole-C-donor in **1-5**, rather than triazole-N-donor in **1-4**^{21 22 23}.

Figure 1.6 Stereoelectronic effect

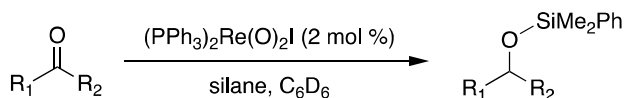


3. Efficient Reduction Methodologies Catalyzed by Oxo-Rhenium Complexes

Reduction of Carbonyl Compounds with Silane/Oxo-Re catalysts

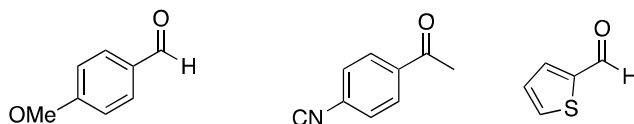
Toste initially discovered the carbonyl hydrosilylation reaction catalyzed by oxo-rhenium complex $\text{ReIO}_2(\text{PPh}_3)_2$ (Figure 1.7)²⁴. This reaction is tolerant to a variety of functional groups such as halo, nitro, amino and cyano. Furthermore, metal-dioxo complex represents as a reduction catalyst here which is reversal from traditional function as oxidation catalyst.

Figure 1.7 Hydrosilylation catalyzed by $\text{ReIO}_2(\text{PPh}_3)_2$



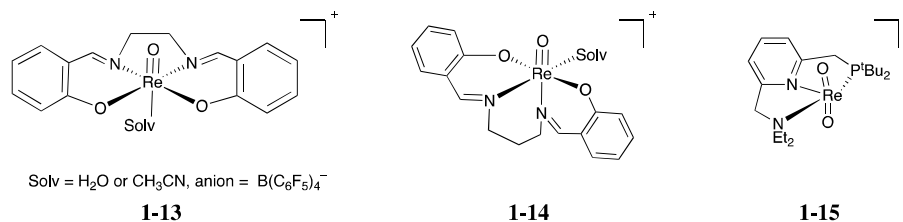
Silane = SiEt_3H , Me_2PhSiH , MePh_2SiH , $t\text{-BuMe}_2\text{SiH}$

Selected examples



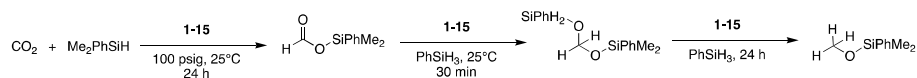
Our group explored the hydrosilylation of high-valent cationic monooxo-rhenium(V) complexes **1-13** and **1-14** towards carbonyl substrates, and dioxo-rhenium(V) complexes **1-15** (Figure 1.8) on CO_2 reduction^{25,26}. These two salen ancillary ligands containing complexes showed excellent catalytic activity under mild, open-flask condition with silyl-protected alcohol as product with the tolerance of a variety of functional groups such as alkene, alkyne, halogens, nitro and esters. The mechanism proceeds through a nonhydride concerted pathway with the formation of η^2 -silane adduct.

Figure 1.8 Cationic salen and pincer rhenium(V) complexes for catalytic hydrosilylation



Recently, our group reported the synthesis of high-valent dioxo-rhenium pincer complex **1-15** and its reactivity for CO₂ reduction with organosilane Me₂PhSiH. This novel methodology is capable of converting CO₂ to silyl formate, silyl formal and silyl-protected methanol over a longer reaction time (Figure 1.9).

Figure 1.9 Hydrosilylative CO₂ reduction catalyzed by **1-15**



Other rhenium oxo complexes MTO (CH₃ReO₃) and ReOCl₃(PPh₃)₂ display similar reactivity for carbonyl aliphatic and aromatic aldehydes²⁷. Among those Re₂O₇ was most effective towards aldehydes, resulting >95 % yield silyl ether in 25 °C within 30 min; whereas MTO and ReOCl₃(PPh₃)₂ were effective towards ketones. Several other high-valent rhenium complexes have been reported in the literature for reductive hydrosilylation reactions of unsaturated compounds²⁸⁻³¹.

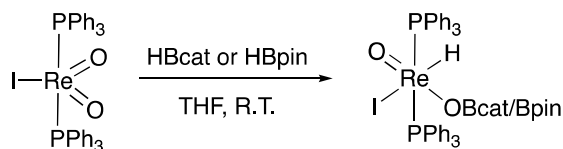
The mechanism for oxo-rhenium catalyzed hydrosilylation reaction is detailed in chapter 3.

Reduction of Sulfoxides with Boranes/Oxo-Re catalysts System

After the discovery of Si–H bond activation catalyzed by oxo-rhenium complexes, Fernandes and co-workers explored the activation of B–H bond with high-valent oxo-rhenium complexes^{32,33 34}. The first example of B–H bond activation was achieved from reaction of $\text{ReIO}_2(\text{PPh}_3)_2$ with the boranes catecholborane (HBcat) and pinacolborane (HBpin). The successful isolation and structural characterization of $(\text{PPh}_3)_2(\text{O})(\text{I})\text{Re}(\text{H})\text{OBcat}$ and $(\text{PPh}_3)_2(\text{O})(\text{I})\text{Re}(\text{H})\text{OBpin}$ showed octahedral geometry rhenium hydrides are formed by addition of B–H bond across oxo-rhenium bond without ligand dissociation (Figure 1.10).

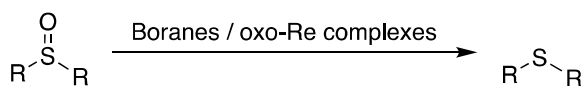
Figure 1.10 Synthesis of high valent rhenium hydrides

$(\text{PPh}_3)_2(\text{O})(\text{I})\text{Re}(\text{H})\text{OBcat}/(\text{PPh}_3)_2(\text{O})(\text{I})\text{Re}(\text{H})\text{OBpin}$

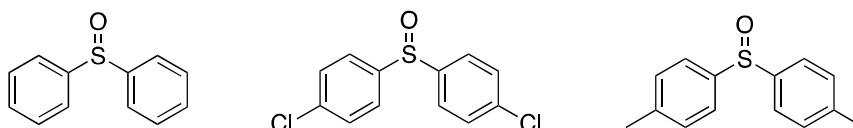


Later they investigated reduction of sulfoxides to sulfides, which is essential in organic synthesis^{35,36} and biochemical reactions³⁷, using boranes HBcat, HBpin, and $\text{BH}_3 \cdot \text{THF}$ in the presence of catalytic amount of oxo-rhenium complexes $\text{ReIO}_2(\text{PPh}_3)_2$, $\text{ReOCl}_3(\text{PPh}_3)_2$, $\text{ReOCl}_3(\text{dppm})$, Re_2O_7 , MTO, and HReO_4 (Figure 1.11). The catalytic system HBcat/ $\text{ReIO}_2(\text{PPh}_3)_2$ (1 mol%), HBcat/ MTO (1 mol%) and HBcat/ Re_2O_7 (1 mol%) demonstrated high efficiency towards deoxygenation of sulfoxides at room temperature.

Figure 1.11 Reduction of sulfoxides with the system boranes/oxo-rhenium complexes



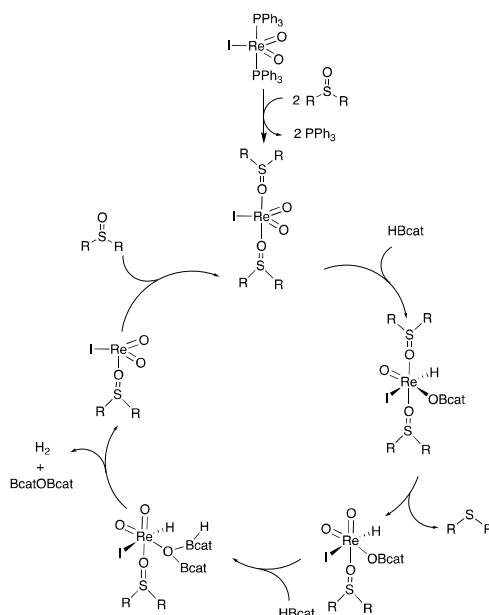
Selected examples



The mechanism was also proposed later for reduction of sulfoxides with catalytic system HBcat/ $\text{ReIO}_2(\text{PPh}_3)_2$ based on the results of DFT computational study (Figure 1.12). These results suggest the catalytic cycle starts with the substitution of two phosphines by two sulfoxides molecule on one active catalyst; whereas one sulfoxide per rhenium complex is reduced. Second step is the formation of octahedral rhenium hydride by addition of first molecule of HBcat, followed by the loss of sulfide R_2S and the oxidation of Re(V) to Re(VII) on the metal center. Second equivalent of HBcat is required to reduce Re(VII) complex back to the initial Re(V) catalyst, as catBOBcat and H_2 are generated at the end.

Literature reported borane activation can be achieved by other transition metals (e.g., Fe, Rh and Pd) but only in low oxidation state^{38 39}.

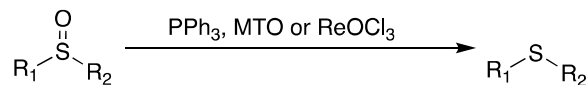
Figure 1.12 Proposed mechanism for the reduction of sulfoxides with the system HBcat/ $\text{ReIO}_2(\text{PPh}_3)_2$



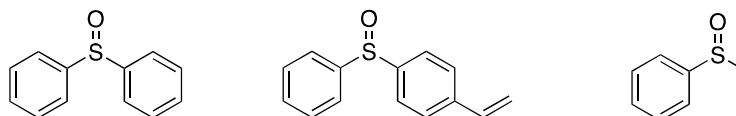
Reduction of Sulfoxides with PPh₃/Oxo-Re catalysts System

Early discovered in 1995 by Espenson and coworkers, high-valent oxo-rhenium complex MTO (CH₃ReO₃) showed high efficiency towards the deoxygenation of a variety of aliphatic and aromatic sulfoxides with triphenylphosphine PPh₃ as reducing agent (Figure 1.13) ⁴⁰.

Figure 1.13 Reduction of sulfoxides with system PPh₃/oxo-rhenium catalysts



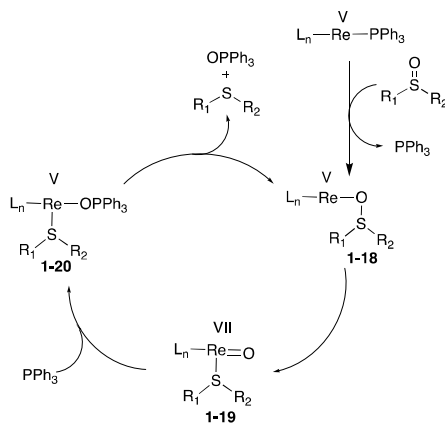
Selected examples



Later in 1996, rhenium(V) catalyst ReOCl₃(PPh₃)₂ was proved to reduce a wide range of aryl and alkyl sulfoxides with triphenylphosphine in air and this reaction was

water tolerant (Figure 1.13)⁴¹. The proposed catalytic cycle (Figure 1.14) begins with the coordination of sulfoxide and dissociation of PPh₃, generating a sulfoxide Re(V) complex **1-18**. An oxidative addition step through S–O cleavage results an electrophilic Re(VII) sulfide complex **1-19**. Phosphine reduction forms a phosphine oxide Re(V) species **1-20** and releases sulfide and phosphine oxide last. The study of reaction rate reveals more basic sulfoxides would react faster due to nucleophilic attack step of the phosphine on protonated sulfoxide oxygen. However, there was no significant impact on steric effect of different aryl sulfoxides.

Figure 1.14 Proposed mechanism for deoxygenation of sulfoxides with system PPh₃/ReOCl₃(PPh₃)₂

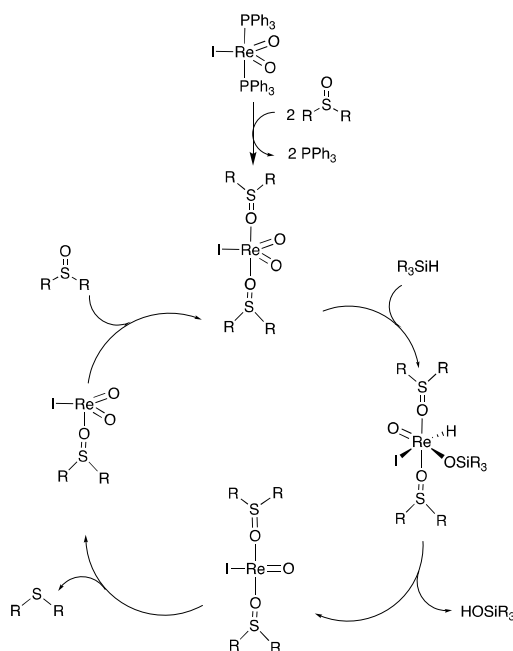


Reduction of Sulfoxides with silane/Oxo-Re catalysts System

Later Fernandes group reported the novel system silane/oxo-rhenium(V) and (VII) for efficient reduction of a variety of aromatic sulfoxides. ReIO₂(PPh₃)₂ was proved to be the most effective catalyst^{42 34}. The substrate scale shows the system can tolerate a large range of functional groups including aldehydes, esters, halogens and nitros. The mechanism proposed for reduction of sulfoxides with

silane/ $\text{ReIO}_2(\text{PPh}_3)_2$ involves the following steps: sulfoxides substitution of phosphine, affording $\text{ReIO}_2(\text{R}_2\text{SO})_2$; addition of Si–H bond of silane with the formation of rhenium hydride species $(\text{R}_2\text{SO})_2(\text{O})\text{IRe}(\text{H})\text{OSiR}_3$. Next step is the elimination of HOSiR_3 with the formation of $\text{Re}(\text{III})$ complex $\text{ReI}(\text{O})(\text{R}_2\text{SO})_2$; rearrangement of this complex can easily liberate R_2S and regenerate $\text{ReIO}_2(\text{R}_2\text{SO})$ (Figure 1.15).

Figure 1.15 Proposed mechanism for the reduction of sulfoxides with the system

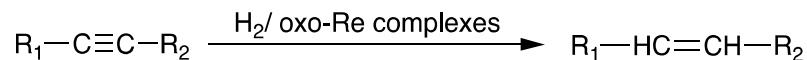


Reduction of Alkynes with $\text{H}_2/\text{Oxo-Re}$ catalyst System

Royo and co-workers discovered high-valent oxo-rhenium(V) complexes CH_3ReO_3 (MTO) and $\text{ReIO}_2(\text{PPh}_3)_2$ are efficient in hydrogenation of alkynes, affording corresponded alkenes in excellent yield under various conditions using hydrogen as reducing agent (Figure 1.16)⁴³. Both catalysts are active towards reduction of 1-hexyne,

phenylacetylene and 3-hexyne. Further mechanism investigation is needed on this hydrogenation process as well as substrate scope extension.

Figure 1.16 Reduction of alkynes catalyzed by oxo-rhenium catalysts

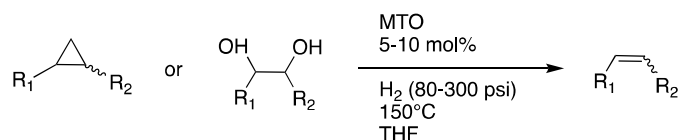


Reduction of Epoxides and Polyols with H₂/Oxo-Re catalysts System

Reduction of high oxygen contents molecules gives possibility of the substitution of fossil fuel by biomass derived chemicals⁴⁴. Rhenium catalyzed doxydehydration (DODH) of polyols is a typical system for upgrading biomass related glycerol and sugar alcohols into corresponding alkenes.

Aiming to utilize biomass derived diols to value-added chemicals, our group in 2009 first described reduction of diols and epoxides, including aromatic epoxides, into corresponding alkenes catalyzed by MTO using hydrogen as a reductant under reasonable mild conditions (150 °C and 5-20 atm), with water as the only byproduct (Figure 1.17)⁴⁵. This described methodology is water and air stable and highly selective towards cis cyclic diols.

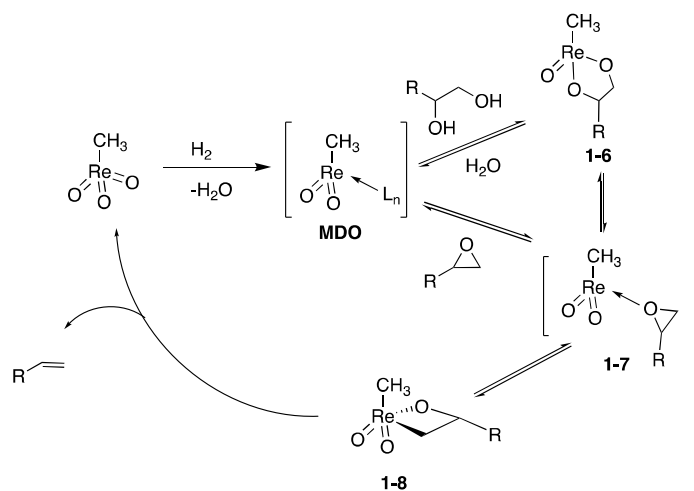
Figure 1.17 Deoxygenation of epoxides and diols



The plausible mechanism proceeded through the formation of rhenium diolate **1-6** or epoxide-rhenium adduct **1-7**, as methyldioxorhenium (MDO) was detected, extruding alkene via metallaoxetane intermediate **1-8** (Figure 1.18).

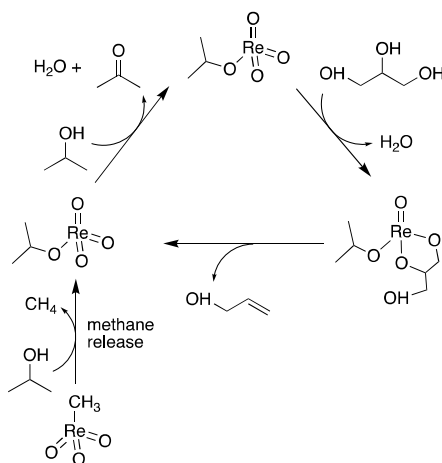
Figure 1.18 Proposed mechanism for deoxygenation of diols with system

H₂/MTO



Mascitti et al. recently suggested an alternative pathway on MTO catalyzed DODH of glycerol, with the prior methane release, based on experimental and theoretical results (Figure 1.19)⁴⁶. DFT calculations prove the release of methane is thermodynamically and kinetically more favorable than direct reduction of MTO, with a reaction free energy of $-18.5 \text{ kcal mol}^{-1}$. In spite the nature of different rhenium complexes discussed here, all catalysts were transformed during an induction period into active Re (VII) alkoxide species. Reduction occurs for MTO catalyzed DODH to convert Re (VII) to Re (V).

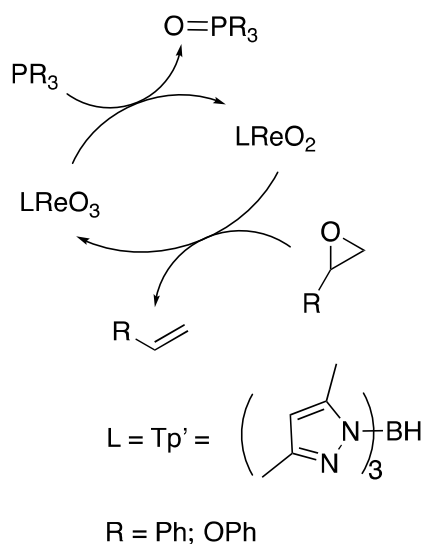
Figure 1.19 Alternative mechanism of MTO catalyzed DODH of glycerol



Reduction of Epoxides with PPh₃/Oxo-Re catalysts System

Early in 1995, MTO was proved to be efficient in catalyzing deoxygenation of aliphatic and aromatic epoxides into olefins with the presence of triphenylphosphine⁴⁰. Later in 2000, another methodology for deoxygenation of epoxide with triphenyl phosphine or triphenyl phosphate as reductant catalyzed by oxo-rhenium complex Tp'ReO₃ (Tp' = tris(3,5-dimethylpyrazolyl)hydridoborate) was reported⁴⁷. A concerted mechanism proposal was proposed for Tp'ReO₃ catalyzed reduction of epoxides (Figure 1.20). A brief induction period was observed suggesting that LReO₃ might represent the resting state of the catalyst that generate either LReO₂ active catalyst or the dimeric form of dioxorhenium(V) intermediate⁴⁸; stoichiometric reaction resulted in a dark green color species, suggesting Re–Re dimer.

Figure 1.20 Reduction of epoxides with system PR₃/Tp'ReO₃



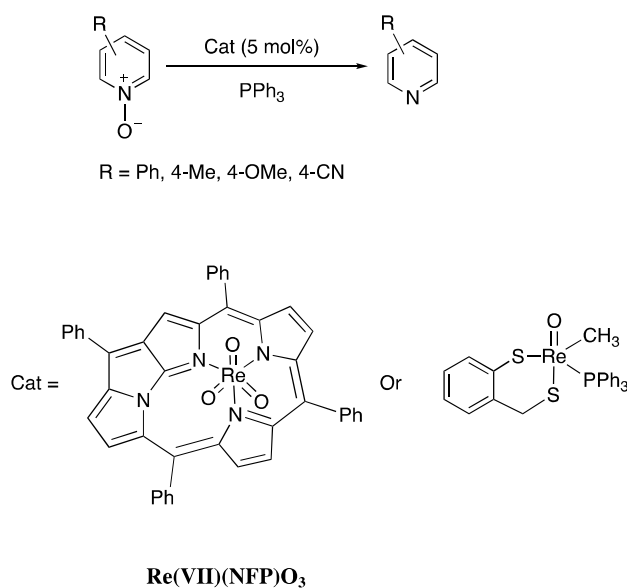
Reduction of Epoxides without Any Reductant

In 2011, Fernandes and coworkers first reported oxo-Re(V) and oxo-Re(VII) complexes catalyzed epoxides deoxygenation without adding any reducing agent in refluxing toluene under air. Among these catalysts $\text{ReIO}_2(\text{PPh}_3)_2$ and $\text{ReOCl}_3(\text{PPh}_3)_2$ showed high reusability towards deoxygenation of 4-chlorostyrene oxide. This novel method achieved high chemoselectivity in the presence of other functional groups including ketone, aldehyde, sulfoxide, amide and cyano in an extended reaction time. In comparison to other oxo-Re catalyzed deoxygenation reactions^{49,50}, this methodology is more economic friendly which minimizes the use and produce of hazardous chemicals. Although the mechanistic study for this reaction is still under investigation, the formation of 1-phenyl-1,2-ethanediol was observed during deoxygenation of styrene oxide. The Lewis acid property of oxo-rhenium complexes should promote hydrolytic epoxide ring opening, and result diol as intermediate before complete deoxygenation to corresponding alkenes.

Reduction of N-oxides with $\text{PPh}_3/\text{Oxo-Re}$ catalysts System

Deoxygenation of pyridine N-oxide derivatives catalyzed with porphyrin rhenium trioxo complexes Re(VII)(NFP)O_3 (NFP = N-fused porphyrin) using phosphine as reductant was explored (Figure 1.21) ⁵¹. This method was tested with a variety of pyridine N-oxides and it is functional groups compatible such as hydroxy, methoxy and cyanide, affording corresponding pyridine products in high yields. This catalytic process exhibited a turnover number of 340,000 and excellent site-selectivity.

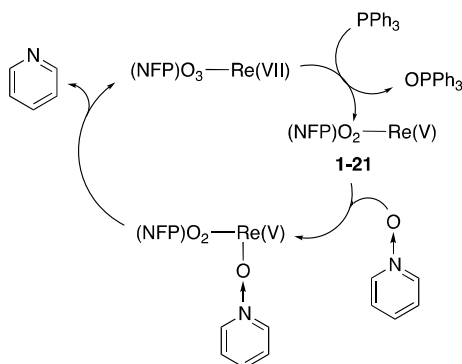
Figure 1.21 Catalytic deoxygenation of pyridine N-oxides



The mechanistic study suggested intermediate Re(V) species **1-21** was the active catalyst, which can be stabilized through coordination with pyridine N-oxide (**Figure 1.22**). The π -electrons around pyridine ring stabilize Re(V) complex until the cleavage of Re-O bond, affording the product and starting Re(VII)(NFP)O_3 . Decomposition of Re(V) complex to Re(III) complex might cause catalyst reactivity shut down. Analogous catalytic pathway was proposed in

several other trioxo-Re(VII) species mediated reductions⁵²⁻⁵⁴. This methodology enriched the field of porphyrinoid chemistry.

Figure 1.22 Proposed mechanism for deoxygenation of pyridine N-oxides



Another oxo-rhenium complex $\text{CH}_3\text{Re(O)(SR)}_2\text{PPh}_3$ (SR = dianion of 2-(mercaptomethyl)thiophenol) is capable of catalyzing deoxygenation of N-oxides to pyridine in high yield (Figure 1.21)⁵⁵. However, the mechanism for this reaction still remains under investigation.

In recent years, frustrated Lewis pair has emerged as a powerful method in small molecule activation and catalysis. While most researchers focused on the development of metal-free FLP catalysis, there have been a few reports on transition metal participated FLP system: metal complexes involved as either Lewis acid or base component^{56 57 58 59 60 61 62 63}. Late transition metals such as rhenium has been demonstrated to capture small molecules and function as frustrated Lewis pair towards catalysis⁶⁴⁻⁶⁶.

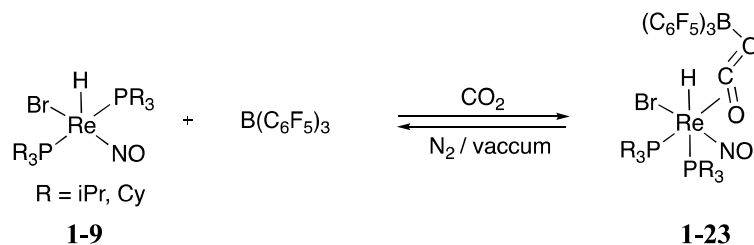
4. Small Molecule Activation through Frustrated Lewis Pair

CO₂ Activation

Berke and co-workers demonstrated activation of CO₂ can be achieved by cooperative Re-H / B(C₆F₅)₃ system with Re-H functioning as Lewis base (Figure 1.23).

It is noteworthy that unsaturated rhenium hydride species $[\text{ReHBr}(\text{NO})(\text{PR}_3)_2]$ (R = iso-propyl or cymene) (**1-9**) only captures CO_2 in addition of Lewis acid $\text{B}(\text{C}_6\text{F}_5)_3$, with CO_2 coordinated between rhenium and borane (**1-23**).

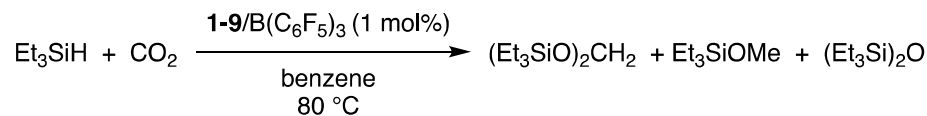
Figure 1.23 CO_2 insertion into Re–H bond



Catalytic reduction of CO_2 by excess of hydrosilane led to formation of silyl products, including $(\text{Et}_3\text{SiO})_2\text{CH}_2$ as the reduced form of CO_2 .

Hydrogenation of CO_2 in the presence of sterically hindered bases (e.g., NEt_3 , $\text{P}(t\text{Bu})_3$, and $\text{HN}(\text{SiMe}_3)_2$) resulted the formation of formate salt $[\text{HCOO}^-][\text{Base}^+]$ (Figure 1.24). Various base strengths were tested and these results elucidated both steric hinderance and basicity affect efficiency of CO_2 hydrogenation.

Figure 1.24 Catalytic reduction of CO_2 by Et_3SiH in Re–H/ $\text{B}(\text{C}_6\text{F}_5)_3$ system

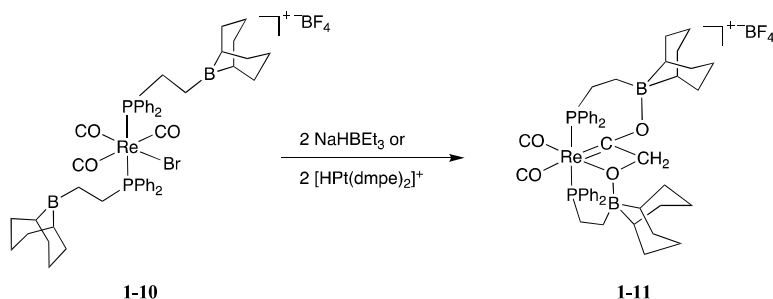


CO Activation

Analogous process is observed in reduction of CO through intramolecular Lewis acid system (Figure 1.25). By incorporating pendant borane into cationic

carbonyl rhenium hydride species **1-10**, hydride transfer reactivity can be promoted, new C–C bond formation is facilitated spontaneously through alkyl migration, with the generation of a novel boroxo carbene rhenium complex **1-11**.

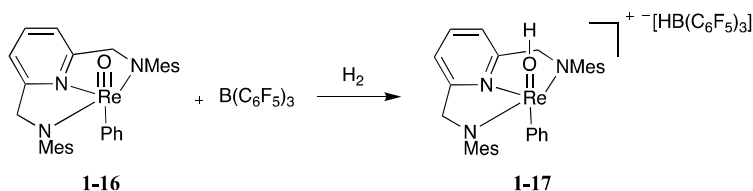
Figure 1.25 Reductive coupling of CO with pendant borane



H₂ Activation

Ison and co-workers reported the catalytic system using Lewis acid-base adduct of high-valent oxo-rhenium pincer complex with B(C₆F₅)₃ in the presence of H₂ to hydrogenate a variety of unactive olefins at 100 °C (Figure 1.26). Mechanistic investigation suggested a non-traditional hydrogenation pathway where the olefin was activated through terminal oxo ligand and not the metal center⁶⁷. According to DFT calculation, FLP **1-16** activates the cleavage of H₂ heterolytically and generates onium hydridoborate **1-17**.

Figure 1.26 oxo-Re complex as a FLP in the activation of H₂

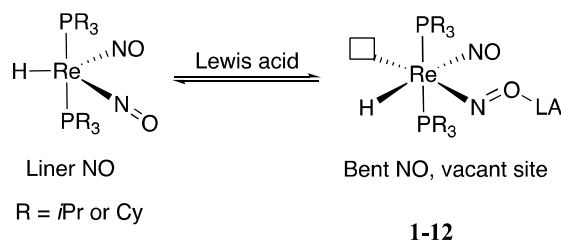


NO Activation

NO-type dinitrosyl rhenium hydride catalyst functionalized as Lewis acid component in alkene hydrogenations was explored by Jiang et al⁶⁸. Denoted as “catalytic

nitrosyl effect”, the catalysis is initiated via NO bending to offer vacant site (Figure 1.27). NO bending process is facilitated by coordination of either neutral or cationic Lewis acids ($B(C_6F_5)_3$ or $[Et]^+$). These electron-deficient five coordinated rhenium hydride intermediates **1-12** can render subsequent alkene insertion and/or H_2 activation.

Figure 1.27 Catalytic nitrosyl effect



5. Conclusions and Future Prospects

This chapter provides an overview of the tridentate pincer ligand design, reduction reactions catalyzed by high-valent oxo-rhenium complexes and small molecule activation by rhenium center through frustrated Lewis pair system. Section 1.2 described key factors in tridentate pincer ligand design that impact desired physical and chemical properties of metal complexes; extends metal’s primary sphere and therefore provide additional opportunities on catalysis. Through both electronic and steric modification of the tridentate pincer ligand platform, coordination sphere as well as catalytic reactivity of metal complexes can be extended. Section 1.3 gives a summarize on a variety of deoxygenative reductions catalyzed by high-valent oxo-rhenium complexes. Using these oxo-rhenium catalysts several functional groups such as carbonyl compounds, sulfoxide, alkyne, epoxides and N-oxides can be reduced to lowered oxygen

content value-added chemicals. In many cases, reduction can be attained under simple, mild and eco-friendly conditions. The activation of small molecules using rhenium complexes as frustrated Lewis pair platform is a new and active area of research and will certainly provide alternatives to existing organometallic framework. In the hope that combination of extended rhenium assisted FLP with well-known suite of ligand design and reduction reactions of oxo-rhenium complexes could lead yet to new chemistry.

6. References

- (1) Gunanathan, C.; Milstein, D. *Chem. Rev.* **2014**, *114* (24), 12024–12087.
- (2) O'Reilly, M. E.; Veige, A. S. *Chem. Soc. Rev.* **2014**, *43* (17), 6325–6369.
- (3) Lee, D. W.; Jensen, C. M.; Morales-Morales, D. *Organometallics*. **2003**, *22* (23), 4744–4749.
- (4) van Koten, G. *Pure. App. Chem.* **2005**, *61*, 1681–1694.
- (5) Vogt, M.; Nerush, A.; Diskin-Posner, Y.; Ben-David, Y.; Milstein, D. *Chem. Sci.* **2014**, *5* (5), 2043–2051.
- (6) Flynn, S. R.; Wass, D. F. *ACS Catal.* **2013**, *3* (11), 2574–2581.
- (7) Lindley, B. M.; van Alten, R. S.; Finger, M.; Schendzielorz, F.; Würtele, C.; Miller, A. J. M.; Siewert, I.; Schneider, S. *J. Am. Chem. Soc.* **2018**, *140* (25), 7922–7935.
- (8) Kosanovich, A. J.; Reibenspies, J. H.; Ozerov, O. V. *Organometallics*. **2016**, *35* (4), 513–519.
- (9) Mazzotta, M. G.; Pichaandi, K. R.; Fanwick, P. E.; Abu-Omar, M. M. *Angew. Chem. Int. Ed.* **2014**, *53* (32), 8320–8322.

- (10) Zhang, X.; Wright, A. M.; DeYonker, N. J.; Hollis, T. K.; Hammer, N. I.; Webster, C. E.; Valente, E. J. *Organometallics*. **2012**, *31* (5), 1664–1672.
- (11) van der Boom, M. E.; Milstein, D. *Chem. Rev.* **2003**, *103* (5), 1759–1792.
- (12) Gagliardo, M.; Amijs, C. H. M.; Lutz, M.; Spek, A. L.; Havenith, R. W. A.; Hartl, F.; van Klink, G. P. M.; van Koten, G. *Inorg. Chem.* **2007**, *46* (26), 11133–11144.
- (13) Jones, N. D.; Cavell, R. G. *J. Organomet. Chem.* **2005**, *690* (24-25), 5485–5496.
- (14) Choi, J.; MacArthur, A.; Brookhart, M.; Goldman, A. S. *Chem. Rev.* **2011**, *111* (3), 1761–1779.
- (15) Wang, Z.; Eberhard, M. R.; Jensen, C. M.; Matsukawa, S.; Yamamoto, Y. *J. Org. Chem.* **2003**, *681* (1-2), 189–195.
- (16) Storey, C. M.; Gyton, M. R.; Andrew, R. E.; Chaplin, A. B. *Chem. Eur. J.* **2020**, *34*, 1468.
- (17) Schmeier, T. J.; Dobereiner, G. E.; Crabtree, R. H.; Hazari, N. *J. Am. Chem. Soc.* **2011**, *133* (24), 9274–9277.
- (18) Dahl, E. W.; Louis-Goff, T.; Szymczak, N. K. *Chem. Commun.* **2017**, *53* (14), 2287–2289.
- (19) Sharninghausen, L. S.; Sinha, S. B.; Shopov, D. Y.; Mercado, B. Q.; Balcells, D.; Brudvig, G. W.; Crabtree, R. H. *Angewandte Chemie*. **2017**, *129* (42), 13227–13231.

- (20) Illam, P. M.; Donthireddy, S. N. R.; Chakrabartty, S.; Rit, A. *Organometallics*. **2019**, *38* (13), 2610–2623.
- (21) Donnelly, K. F.; Petronilho, A.; Albrecht, M. *Chem. Commun.* **2013**, *49* (12), 1145–1159.
- (22) Mathew, P.; Neels, A.; Albrecht, M. *J. Am. Chem. Soc.* **2008**, *130* (41), 13534–13535.
- (23) Krüger, A.; Albrecht, M. *Aust. J. Chem.* **2011**, *64* (8), 1113–1117.
- (24) Kennedy-Smith, J. J.; Nolin, K. A.; Gunterman, H. P.; Toste, D. *J. Am. Chem. Soc.* **2003**, *125* (14), 4056–4057.
- (25) Du, G.; Abu-Omar, M. M. *Organometallics*. **2006**, *25* (20), 4920–4923.
- (26) Mazzotta, M. G.; Xiong, M.; Abu-Omar, M. M. *Organometallics*. **2017**, *36* (9), 1688–1691.
- (27) Royo, B.; Romão, C. C. *J. Mol. Catal. A: Chem.* **2005**, *236* (1-2), 107–112.
- (28) Gu, P.; Wang, W.; Wang, Y.; Wei, H. *Organometallics*. **2012**, *32* (1), 47–51.
- (29) Wang, J.; Wang, W.; Huang, L.; Yang, X.; Wei, H. *ChemPhysChem*. **2015**, *16* (5), 1052–1060.
- (30) Nolin, K. A.; Ahn, R. W.; Toste, D. *J. Am. Chem. Soc.* **2005**, *127* (36), 12462–12463.
- (31) Rende, D. E.; Kim, R.; Beck, C. M.; Wojcicki, A. *Inorganica Chimica Acta*. **1995**, *240* (1-2), 435–439.

- (32) Fernandes, A. C.; Fernandes, J. A.; Romão, C. C.; Veiros, L. F.; Calhorda, M. J. *Organometallics*. **2010**, *29* (21), 5517–5525.
- (33) Sousa, S. C. A.; Bernardo, J. R.; Romão, C. C.; Fernandes, A. C. *Tetrahedron*. **2012**, *68* (39), 8194–8197.
- (34) Cabrita, I.; Sousa, S. C. A.; Fernandes, A. C. *Tetrahedron Lett.* **2010**, *51* (47), 6132–6135.
- (35) Fujiki, K.; Kurita, S. *Synth. Commun.* **2010**, *40*, 1794–1801.
- (36) Abo, M.; Dejima, M.; Asano, F.; Okubo, A.; Yamazaki, S. *Tetrahedron: Asymmetry*. **2000**, *11* (3), 823–828.
- (37) Nicolás, E.; Vilaseca, M.; Giralt, E. *Tetrahedron*. **1995**, *51* (19), 5701–5710.
- (38) Vogels, C. M.; Westcott, S. A. *Curr. Org. Chem.* **2005**, *9* (7), 687–699.
- (39) Beletskaya, I.; Pelter, A. *Tetrahedron*. **1997**, *53* (14), 4957–5026.
- (40) Zhu, Z.; Espenson, J. H. *J. Mol. Catal. A: Chem.* **1995**, *103* (2), 87–94.
- (41) Arterburn, J.; Perry, M. *Tetrahedron Lett.* **1996**, 7941–7944.
- (42) Sousa, S. C. A.; Fernandes, A. C. *Tetrahedron Lett.* **2009**, *50* (49), 6872–6876.
- (43) Reis, P. M.; Costa, P. J.; Romão, C. C.; Fernandes, J. A.; Calhorda, M. J.; Royo, B. *Dalton Trans.* **2008**, *125* (13), 1727–1728.

- (44) Dethlefsen, J. R.; Dethlefsen, J. R.; Fristrup, P.; Fristrup, P. *ChemSusChem*. **2015**, *8* (5), 767–775.
- (45) Ziegler, J.; Zdilla, M.; Evans, A.; Abu-Omar, M. *Inorg. Chem.* **2009**, 9998–10000.
- (46) Lupacchini, M.; Mascitti, A.; Canale, V.; Tonucci, L.; Colacino, E.; Passacantando, M.; Marrone, A.; d'Alessandro, N. *Catal. Sci. Technol.* **2019**, *9* (12), 3036–3046.
- (47) Gable, K.; Brown, E. C. *Organometallics*. **2000**, *19* (5), 944–946.
- (48) Paulo, A.; Domingos, A.; Marcalo, J.; de Matos, A. P.; Santos, I. *Inorg. Chem.* **1995**, *34* (8), 2113–2120.
- (49) Vkuturi, S.; Chapman, G.; Ahmad, I.; Nicholas, K. M. *Inorg. Chem.* **2010**, *49* (11), 4744–4746.
- (50) Gable, K. P.; Brown, E. C. *Synlett* **2003**, *2003* (14), 2243–2245.
- (51) Toganoh, M.; Fujino, K.; Ikeda, S.; Furuta, H. *Tetrahedron Lett.* **2008**, *49* (9), 1488–1491.
- (52) Gable, K. P.; Zhuravlev, F. A.; Yokochi, A. F. T. *Chem. Commun.* **1998**, *0* (7), 799–800.
- (53) Gable, K.; Brown, E. C. *J. Am. Chem. Soc.* **2003**, *125* (36), 11018–11026.
- (54) Lahti, D. W.; Espenson, J. H. *J. Am. Chem. Soc.* **2001**, *123* (25), 6014–6024.
- (55) Wang, Y.; Espenson, J. H. *Org. Lett.* **2000**, *2* (22), 3525–3526.
- (56) Metters, O. J.; Forrest, S. J. K.; Sparkes, H. A.; Manners, I.; Wass, D. F. *J. Am. Chem. Soc.* **2016**, *138* (6), 1994–2003.

- (57) Flynn, S. R.; Metters, O. J.; Manners, I.; Wass, D. F. *Organometallics*. **2016**, *35* (6), 847–850.
- (58) Cui, P.; Comanescu, C. C.; Iluc, V. M. *Chem. Commun.* **2015**, *51* (28), 6206–6209.
- (59) Xu, X.; Kehr, G.; Daniliuc, C. G.; Erker, G. *J. Am. Chem. Soc.* **2015**, *137* (13), 4550–4557.
- (60) Dobrovetsky, R.; Stephan, D. W. *Isr. J. Chem.* **2015**, *55* (2), 206–209.
- (61) Boone, M. P.; Stephan, D. W. *Organometallics*. **2013**, *33* (1), 387–393.
- (62) Frömel, S.; Kehr, G.; Fröhlich, R.; Daniliuc, C. G.; Erker, G. *Dalton Trans.* **2013**, *42* (40), 14531–14536.
- (63) Xu, X.; Kehr, G.; Daniliuc, C. G.; Erker, G. *Organometallics*. **2013**, *32* (24), 7306–7311.
- (64) Jiang, Y.; Blacque, O.; Fox, T.; Berke, H. *J. Am. Chem. Soc.* **2013**, *135* (20), 7751–7760.
- (65) Miller, A. J. M.; Labinger, J. A.; Bercaw, J. E. *J. Am. Chem. Soc.* **2008**, *130* (36), 11874–11875.
- (66) Lambic, N. S.; Sommer, R. D.; Ison, E. A. *J. Am. Chem. Soc.* **2016**, *138* (14), 4832–4842.
- (67) Boone, M. P.; Stephan, D. W. *J. Am. Chem. Soc.* **2013**, *135* (23), 8508–8511.

(68) Jiang, Y.; Huang, W.; Schmalle, H. W.; Blacque, O.; Fox, T.; Berke, H.
Organometallics. **2013**, 32 (23), 7043–7052.

Chapter II. Synthesis of Pincer Rhenium Complexes

1. Introduction

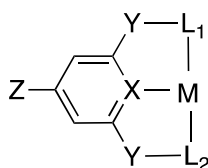
History of Rhenium element

Rhenium is a group 7 transition metal in the same group as manganese, technetium, and bohrium. Discovered in 1908 by Ogawa, a Japanese chemist, rhenium was the second-last natural stable element (the last one is hafnium) and named after the river Rhine in Europe. However, Ogawa incorrectly reported this new element nipponium which is believed today that it was in fact rhenium. It was not until 1925 that rhenium was officially announced by German chemists Noddack, Tacke, and Berg^{1 2}.

Typical for a transition metal, rhenium is used as a catalyst for emissive probe filaments, utilization of petroleum and extrardentary heat-resistant alloys^{3,4}. The chemistry of rhenium is rather diverse. It shows the largest range of oxidation states of any known element, from -1, 0, +1 and so on all the way up to +7 (most common oxidation state). It is also the first metal–metal quadruple bond discovered in history, in the form of $[\text{Re}_2\text{Cl}_8]^{2-}$ ⁵. Since rhenium is quite rare and is available only in trace amount, the price of rhenium metal is relatively high; however, it is cheaper than platinum, palladium, rhodium and ruthenium, which play central roles in catalytic reactions⁶. The reactivity of rhenium has not been explored as extensively as that of other transition complexes, especially as catalyst for organic synthesis⁷.

Pincer ligand complex

Figure 2.1 Steric and electronic control over pincer ligand



X: electronic control (C, N)

Y: introduction of chirality (CH₂, O, NH)

L: determines the hemilability of the pincer (P, N, O)

Z: determines electronic density of central donor (Halogen, R, RO)

Pincer ligands are tridentate ligand and have distinctive combination of properties. The

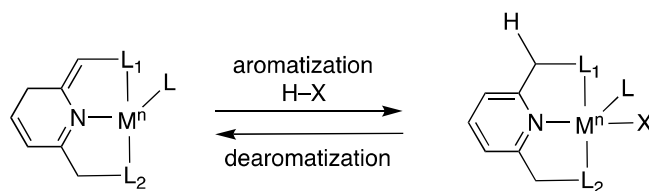
more rigid pincers can give exceptionally efficient ligands for asymmetric catalysis ⁸.

By tuning the electronic and steric properties of the pincer ligand, the nature of the complex can be modified with a fixed coordination geometry (Figure 2.1). To be more specific, the central donor atom X (typically C or N) can have a significant electronic impact, particularly through *trans* influence ⁹. The size of the linker arm Y determines the ring size and therefore influence the bite angle. Pincer ligand may introduce chirality into the complex by incorporating chiral L groups ¹⁰. Fine controlling of Z, a substituent on the central aromatic ring, can also modulate the electronic properties of the pincer ligand

11.

Bond Activation by MLC

Figure 2.2 Metal-ligand cooperation based on aromatization-dearomatization



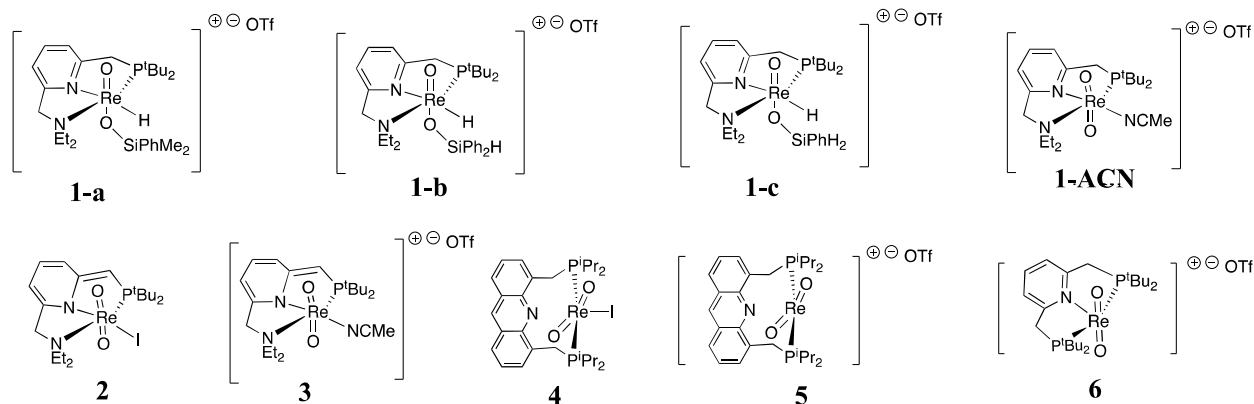
In conventional metal-based homogeneous catalyst, catalysis is essentially performed by the metal center, with the ligand not actively participating in bond making and breaking process. However, by incorporating bifunctional mode, both metal center and ligand participate in catalysis (Figure 2.2)¹². The bifunctional transition metal-based catalyst offers a great opportunity for stereoselective molecular transformation. Pincer complexes have found in various applications in synthesis, bond activation and catalysis^{12 13 15}. These bulky and electron rich ligand framework can also stabilize unsaturated complex. A new mode of bond activation by metal-ligand cooperation through aromatization-dearomatization of the pincer ligand was first discovered in 2005 by Milstein and coworkers¹⁴. The dearomatized complex can then activate chemical bond H-Y ($Y = H, OR, NR_2, C$) and regain aromaticity.

Organometallic chemistry and homogeneous catalysis can benefit from our ability to deploy a wide range of ligands with highly distinctive effects on reactivity of the

resulting complex. Early work emphasized monodentate and chelate ligands¹⁵. But in the last 15 years, pincer ligands have risen to prominence for their versatility and ease of use¹⁸⁻²⁰. The reactivity of rhenium pincer complexes has not been explored as extensively as that of other transition metal complexes.

In this Chapter, we report the isolation of rhenium hydride pincer complexes (**1-a**, **1-b**, **1-c**), which are considered potential active species in hydride mechanism (detailed in chapter 3). An equilibrium process was studied with solvent coordinated rhenium complex **1-ACN**. Dearomatized complexes (**2** and **3**) derived from **1** for MLC type catalysis of small molecules were isolated and characterized, and further implementation of the dearomatized complex possessing a PNN pincer system. In addition, complexes **4-6** were isolated by fine tuning the steric and electronic properties of the pincer ligand.

Scheme 2.1 Synthesis of PNN and PNP Rhenium Pincer Complexes



2. Experimental

a. General Consideration

All reactions were performed in a nitrogen-filled glove box. Solvents were degassed and purified with a solvent purification system (Pure Process Technology INC) prior to use. CD_2Cl_2 was dried with CaH_2 , distilled under argon and stored over molecular sieves.

^1H and ^{13}C NMR spectra were recorded on 400 MHz, 500 MHz or 600 MHz spectrometers using residue solvent peaks as reference (CDCl_3 , ^1H : 7.26 ppm; ^{13}C : 77.00 ppm. CD_2Cl_2 , ^1H : 5.32 ppm; ^{13}C : 53.84 ppm.). ^{31}P NMR spectra were recorded on Agilent 400 MHz spectrometer and reference versus phosphoric acid external standard (H_3PO_4 , ^{31}P : 0.00 ppm). ^{19}F NMR spectra were recorded on Agilent 400 MHz spectrometer and referenced versus trifluoroacetic acid external standard (CF_3COOH , ^{19}F : -76.55 ppm).

For X-ray crystal structure determination, the crystal was mounted on a cryo-loop and transferred to a Bruker Kappa APEX II diffractometer. The APEX2 program was used to determine the unit cell parameters and data collection (10 sec / frame, 0.5 deg. /frame Omega scan). The data were collected at 100k with Oxford cryo-system. The raw frame data were processed using SAINT program. The absorption correction was applied using program SADABS. Subsequent calculations were carried out using SHELXTL

program. The structure was solved by direct methods and refined on F² by full-matrix least-squares techniques.

ESI mass spectra were acquired with a Waters Micromass LCT-Premier mass spectrometer. Samples were diluted to an appropriate concentration and infused directly using either a syringe pump or a Waters Alliance 2695 autosampler. Accurate mass data was acquired using poly(ethylene glycol) or poly(ethylene glycol) monomethyl ether as an internal calibrant, as appropriate.

Experimental Procedure for titration:

Titration experiments for equilibrium constants were performed in degassed CD₂Cl₂ solution (1.0 mL) at 298.1 ± 0.1 K with 0.0126 M **1**. A threefold concentration series of ACN (0.057, 0.095, and 0.19 M) was added to the mixture.

b. Synthesis of [(PNN)Re(H)(O)(OSiMe₂Ph)][OTf] (1-a**)**

To a solution of [Re(O)₂(PNN)][OTf] (**1**) (21 mg, 0.03 mmol) in CD₂Cl₂ (1.0 mL), which was synthesized in accordance with a published procedure¹⁶, Me₂PhSiH (5 μL, 0.03 mmol) was added at ambient conditions.

¹H NMR (500 MHz, CD₂Cl₂) **1a**: δ 8.27 (t, *J* = 8 Hz, 1H), 8.13 (d, *J* = 8 Hz, 1H), 7.87 (d, *J* = 8 Hz, 1H), 7.67 (d, *J* = 14 Hz, 1H), 7.36 (m, 1H), 7.25 (t, *J* = 7 Hz 2H), 7.00 (m, 2H), 4.81 (d, *J* = 16 Hz, 1H), 4.53 (d, *J* = 16 Hz, 1H), 4.43 (m, 2H), 3.17 (m, 1H), 3.06 (m, 1H), 2.84 (m, 1H), 2.42 (m, 1H), 1.46 (m, 18H), 1.15 (m, 5H), 0.19 (s, 3H), 0.07 (s, 3H).

^{13}C NMR (126 MHz, CD_2Cl_2): δ 164.0, 160.0, 144.4, 133.1, 130.3, 128.6, 125.1, 123.1, 69.3, 55.1, 51.2, 39.8 (d, $J = 24$ Hz), 38.7 (d, $J = 18$ Hz), 36.6 (d, $J = 17$ Hz), 30.3, 28.9, 13.3, 9.6, 1.8.

$^{31}\text{P}\{^1\text{H}\}$ NMR (202 MHz, CD_2Cl_2): δ 60.3.

$^{29}\text{Si}\{^1\text{H}\}$ INEPT NMR (99 MHz, CD_2Cl_2): δ 5.8.

ESI-MS (*m/z and relative abundance*): obs. 675/677 (56/100) ($[\text{M}]^+$); calc. 675/677 (60/100).

c. Synthesis of [(PNN)Re(H)(O)(OSiHPh₂)](OTf) (1-b)

To a solution of **1** (21 mg, 0.03 mmol) in CD_2Cl_2 (1.0 mL), Ph_2SiH_2 (4 μL , 0.03 mmol) was added at ambient conditions.

^1H NMR (500 MHz, CD_2Cl_2) **1b**: δ 8.27 (m, *Re-H overlapped*, 2H), 8.14 (d, $J = 7.9$ Hz, 1H), 7.85 (d, $J = 7.9$ Hz, 1H), 7.37 (m, 6H), 7.20 (t, $J = 7.7$ Hz, 2H), 6.88 (d, $J = 7.9$ Hz, 2H), 5.04 (s, 1H), 4.70 (d, $J = 16.9$ Hz, 1H), 3.51 (d, $J = 16.9$ Hz, 1H), 3.40 (m, 1H), 3.27 (m, 1H), 2.61 (m, 1H), 2.12 (m, 1H), 1.58 (t, $J = 7.2$ Hz, 3H), 1.51 (d, $J = 15.3$ Hz, 9H), 1.26 (d, $J = 14.1$ Hz, 9H), 0.93 (t, $J = 7.2$ Hz, 3H).

^{13}C NMR (500 MHz, CD_2Cl_2): δ 163.68, 159.91, 144.49, 135.40, 135.09, 134.64, 131.19, 128.72, 128.36, 123.22, 122.61, 71.01, 57.02, 50.69, 39.78 (d, $J = 24.1$ Hz), 39.37 (d, $J = 23.9$ Hz), 38.81 (d, $J = 18.7$ Hz), 29.99, 28.91, 27.68, 14.59, 9.24.

$^{31}\text{P}\{^1\text{H}\}$ NMR (400 MHz, CD_2Cl_2): δ 60.9.

$^{29}\text{Si}\{^1\text{H}\}$ INEPT NMR (400 MHz, CD_2Cl_2): δ -0.10

ESI-MS (*m/z and relative abundance*): obs. 723/725 (63/100) ($[\text{M}]^+$); calc. 723/725 (60/100).

d. Synthesis of [(PNN)Re(H)(O)(OSiH₂Ph)][OTf] (1-c)

To a solution of **1** (21 mg, 0.03 mmol) in CD₂Cl₂ (1.0 mL), PhSiH₃ (4 μL, 0.03 mmol) was added at ambient conditions.

¹H NMR (500 MHz, CD₂Cl₂) **1c**: δ 8.21 (t, *J* = 8 Hz, 1H), 8.02 (m, 2H, *Re-H overlapped*), 7.97 (d, *J* = 8 Hz, 1H), 7.40 (t, *J* = 8 Hz, 1H), 7.30 (t, *J* = 8 Hz, 2H), 7.16 (d, *J* = 7 Hz, 2H), 5.23 (d, *J* = 16 Hz, 1H), 4.76 (d, *J* = 16 Hz, 1H), 4.13 (m, 1H), 3.49 (m, 1H), 3.27 (m, 2H), 3.20 (m, 1H), 1.46 (m, 18H), 1.33 (m, 6H), 0.09.

¹³C{¹H} NMR (126 MHz, CD₂Cl₂): δ 163.6, 159.8, 144.5, 134.3, 131.2, 128.8, 125.3, 123.4, 71.2, 57.1, 50.9, 39.4 (d, *J* = 25 Hz), 38.4 (d, *J* = 18 Hz), 37.5 (d, *J* = 17 Hz), 29.9, 29.0, 13.7, 9.5.

³¹P{¹H} NMR (202 MHz, CD₂Cl₂): δ 61.7.

²⁹Si{¹H} INEPT NMR (99 MHz, CD₂Cl₂): δ -23.9.

ESI-MS (*m/z and relative abundance*): obs. 647/649 (52/100) ([M]⁺); calc. 647/649 (60/100).

e. Synthesis of [(PNN)Re(O)₂(ACN)][OTf] (1-ACN)

To a suspension of **1** (51.0 mg, 0.10 mmol) in acetonitrile (2.0 mL), silver triflate (21.0 mg, 0.10 mmol) was added and the reaction mixture was stirred for 0.5 h in the dark. The solution was filtered to remove the silver iodide precipitate and the solvent was removed under vacuum to yield a crude product, which was subsequently washed with diethyl ether (2.0 mL). Yield 61.0 mg (MW 731, 83%).

^1H NMR (500 MHz, CD_3CN) **1-ACN**: δ 8.09 (t, $J = 7.5$ Hz, 1H), 7.87 (d, $J = 7.9$ Hz, 1H), 7.67 (d, $J = 7.7$ Hz, 1H), 4.78 (s, 2H), 4.14 (d, $J = 10.0$ Hz, 2H), 3.30 (m, 2H), 3.19 (m, 2H), 1.37 (d, $J = 14.2$ Hz, 19H), 1.25 (t, $J = 7.2$ Hz, 6H).

^{13}C NMR (500 MHz, CD_3CN): δ 166.18, 162.62, 142.44, 123.30, 123.24, 121.72, 68.78, 49.98, 39.68, 39.47, 35.82 (d, $J = 18.7$ Hz), 28.47, 9.20.

$^{31}\text{P}\{^1\text{H}\}$ NMR (400 MHz, CD_3CN): δ 52.3.

ESI-MS (*m/z* and relative abundance): obs. 580/582 (54/100) ($[\text{M}]^+$); calc. 580/582 (60/100).

Table 2.1. Crystal data and structure refinement for **1-ACN**.

Empirical formula	C ₂₂ H ₃₆ F ₃ N ₃ O ₅ P Re S	
Formula weight	728.77	
Temperature	100(2) K	
Wavelength	0.71073 Å	
Crystal system	Monoclinic	
Space group	P2 ₁ /n	
Unit cell dimensions	a = 14.773(3) Å	a = 90°.
	b = 24.983(5) Å	b = 111.537(6)°.
	c = 16.283(3) Å	g = 90°.
Volume	5590.4(19) Å ³	
Z	8	
Density (calculated)	1.732 Mg/m ³	
Absorption coefficient	4.535 mm ⁻¹	

F(000)	2896
Crystal size	0.100 x 0.100 x 0.050 mm ³
Theta range for data collection	1.572 to 26.455°.
Index ranges	-18<=h<=18, -28<=k<=30, -19<=l<=19
Reflections collected	24516
Independent reflections	10732 [R(int) = 0.1291]
Completeness to theta = 25.242°	98.3 %
Absorption correction	Semi-empirical from equivalents
Max. and min. transmission	0.7454 and 0.5971
Refinement method	Full-matrix least-squares on F ²
Data / restraints / parameters	10732 / 52 / 537
Goodness-of-fit on F ²	0.940
Final R indices [I>2sigma(I)]	R1 = 0.0764, wR2 = 0.1335
R indices (all data)	R1 = 0.1826, wR2 = 0.1749
Extinction coefficient	n/a
Largest diff. peak and hole	2.702 and -1.822 e.Å ⁻³

f. Synthesis of (PNN*)Re(O)₂I (**2**)

To a suspension of Re(O)₂(PNN)I (200.4 mg, 0.30 mmol) in cold -40 °C THF (8.0 mL), a solution of LiHMDS (58.0 mg, 0.30 mmol) in -40 °C THF (2.0 ml) was added. The two solutions were combined with an instant color change from orange to dark red. The solvent was removed in vacuo and the crude product was washed with pentane (3 × 10.0 mL) to afford **2** as dark red powder. Yield 150 mg (MW 667, 75%).

^1H NMR (500 MHz, CD_3CN) **2**: δ 8.09 (t, $J = 7.5$ Hz, 1H), 7.87 (d, $J = 7.9$ Hz, 1H), 7.67 (d, $J = 7.7$ Hz, 1H), 4.78 (s, 2H), 4.14 (d, $J = 10.0$ Hz, 2H), 3.30 (m, 2H), 3.19 (m, 2H), 1.37 (d, $J = 14.2$ Hz, 19H), 1.25 (t, $J = 7.2$ Hz, 6H).

^{13}C NMR (500 MHz, CD_3CN): δ 166.18, 162.62, 142.44, 123.30, 123.24, 121.72, 68.78, 49.98, 39.68, 39.47, 35.82 (d, $J = 18.7$ Hz), 28.47, 9.20.

$^{31}\text{P}\{^1\text{H}\}$ NMR (400 MHz, CD_3CN): δ 52.3.

ESI-MS (*m/z and relative abundance*): obs. 665/667 (54/100) ($[\text{M}]^+$); calc. 665/667 (60/100).

g. Synthesis of $[(\text{PNN}^*)\text{Re}(\text{O})_2(\text{ACN})][\text{OTf}]$ (**3**)

To a suspension of **2** (67.0 mg, 0.10 mmol) in acetonitrile (2.0 mL), silver triflate (21.0 mg, 0.10 mmol) was added and the reaction mixture was stirred for 0.5 h in the dark. The solution was filtered to remove the silver iodide precipitate and the solvent was removed under vacuum to yield a crude product, which was subsequently washed with diethyl ether (2.0 mL). Yield 64.0 mg (MW: 730, 87%).

^1H NMR (500 MHz, CD_3CN) **3**: δ 8.09 (t, $J = 7.5$ Hz, 1H), 7.87 (d, $J = 7.9$ Hz, 1H), 7.67 (d, $J = 7.7$ Hz, 1H), 4.78 (s, 2H), 4.14 (d, $J = 10.0$ Hz, 2H), 3.30 (m, 2H), 3.19 (m, 2H), 1.37 (d, $J = 14.2$ Hz, 19H), 1.25 (t, $J = 7.2$ Hz, 6H).

^{13}C NMR (500 MHz, CD_3CN): δ 166.18, 162.62, 142.44, 123.30, 123.24, 121.72, 68.78, 49.98, 39.68, 39.47, 35.82 (d, $J = 18.7$ Hz), 28.47, 9.20.

$^{31}\text{P}\{^1\text{H}\}$ NMR (400 MHz, CD_3CN): δ 52.3.

ESI-MS (*m/z and relative abundance*): obs. 579/581 (67/100) ($[\text{M}]^+$); calc. 579/581 (60/100).

h. Synthesis of (ⁱPrPNPⁱPr)Re(O)₂I (**4**)

To a suspension of (PPh₃)₂ReIO₂ (82.0 mg, 0.1 mmol) in THF (10.0 mL), ⁱPrPNPⁱPr ligand (50.0 mg, 0.12 mmol) was added and stirred for 5 min at ambient temperature. Crystal formation was noticed within several minutes of reaction. The solution was filtered and bright orange crystals of **4** were obtained. Yield 54.0 mg (MW 800, 67 %).

¹H NMR (500 MHz, CD₂Cl₂) **4**: δ 8.92 (s, 1H), 8.04 (d, *J* = 8.46 Hz, 2H), 7.81 (d, *J* = 6.88 Hz, 2H), 7.50 (t, *J* = 8.00 Hz, 2H), 4.94 (d, *J* = 12.36 Hz, 2H), 3.86 (m, 2H), 2.80 (m, 2H), 1.71 (q, 6H), 1.58 (q, 6H), 1.51 (q, 6H), 1.28 (q, 6H), 0.76 (q, 6H).

³¹P{¹H} NMR (400 MHz, CD₂Cl₂): δ 61.3.

ESI-MS (*m/z and relative abundance*): obs. 783/785 (65/100) ([M]⁺); calc. 783/785 (60/100).

Table 2.2. Crystal data and structure refinement for (ⁱPrPNPⁱPr)Re(O)₂I (**4**)

Empirical formula	C ₂₇ H ₃₉ I N O ₂ P ₂ Re	
Formula weight	784.63	
Temperature	100(2) K	
Wavelength	0.71073 Å	
Crystal system	Orthorhombic	
Space group	Pbca	
Unit cell dimensions	a = 15.0049(6) Å	a = 90°.
	b = 15.3540(7) Å	b = 90°.
	c = 24.5257(10) Å	g = 90°.
Volume	5650.4(4) Å ³	

Z	8
Density (calculated)	1.845 Mg/m ³
Absorption coefficient	5.532 mm ⁻¹
F(000)	3056
Crystal size	0.100 x 0.100 x 0.050 mm ³
Theta range for data collection	1.661 to 30.401°.
Index ranges	-20<=h<=20, -21<=k<=16, -22<=l<=34
Reflections collected	42117
Independent reflections	7754 [R(int) = 0.0750]
Completeness to theta = 25.242°	100.0 %
Absorption correction	Semi-empirical from equivalents
Max. and min. transmission	0.7460 and 0.6834
Refinement method	Full-matrix least-squares on F ²
Data / restraints / parameters	7754 / 0 / 315
Goodness-of-fit on F ²	1.019
Final R indices [I>2sigma(I)]	R1 = 0.0348, wR2 = 0.0493
R indices (all data)	R1 = 0.0676, wR2 = 0.0557
Extinction coefficient	n/a
Largest diff. peak and hole	0.978 and -0.955 e.Å ⁻³

i. Synthesis of [(ⁱPrPNPⁱPr)Re(O)₂][OTf] (5)

To a suspension of **4** (80.0 mg, 0.10 mmol) in THF (2.0 mL), silver triflate (21.0 mg, 0.10 mmol) was added and the reaction mixture was stirred for 0.5 h in the dark. The solution was filtered to remove the silver iodide precipitate and the solvent was removed under vacuum to yield a crude product, which was subsequently washed with diethyl ether (2.0 mL). Yield 82 mg (MW 949, 86%).

^1H NMR (500 MHz, CD_2Cl_2) **5**: δ 8.33 (s, 1H), 7.94 (d, $J = 9.32$ Hz, 2H), 7.80 (d, $J = 6.80$ Hz, 2H), 7.33 (m, 2H), 4.83 (m, 2H), 3.73 (m, 2H), 2.75 (m, 2H), 1.70 (q, 6H), 1.55 (q, 6H), 1.51 (q, 6H), 1.25 (q, 6H), 0.73 (q, 6H).

$^{31}\text{P}\{^1\text{H}\}$ NMR (400 MHz, CD_2Cl_2): δ 57.6.

ESI-MS (*m/z* and relative abundance): obs. 656/658 (63/100) ($[\text{M}]^+$); calc. 656/658 (60/100).

j. Synthesis of [(^tbuPNP^tbu)Re(O)₂][OTf] (6**)**

To a solution of (^tbuPNP^tbu)Re(O)₂I (MW 741, 74 mg, 0.1 mmol) in THF (2.0 mL), which was synthesized in accordance with a published procedure¹⁷, silver triflate (21.0 mg, 0.10 mmol) was added and the reaction mixture was stirred for 0.5 h in the dark. The solution was filtered to remove the silver iodide precipitate and the solvent was removed under vacuum to yield a crude product, which was subsequently washed with diethyl ether (2.0 mL). Yield 61.0 mg (MW 731, 83%).

^1H NMR (500 MHz, CDCl_3) **6**: δ 7.99 (s, 1H), 7.86 (d, $J = 8.00$ Hz, 2H), 4.90 (m, 2H), 4.09 (m, 2H), 1.50 (s, 36H)

^{13}C NMR (500 MHz, CDCl_3): δ 167.08, 142.20, 123.06, 41.54, 37.43, 29.48.

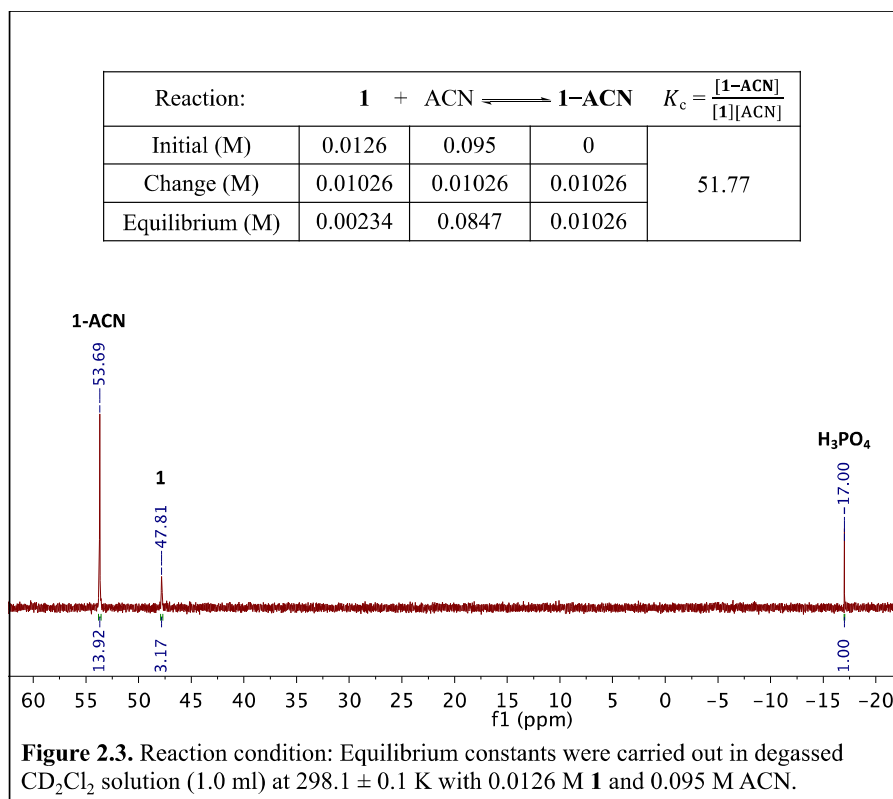
$^{31}\text{P}\{^1\text{H}\}$ NMR (400 MHz, CD_2Cl_2): δ 35.95.

ESI-MS (*m/z and relative abundance*): obs. 612/614 (65/100) ($[\text{M}]^+$); calc.
612/614 (60/100).

3. Results and discussion

a. Determination of Equilibrium Constant

Figure 2.3 Determination of Equilibrium Constant



The removal of solvent molecules coordinated on metal center plays a substantial role in potential applications since this process offers one more vacant site¹⁸. In this study, we demonstrate a coordination exchange (CE) process executed initially with DCM and subsequently with ACN. A color change of **1**, from orange to yellow, was observed after treatment with ACN at room temperature, which provided initial evidence because the color can be influenced by the coordination environment around the Re^{5+} center¹⁹.

To provide more concrete evidence on this CE process, we designed ^{31}P NMR experiment conducted in NMR tubes. Aliquot of CD_3CN was added into a NMR tube with **1** immersed in CD_2Cl_2 solvent. Equilibrium was achieved between **1** ($^{31}\text{P} = 47.81$ ppm) and **1-ACN** ($^{31}\text{P} = 53.69$ ppm) (Figure 2.3). The quantity of **1** and **1-ACN** was calibrated with an internal standard H_3PO_4 . And the equilibrium constant of CE process

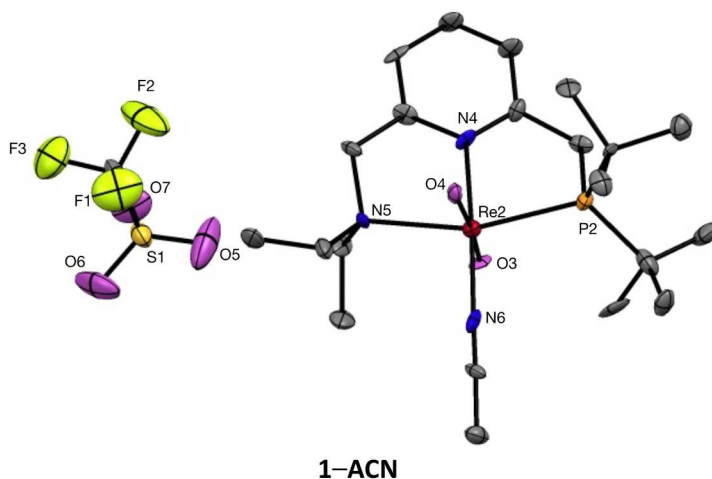
was determined by monitoring ^{31}P NMR peaks for **1** and **1-ACN** derived from three independent titration experiments.

It is important to determine the equilibrium constant for coordination/dissociation of solvent ligand to metal complexes since this is thought to be a key step for kinetic and mechanistic studies. Although rhenium-acetonitrile coordinated complexes *fac*-[ReBr(CO)₃(Hpz)(NCMe)] and *fac*-[ReBr(CO)₃(Hdmpz)(NCMe)] (Re–N = 2.139 Å) has been reported before in literature,²⁰ their equilibrium constants for their formation have not been reported. The titration experiment for measuring equilibrium constant of coordination/dissociation of ACN ligand, or the cleavage of Re–N bond allow for a detailed investigation of the factors responsible for significant rate enhancement and new catalyst design. The presence of a vacant site on rhenium is essential for catalysis considering that fact that solvent coordination could also inhibit catalysis. The effect of reaction medium is discussed in detail in chapter 4.

In this chapter, we report that the equilibrium constant for Re–N bond: $K_c = 52 \text{ M}^{-1}$ at 298K. This provides a reference value that can be used to estimate the equilibrium position of pincer rhenium complex reaction with ACN.

b. Structural Discussion of [(PNN)Re(O)₂(ACN)][OTf] (1-ACN)

Figure 2.4 ORTEP drawing (50% thermal ellipsoids) of **1-ACN** with partial atom labeling. Hydrogen atoms are omitted for clarity. Selected bond lengths (Å) and angles (°): N(4)–Re(2), 2.083(12); N(5)–Re(2), 2.298(12); N(6)–Re(2), 2.114(13); P(2)–Re(2), 2.413(4); O(3)–Re(2), 1.735(10); O(4)–Re(2), 1.758(10); O(3)–Re(2)–O(4), 173.9(4); N(4)–Re(2)–N(6), 176.9(5); N(5)–Re(2)–P(2), 159.9(3).



The acetonitrile coordinated complex **1-ACN** was fully characterized by multinuclear NMR and X-ray crystallographic studies (Figure 2.4). The ¹⁹F NMR spectrum exhibited one signal as a sharp singlet and was assigned to triflate counterion (-78.68 ppm). ¹³C NMR spectrum exhibited signal at 121.72 ppm and 9.2 ppm were assigned to CH₃CN and CH₃CN respectively.

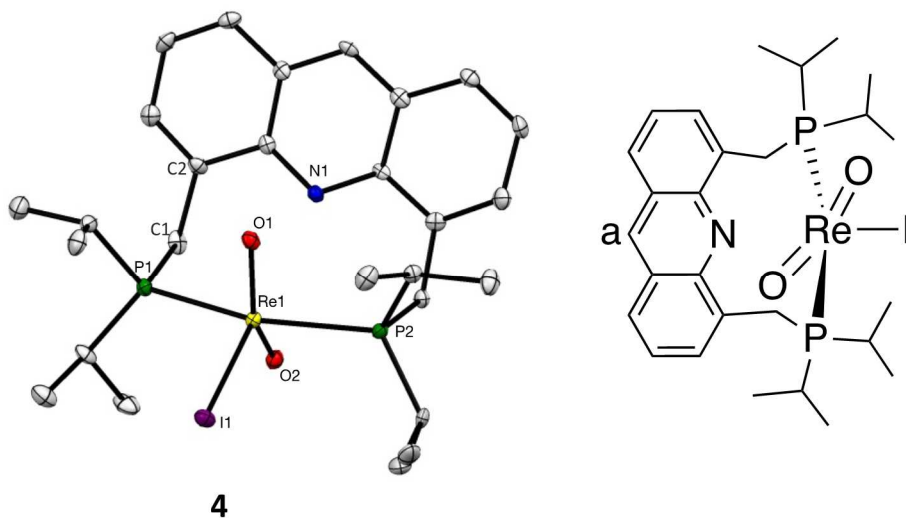
X-ray crystallographic studies confirmed the structure of complex **1-ACN**. The cationic portion adopts a slightly distorted octahedral geometry, formed by the tridentate PNN pincer ligand, two oxo ligand *trans* to each other, and an acetonitrile molecule. The main distortion of the ideal octahedral geometry is due to $\angle\text{N5-}\text{Re2-}\text{P2} = 159.9^\circ$. The

Re2–N6 bond distance (2.101 Å) is in agreement with those found in the literature for compound containing Re(V).²¹

The coordination between rhenium center ACN ligand does not influence bond distance between and pyridine N (Re2–N4 = 2.083 Å). The structure presents a nearly linear O3=Re=O4 with a angle 173.9(4)° with two oxo ligands positioned trans to one another. The N≡C bond in coordinated N≡CCH₃ molecule is somewhat stronger, which is confirmed by a decrease of its length (N≡C, 1.147 Å) compared to a free acetonitrile molecule (N≡C, 1.158 Å)²². The π -acceptor ability of nitrile group is almost not manifested in this case, because the electron density on rhenium metal atom is lower. The ³¹P{¹H} NMR of **1**–ACN (53.69 ppm) shifted downfield by 5.88 ppm compared to **1**, which also reflecting the decrease in electron density at the rhenium center by electron withdrawing ACN ligand.

c. Structural Discussion of (ⁱPrPNPⁱPr)Re(O)₂I (**4**)

Figure 2.5 ORTEP drawing (50% thermal ellipsoids) of (ⁱPrPNPⁱPr)Re(O)₂I (**4**) with partial atom labeling. Hydrogen atoms are omitted for clarity. Selected bond lengths (Å) and angles (°): I(1)–Re(1), 2.6665(3); O(1)–Re(1), 1.738(3); O(2)–Re(1), 1.744(3); P(1)–Re(1), 2.4464(10); P(2)–Re(1), 2.4650(11); C(2)–C(1)–P(1), 117.4(3); O(1)–Re(1)–O(2), 143.56(13); P(1)–Re(1)–P(2), 160.26(4); O(1)–Re(1)–I(1), 107.44(9); O(2)–Re(1)–I(1), 108.99(9); P(1)–Re(1)–I(1), 99.74(3); P(2)–Re(1)–I(1), 99.26(3).



We recently synthesized novel acridine-based rhenium pincer complex ReO₂I(A-ⁱPr-PNP) (**4**) [A-ⁱPr-PNP = 4,5-bis-(diisopropylphosphinomethyl)acridine]. Salt metathesis of **4** with AgOTf afforded cationic complex **5**. The structure of **4**, determined by X-ray diffraction, reveals a distorted trigonal bipyramidal geometry around rhenium center with (Figure 2.5) and the iodide ligand is in the equatorial plane with two oxo

ligands. Of note is the significantly smaller O–Re1–O angle (143.56 (13)°) comparing to **1**–ACN (173.9(4)°): two oxo ligands are trans to one another.

Coordination between rhenium center and acridinyl nitrogen atom is not achieved due to unusually long Re N distance (3.207 Å, compared with 2.497 Å in RuHCl(CO)(A-ⁱPr-PNP)²³. Upon complexation, the acridine ligand becomes bent at the middle of aryl ring to adopt a boat-shaped structure with a dihedral angle of ∠P1–C1–P2 = 117.4°. The ¹H NMR of **4** shows two doublet triplets at 4.94 and 3.86 ppm (²J_{HH} = 11.7 Hz, ²J_{PH} = 3.3 Hz) which correspond to methylene “arm” protons. One singlet resonance for acridine ring proton “a” appears at 8.92 ppm, representing a downfield shift of 0.31 ppm relative to the corresponding proton of ligand ⁱPrPNPⁱPr (8.61 ppm), suggesting diminished aromaticity of acridine upon complexation with rhenium.

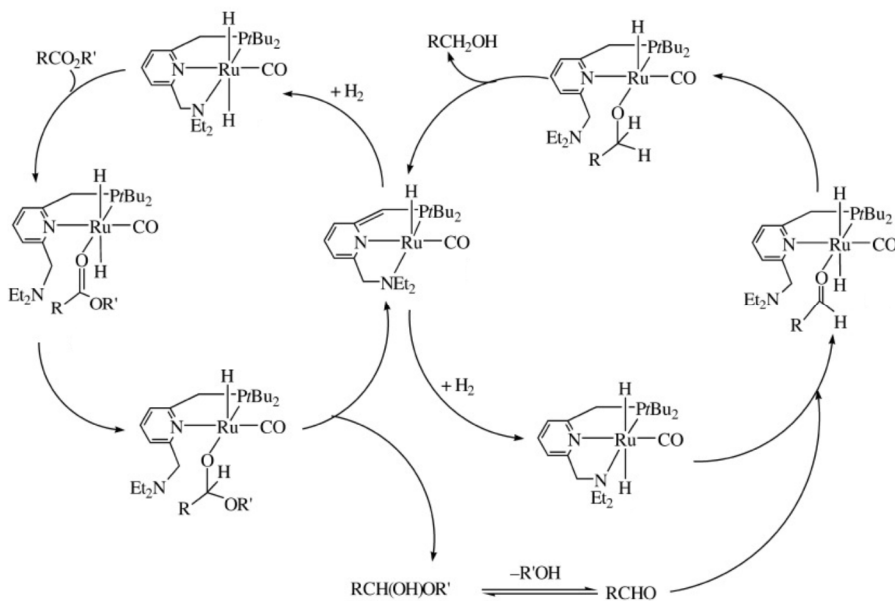
d. Pincer Hemilabile Effect

In 1979, Heffery and Rauchfuss first discovered hemilabile property of ligands in coordination chemistry and refers to one of the donor groups on pincer ligand, not strongly bonded to metal center, can reversibly dissociate in solution to open a vacant site for catalysis.²⁴ Hemilability for pincer-type complexes is a key factor in catalyst design and promoting catalytic efficiency.^{8,25-27}

The presence of one open coordination site on rhenium is essential for catalysis. A control experiment proves that catalyst efficiency has been shut down when hydrosilylation was mediated by Re(O)₂(PNN)I, in which rhenium center was six ligands coordinated. A plausible rationale for opening a vacant site is through dissociation of hemilabile amine on pincer ligand (Figure 2.6).²⁸ Pincer ruthenium hydride complex is capable of opening the chelate ring to provide a coordination site for ester addition.

Dissociation of the amine “arm” in PNN rhenium hydride might also provide a second vacant site for aldehyde coordination. However, this is difficult with rhenium hydride complex (**1-a**, **1-b**, **1-c**) when introducing aldehydes. The detailed mechanism was discussed in chapter 5 as rhenium hydride is not the active species and hydrosilylation proceeds through a nonhydride Lewis acid pathway. An analogous pincer oxo-rhenium complex **6** was prepared to investigate catalytic efficacy compared to **1**. This ^tBuPNP^tBu pincer complex **6**, without an amine donor comparing to **1**, does not have any hemilability through catalysis. It is noteworthy that hydrosilylation catalyzed by **6** revealed comparable reaction chemoselectivity and kinetics, showing an induction period at first 10 minutes. This result is highly suggestive that dissociation of amine arm or the ligand is not necessary in this mechanism.

Figure 2.6 Pincer ligand hemilability



4. Conclusion

To conclude, we report the synthesis of Re-H complex (**1-a**, **1-b**, **1-c**) by stoichiometric experiment of **1** with various organosilanes. This result suggests that silane is activated in the absence of substrate. Further hydride mechanism study can be carried out starting from these potential active species with the assumption that the mechanism proceeds through a hydride pathway. An equilibrium process between **1** and **1-ACN** was monitored, and equilibrium constant ($K_c = 52 \text{ M}^{-1}$) was determined by quantitative ^{31}P -NMR with solvent ligand coordinated rhenium complex **1-ACN**. Dearomatized complexes **2** and **3** are derived from **1** for MLC type catalysis. Last but not the least, complexes **4-6** was isolated by fine tuning the steric and electronic properties of pincer ligand frameworks. These discovers shows the unprecedented level of coordination sphere of pincer rhenium complexes and we believe the full power of pincer ligand has yet to be explored.

5. References

- (1) Yoshihara, K. *Proc. Jpn. Acad., Ser. B* **2008**, *84* (7), 232–245.
- (2) Scerri, E. *Nat. Chem.* **2010**, *2* (7), 598–598.
- (3) Fink, P. J.; Miller, J. L.; Konitzer, D. G. *JOM* **2010**, *62* (1), 55–57.

- (4) Wilson, E. H.; Jeong, J.; Hershkowitz, N. *Rev. Sci. Instrum.* **2002**, *73* (5), 2033–2037.
- (5) Cotton, A.; Walton, R. A. *Reductions in Organic Synthesis: Recent Advances and Practical Applications*; Oxford Univ. Press, 1996.
- (6) Hagelucken, C. *Metall.* **2006**, *1*, 31–24.
- (7) Hua, R.; Jiang, J. *Curr. Org. Synth.* **2007**, *4* (2), 151–174.
- (8) Peris, E.; Crabtree, R. H. *Chem. Soc. Rev.* **2018**, *47* (6), 1959–1968.
- (9) Choi, J.; MacArthur, A.; Brookhart, M.; Goldman, A. S. *Chem. Rev.* **2011**, *111* (3), 1761–1779.
- (10) Deng, Q.-H.; Melen, R. L.; Gade, L. H. *Collect. Czech. Chem. Commun.* **2014**, *47* (10), 3162–3173.
- (11) Prakash, O.; Joshi, H.; Kumar, U.; Sharma, A. K.; Singh, A. K. *Dalton Trans.* **2015**, *44* (4), 1962–1968.
- (12) Balaraman, E.; Gnanaprakasam, B.; Shimon, L. J. W.; Milstein, D. *J. Am. Chem. Soc.* **2010**, *132* (47), 16756–16758.
- (13) Sebelius, S. *Palladium-Catalyzed Synthesis and Transformation of Organoboranes*, AB Danagårds Grafiska, Ekonomi-Print Krokodilen, 2006.
- (14) Zhang, J.; Leitus, G.; Ben-David, Y.; Milstein, D. *J. Am. Chem. Soc.* **2005**, *127* (31), 10840–10841.
- (15) Milstein, D. *Pure Appl. Chem.* **2003**, *75* (4), 445–460.
- (16) Mazzotta, M. G.; Pichaandi, K. R.; Fanwick, P. E.; Abu-Omar, M. M. *Angew. Chem. Int. Ed.* **2014**, *53* (32), 8320–8322.

- (17) Korstanje, T. J.; Lutz, M.; Jastrzebski, J. T. B. H.; Klein Gebbink, R. J. M. *Organometallics*. **2014**, *33* (9), 2201–2209.
- (18) Kim, H. K.; Yun, W. S.; Kim, M.-B.; Kim, J. Y.; Bae, Y.-S.; Lee, J.; Jeong, N. *C. J. Am. Chem. Soc.* **2015**, *137* (31), 10009–10015.
- (19) Bae, J.; Choi, J. S.; Hwang, S.; Yun, W. S.; Song, D.; Lee, J.; Jeong, N. C. *ACS Appl. Mater. Interfaces*. **2017**, *9* (29), 24743–24752.
- (20) Arroyo, M.; Miguel, D.; Villafañe, F.; Nieto, S.; Pérez, J.; Riera, L. *Inorg. Chem.* **2006**, *45* (17), 7018–7026.
- (21) Heath, G.; McGrady, J.; Raptis, R.; Willis, A. C. *Inorg. Chem.* **1996**, *35* (23), 6838–6843.
- (22) Volkov, S. V.; Mykhalichko, B. M.; Pekhn'ov, V. I.; Yanko, O. G.; Murillo, C. A.; Khar'kova, L. B.; Arsenin, K. I. *Russ. J. Inorg. Chem.* **2007**, *52* (2), 186–190.
- (23) Gunanathan, C.; Shimon, L. J. W.; Milstein, D. *J. Am. Chem. Soc.* **2009**, *131* (9), 3146–3147.
- (24) Jeffrey, J. C.; Rauchfuss, T. *Organometallics*. **1979**, *18*, 1979.
- (25) Younus, H. A.; Ahmad, N.; Su, W.; Verpoort, F. *Coor. Chem. Rev.* **2014**, *276*, 112–152.
- (26) Elena Poverenov; Mark Gandelman; Linda J W Shimon; Haim Rozenberg; Yehoshoa Ben-David, A.; David Milstein. *Organometallics*. **2005**, *24* (6), 1082–1090.
- (27) Wang, Z.; Eberhard, M. R.; Jensen, C. M.; Matsukawa, S.; Yamamoto, Y. *J. Org. Chem.* **2003**, *681* (1-2), 189–195.

- (28) Zhang, J.; Leitus, G.; Ben-David, Y.; Milstein, D. *Angew. Chem. Int. Ed.* **2006**, *45* (7), 1113–1115.

Chapter III. Carbon Dioxide Reduction to Silyl-Protected Methanol Catalyzed by an Oxorhenium Pincer PNN Complex

This work represented in this chapter was published on *Organometallics*. Copyright to American Chemical Society.

Citation: Mazzotta, M. G.; Xiong, M.; Abu-Omar, M. M. *Organometallics*. **2017**, *36* (9), 1688–1691.

1. Introduction

The Importance of CO₂ Fixation:

Catalytic reduction of CO₂ to formate or methanol is an active area of research because of interest in its use as a C1 synthon and ultimate source of fossil fuel, which remains a major challenge.^{1–5} The rising concentration of CO₂ and other greenhouse gases in atmosphere not only impact climate change, but also ocean acidification, since atmospheric CO₂ results a major sink in ocean.⁶ Photosynthesis process fix a very large

scale of CO₂, with an estimation of 385×10^9 tons annually, and this grows by a factor of 2.⁷

While a number of heterogeneous transition-metal catalysts are capable of hydrogenating CO₂ to formic acid, most methodologies require high temperature and pressure.⁶⁻⁹ A growing number of homogeneous catalytic systems have been reported to achieve hydrogenation of CO₂ to methanol under mild conditions.¹⁻⁵

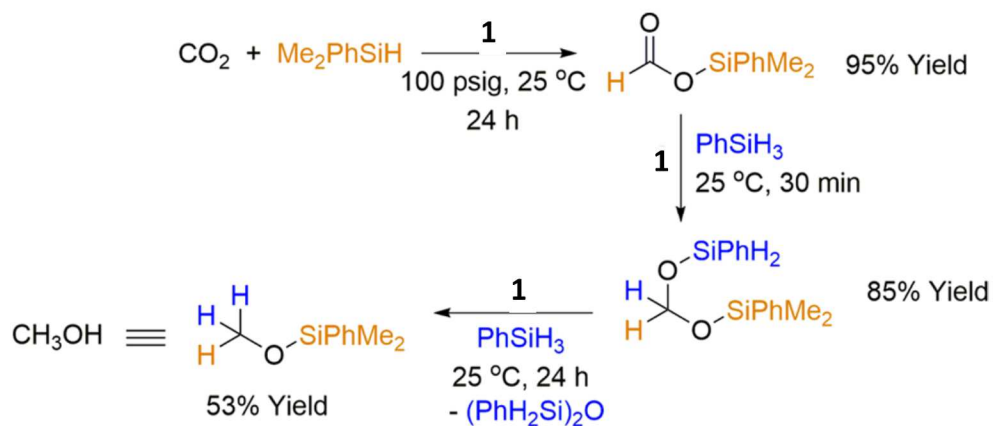
Hydrosilylative reduction of CO₂:

The inherent stability of the Si–O bond and the propensity for Si–H bond scission to form metal hydrides render organosilanes ideal for CO₂ reduction.¹⁰⁻¹⁵ Hydrosilylation of CO₂ generally yields silyl formate and silyl formal, which are versatile products that can be used as building blocks for making organic molecules and polymers.¹⁶

Ruthenium- and iridium-catalyzed hydrosilylations of CO₂ have produced silyl formate with varying quantities of siloxane byproduct. However, most systems require high CO₂ pressure, display low catalytic activity, or cannot convert CO₂ directly to methanol in a single-pot reaction.¹⁷

We have recently reported the synthesis of the high-valent dioxorhenium PNN pincer complex [(PNN)Re(O)₂][OTf] (**1**; OTf = CF₃SO₃⁻).¹⁸ In this chapter, we describe the catalytic conversion of CO₂ to silyl formate under mild conditions (25 °C, 100 psig) with Me₂PhSiH as the reductant. In a subsequent step, and with the same catalyst, silyl formate is reduced further to silyl methanol via silyl formal with the addition of PhSiH₃ (Scheme 3.1).

Scheme 3.1



2. Experimental

General Consideration

All reactions were performed in a nitrogen-filled glove box (≤ 1.2 ppm O_2) or using standard Schlenk techniques under argon. Solvents were degassed and purified with a solvent purification system (Pure Process Technology, Inc.) prior to use. CD_2Cl_2 was dried with CaH_2 , distilled under argon and stored over molecular sieves overnight prior to use. Organosilanes and all other compounds were obtained from commercial sources, degassed and stored over molecular sieves prior to use. Carbon dioxide was obtained from Matheson (Research Purity, 99.999%) and used as received.

One-dimensional NMR spectra were recorded on a Bruker DRX-500 NMR spectrometer equipped with a 5 mm broadband (BBO) probe or a Bruker AV400 instrument. Bruker TopSpin software (version 1.3) was used for data acquisition and MestReNova (version 8) was used for processing spectra. All spectra obtained were referenced to residual solvent peaks.

Electrospray ionization analyses were carried out on a Waters Micromass ZQ (Waters Corp, Milford, MA) mass spectrometer system. The cone voltage was set to 10 V for all mass spectral analyses. Typical background source pressure was 1.2×10^{-5} torr as read by an ion gauge. The sample flow rate was approximately 8 mL/min. The drying gas was nitrogen. The LCQ is typically scanned to 2000 amu. High-resolution electrospray ionization mass spectrometry measurements were performed by the Purdue University Campus Wide Mass Spectrometry Center using a FinniganMAT XL95 (FinniganMAT Corp., Bremen, Germany) mass spectrometer in peak-matching mode. The instrument was calibrated to a resolution on 10,000 with a 10% valley between peaks using the appropriate polypropylene glycol standards. Elemental analysis (C,H,N) was performed by Atlantic Microlab, Inc. (Norcross, GA).

General Procedure for NMR scale Hydrosilylation of CO₂

Me₂PhSiH (0.060 g, 0.44 mmol) was added to a solution of [Re(O)₂(PNN)][OTf], **1**, (0.015 g, 0.02 mmol) in 500 μL CD₂Cl₂ with toluene internal standard (50 μL, 0.47 mmol) in a heavy wall precision pressure/vacuum valve NMR sample tube (Wilmad LabGlass) equipped with PTFE screw cap. The tube was connected to a homebuilt brass-tubing manifold, connected to both a rotary vane vacuum pump and the CO₂ cylinder,

and evacuated quickly (less than 2 seconds) to remove the headspace gas. Using the evacuated setup, the tube was then pressurized with CO₂ (100 psi), sealed tightly, inverted, allowed to stand for specific times, and NMR spectra acquired. To maintain a constant temperature of the reaction, the pressurized tube was immersed in a water bath regulated at 25 °C. Conversions and yields were determined on basis of the ¹H peak intensity ratio of the organosilane starting material, product and C₆H₅CH₃.

After completion of the first hydrosilylation step (as indicated by ¹H NMR), the sample was cycled into the glove box appropriately and depressurized. PhSiH₃ (0.090 g, 0.83 mmol) was added to the solution, and the tube was pressurized using the same procedure as described above. To maintain a constant reaction temperature, the pressurized tube was immersed in a water bath regulated at 25 °C.

General Procedure for Hydrosilylation of CO₂ in Fisher-Porter Tube

Me₂PhSiH (0.060 g, 0.44 mmol) was added to a solution [Re(O)₂(PNN)][OTf], **1**, (0.015 g, 0.02 mmol) in 800 μL CD₂Cl₂ with toluene internal standard (50 μL, 0.47 mmol) in a 3- oz Fisher-Porter tube (Andrews Glass). The tube was connected to a homebuilt brass-Swagelok manifold, connected to both a rotary vane vacuum pump and the CO₂ cylinder, and evacuated quickly (less than 2 seconds) to remove headspace gas. Using the evacuated setup, the tube was then pressurized with CO₂ (100 psi), sealed tightly and allowed to stand for specific times and subjected to NMR spectroscopy. To

maintain a constant reaction temperature, the pressurized tube was immersed in a water bath regulated at 25 °C. Conversions and yields were determined on basis of the ^1H peak intensity ratio of the organosilane starting material, product and $\text{C}_6\text{H}_5\text{CH}_3$.

After completion of the first hydrosilylation step (as indicated by ^1H NMR), the tube was cycled into the glove box appropriately and depressurized. PhSiH_3 (0.090 g, 0.83 mmol) was added to the solution, and the tube was pressurized using the same procedure as described above. To maintain a constant reaction temperature, the pressurized tube was immersed in a water bath regulated at 25 °C. Alternatively, the reduction of the silyl formate was monitored by combining silyl formate, obtained from either product isolated on bulk scale or material synthesized from literature sources¹, under the same conditions as above.

Control Experimental Procedure: Me_2PhSiH (0.060 g, 0.44 mmol) was added to a solution 800 μL CD_2Cl_2 with toluene internal standard (50 μL , 0.47 mmol) in a 3-oz Fisher-Porter tube (Andrews Glass). An additional control consisting of, Me_2PhSiH (0.060 g, 0.44 mmol) and a solution of AgOTf (0.011 g, 0.044 mmol) 800 μL CD_2Cl_2 with toluene internal standard (50 μL , 0.47 mmol) in a 3-oz Fisher-Porter tube (Andrews Glass) was also prepared. The tube was connected to a homebuilt brass-Swagelok manifold, connected to both a rotary vane vacuum pump and the CO_2 cylinder, and evacuated quickly (less than 2 seconds) to remove headspace gas. Using the evacuated setup, the tube was then pressurized with CO_2 (100 psi), sealed tightly and allowed to stand for specific times and subjected to NMR spectroscopy. To maintain a constant reaction temperature, the pressurized tube was immersed in a water bath regulated at 25

°C. Conversions and yields were determined on basis of the ^1H peak intensity ratio of the organosilane starting material, product and $\text{C}_6\text{H}_5\text{CH}_3$.

Synthesis of [(PNN)Re(OTf)(O)(OSiMe₃)] [OTf] (**1-OTf**)

To a solution of $[\text{Re}(\text{O})_2(\text{PNN})][\text{OTf}]$, **1**, (0.38 M, 0.03 mmol) in dichloromethane, Me_3SiOTf (6 μL , 0.03 mmol) was added at ambient conditions. The solvent was removed *in vacuo* and the solid material was washed with pentane (2 mL) then dried to afford **5** as a dark violet powder. Yield 23.8 mg (85 %). X-ray quality crystals were obtained by adding diethyl ether to a solution of **1-OTf** in dichloromethane at -40 °C overnight. ^1H NMR (500 MHz, CD_2Cl_2): δ 8.40 (m, 2H), 8.17 (d, $J = 8$ Hz, 1H), 5.14 (d, $J = 16$ Hz, 1H), 4.91 (d, $J = 16$ Hz, 1H), 4.66 (m, 1H), 4.13 (m, 1H), 3.49 (m, 1H), 3.27 (m, 2H), 3.20 (m, 1H), 1.46 (m, 18H), 1.33 (m, 6H), 0.09 (s, 9H). $^{13}\text{C}\{^1\text{H}\}$ NMR (126 MHz, CD_2Cl_2): δ 169.2, 163.9, 147.5, 125.4, 124.0, 70.5, 41.8 (d, $J = 25$ Hz), 39.6 (d, $J = 16$ Hz), 36.6 (d, $J = 16$ Hz), 30.0, 28.9, 10.3, 8.9, 3.4, 0.5. $^{31}\text{P}\{^1\text{H}\}$ NMR (202 MHz, CD_2Cl_2): δ 42.8. $^{29}\text{Si}\{^1\text{H}\}$ INEPT NMR (99 MHz, CD_2Cl_2): δ 24.9. Elemental analysis obs. (cal.): C, 31.68 (31.61); H, 4.83 (4.86); N, 3.09 (3.07). ESI-MS (*m/z and relative abundance*): obs. 761/763 (68/100) (M^+); calc. 761/763 (60/100).

X-ray Details

Table 3.1 Crystal Data and Structure Refinement for **1-OTf**

Formula	$\text{C}_{24}\text{H}_{44}\text{F}_6\text{N}_2\text{O}_8\text{PReS}$ 2Si
---------	--

Formula	912.01
Weight	
Space Group	P 21 21 21 (No. 19)
a, Å	12.2352(4)
b, Å	13.1124(3)
c, Å	22.2118(4)
β, deg	90.00
V, Å ³	3563.50(16)
Z	4
d _{calc} , g cm ⁻³	1.700
Crystal Dimensions, mm	0.23x0.20x0.15
Temperature, K	200
Radiation (wavelength, Å)	Cu Ka (1.54184)
Monochromator	confocal optics
Linear Abs Coef, mm ⁻¹	9.198
Absorption Correction Applied	empirical ^a
Transmission Factors: min, max	0.07, 0.25
Diffractometer	Rigaku RAPID-II
h, k, l Range	-14 to 14 -16 to 16 - 26 to 26
2θ Range, deg	3.98-144.51
Mosaicity, deg	0.33
Program Used	SHELXTL
F000	1824.0
Data Collected	20750
Unique Data	5714
Rint	****

Data Used in Refinement	5714
Cutoff Used in R- Factor Calculations	2 Fo2>2.0s(Fo)
Data with I > 2.0σ(I)	5671
Number of Variables	417
Largest Shift/esd in Final Cycle	0.00
R(Fo)	0.049
Rw(Fo2)	0.130
Goodness of Fit	1.047
Absolute Structure Determination	Flack Parameter ^b (0.50(2))

^a Otwinowski Z. & Minor, W. *Methods Enzymol.* **1996**, 276307.

^b Flack, H. D. *Acta Cryst., Sect. A* **1983**, A39, 876.

3. Results and Discussion

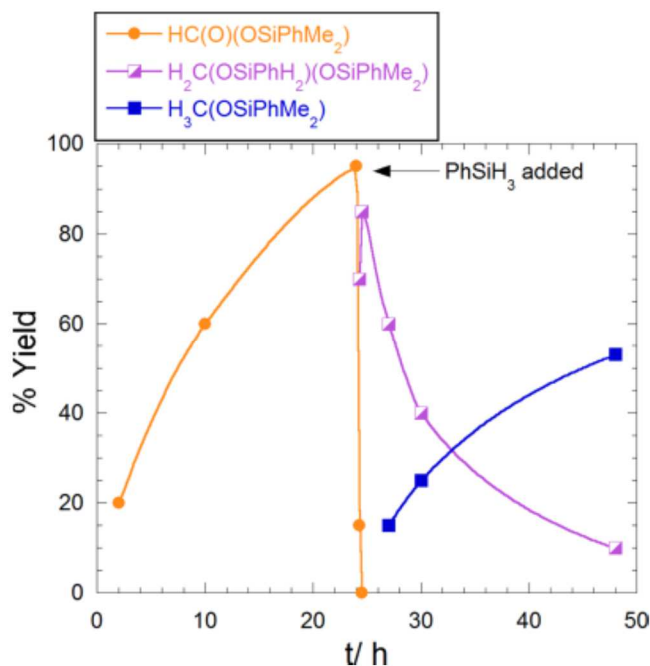
d. Hydrosilylation of CO₂ to silyl formate, bis(silyl) formal and silyl methanol

Reaction of CO₂ (100 psig) with Me₂PhSiH (0.44 mmol) in CH₂Cl₂ (DCM) at 25 °C in the presence of a catalytic amount of **1** (0.02 mmol, 4.5 mol %) produces the silyl formate HC(O)(OSiMe₂Ph) in 95% yield (by NMR). The characteristic singlet at δ 8.1 (¹H NMR) of HC(O)(OSiMe₂Ph) was used to confirm the product {Lalrempuia:2012fy}. Furthermore, a singlet at δ 161 in the ¹³C {¹H} NMR spectrum was

observed when $^{13}\text{CO}_2$ was employed. The remaining features of the ^1H and ^{13}C spectra were fully consistent with $\text{HC(O)}(\text{OSiMe}_2\text{Ph})$ as the product.

The use of Me_2PhSiH gave clean conversion to silyl formate. Additional reductant and increased temperature did not result in further reduction of the silyl formate. However, upon addition of a primary silane, PhSiH_3 (0.88 mmol), further reduction of silyl formate was observed. Initially rapid conversion (within 30 min) yielded silyl formal in 85% yield (Figure 3.1). This conversion is marked by the characteristic resonance of the formal protons at δ 5.2 (^1H NMR). Over a longer reaction time of 24 h, the silyl formal is reduced to silyl methanol¹³⁻¹⁵ in approximately 53% yield (Figure 3.1). A unique characteristic of this system is the kinetic resolution of the different reduction products. One can select for silyl formate by using a tertiary silane such as Me_2PhSiH , stop at the silyl formal with PhSiH_3 and halt the reaction after 30 min, or go all the way to silyl methanol after 24 h reaction with 2 equiv of PhSiH_3 . The reaction profile in Figure 3.1 shows that the hydrosilylation of CO_2 to silyl formate takes place over the course of 24 h with excellent chemoselectivity (no formal observed). Upon addition of 2 equiv of PhSiH_3 , the immediate formation of the bis(silyl)formal was observed, along with the simultaneous, and extremely rapid, consumption of the formate. Reduction of the bis(silyl)formal to silyl methanol proceeds over the course of 24 h; a longer reaction time gave no additional production of silyl methanol or further reduction to methane.

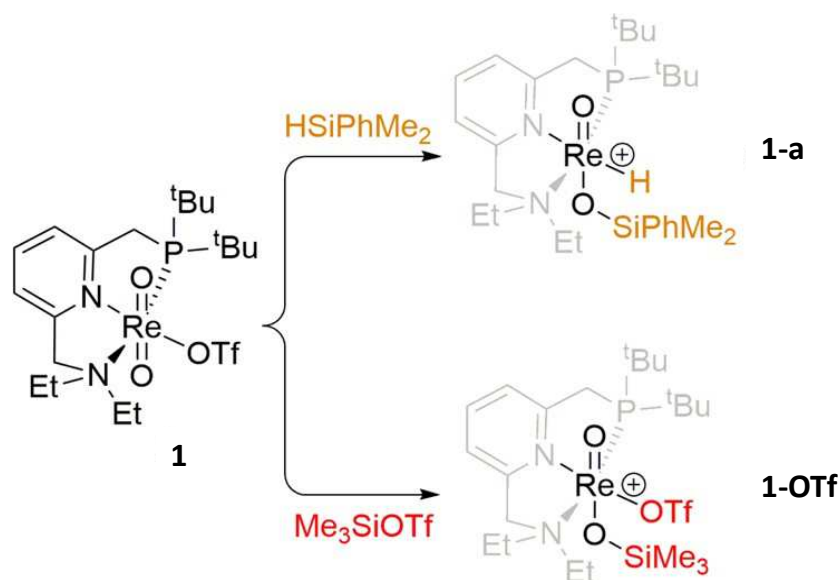
Figure 3.1 Typical time profile. Conditions: Conditions: CO₂ 100 psi, Me₂PhSiH (0.44 mmol) in DCM at 25 °C. At 24 h PhSiH₃ (0.88 mmol) was added. The lines are to guide the eye.



e. Isolation and identification of oxo-rhenium complexes **1-a** and **1-OTf**

Attempts to perform this reaction all in a single step (Me₂PhSiH + PhSiH₃ + CO₂) rather than by sequential addition of organosilanes were unsuccessful. This puzzling result indicated that two distinct and silane-dependent oxorhenium species were responsible for the respective catalytic products, and thus, we sought to confirm this hypothesis. Reaction of **1** with 1 equiv of Me₂PhSiH in DCM yielded a clean reaction to afford the siloxy hydride [(PNN)Re(H)(O)- (OSiMe₂Ph)][OTf] (**1-a**) (Scheme 3.2), which is analogous to (PPh₃)₂Re(H)(O)(OSiMe₂Ph)(I) reported by Toste and co-workers.¹⁹

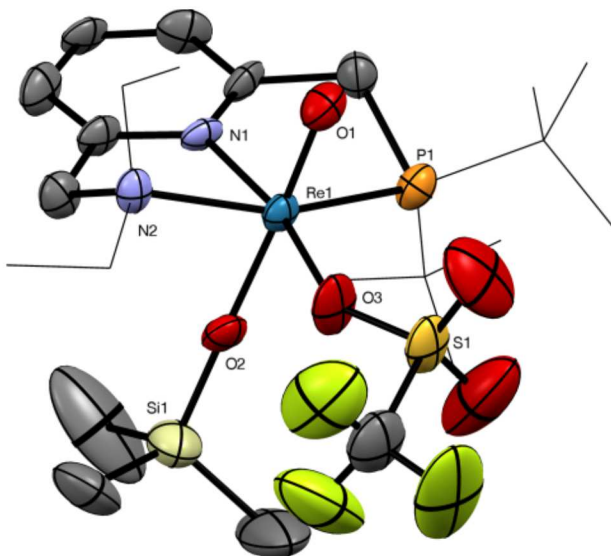
Scheme 3.2



The $^{31}\text{P}\{^1\text{H}\}$ NMR spectrum of **1-a** exhibits a singlet at δ 60 and the ^1H NMR spectrum a doublet at δ 7.7 ($J = 14$ Hz), which is assigned to Re–H. Toste and co-workers observed the Re–H in $(\text{PPh}_3)_2\text{Re}(\text{H})(\text{O})(\text{OSiMe}_2\text{Ph})(\text{I})$ at δ 6.5. Our assignment of the Re–H was confirmed by using Me_2PhSiD , which had a signal at δ 7.7 in the ^2H spectrum and was absent from the ^1H spectrum. Additionally, the $^1\text{H}\{^{31}\text{P}\}$ NMR spectrum of **1-a** gave a singlet at δ 7.7, verifying that the coupling is to the P of the PNN ligand. Attempts to obtain single crystals of **1-a** were not successful, in part because of its reactivity. Nevertheless, reaction of 1 equiv of Me_3SiOTf with complex **1** gave the analogous siloxy

triflate [(PNN)Re(O)(OTf)(OSiMe₃)] [OTf] (**1-OTf**). X-ray- quality crystals of **1-OTf** allowed structural determination (Figure 3.2), providing credence to the proposed addition of a Si–X bond across the oxo ligand of **1**. Many features of the ¹H NMR spectrum of **1-OTf** resemble those observed for **1-a**, further supporting the proposed siloxy hydride species.

Figure 3.2 ORTEP drawing of the molecular structure of **1-OTf**. Hydrogen atoms and the outer-sphere triflate anion are omitted for clarity.

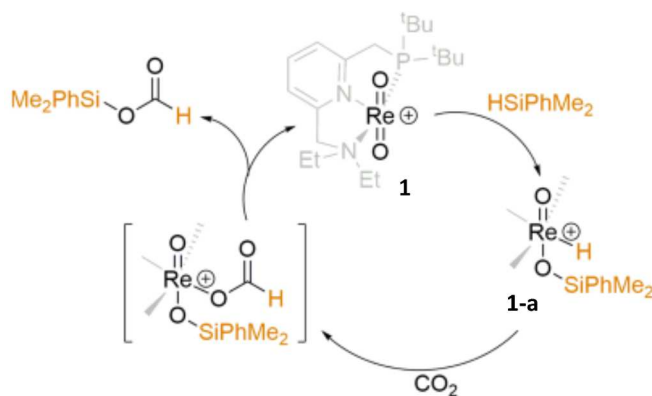


f. Mechanistic study and proposed catalytic cycle

Stoichiometric reaction of **1-a** with CO₂ produces silyl formate at a comparable rate to that of the catalytic reaction, thus implicating this species as a viable active complex for CO₂ hydrosilylation. It is conceivable that initially PhMe₂SiH associates as a η^1 - or η^2 -silane to Re, as has been reported by our group; however, we were not able to definitively observe such a silane adduct.^{20,21} Wei and co-workers have extensively

reported with computational studies that silane adducts (primarily the η^1 complex) are pervasive in oxorhenium-catalyzed hydrosilylations and may even function as the active catalyst.²² The $[\text{Re}(\text{O})_2(\text{PNN})]^+$ complex is Lewis acidic and thus activates the Si–H bond by addition across the Re–O bond. To establish the need for the rhenium center, we performed the reaction with only AgOTf, CO_2 , and PhMe_2SiH under identical conditions and found no formation of silyl formate. The reaction between **1-a** and CO_2 likely proceeds through formation of rhenium formate, as has been detailed extensively by Darensbourg,^{23,24} followed by silylium transfer, as has been shown by Oro, Piers, and Stephan.^{11,25,26} A complete catalytic cycle for the first-step reduction of CO_2 is shown in Scheme 3.3.

Scheme 3.3

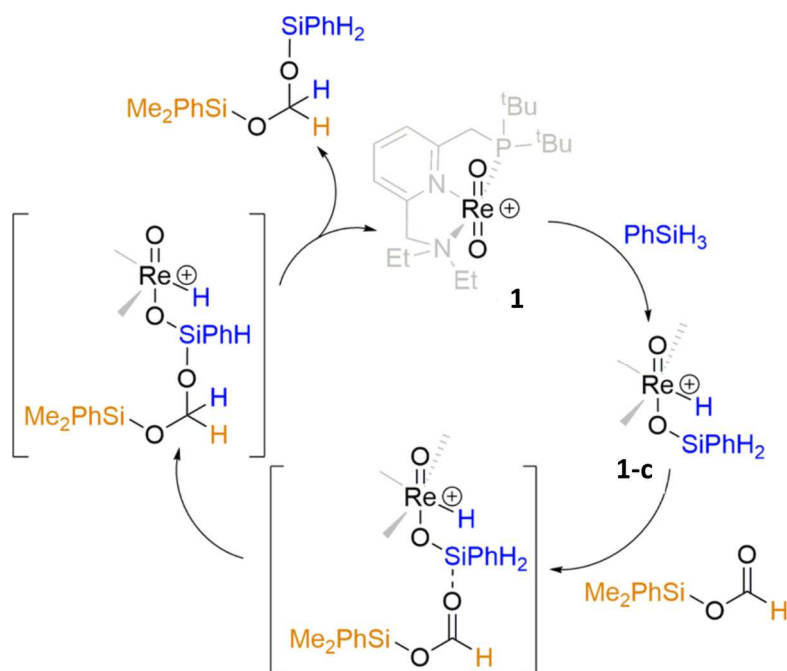


The reduction of silyl formate to formal and all the way to silyl methanol is proposed to proceed initially via a mechanism similar to that in Scheme 3.3, with the exception of having $[-\text{SiPhH}_2]$ on the oxo ligand. This subtle difference appears to influence the subsequent reactivity in a significant way. The evidence for this claim is

presented next. Reaction of **1** with 1 equiv of PhSiH₃ in DCM yielded compound **1-c**, which has spectroscopic features similar to those of **1-a**. The ¹H NMR resonance of the Re–H appears as a doublet at δ 8.0. An AB quartet, with signals at δ 4.50 and 4.64, was identified as two diastereotopic protons of the –SiPhH₂ moiety, which we tentatively propose as residing on one of the oxo ligands, as observed with the Si–Me groups of **1-a**.²⁷ While structurally similar, complexes **1-a** and **1-c** differ dramatically in their reactivity. Fernandes and co-workers have articulated similar observations as to the enhanced reactivity of their oxorhenium catalysts with the use of primary versus secondary organo- silanes.²⁸ Zheng and Chan proposed a unique mechanism for ketone hydrosilylation with Rh complexes that was specific to primary versus secondary organosilanes.²⁹ We propose a similar mechanistic distinction for oxorhenium hydrosilylation catalysis. In this mechanism, the silane undergoes an initial oxidative addition on Rh followed by the ketone (or formal) coordinating to the silicon and inserting into an Si–H bond. We postulate a similar sequence of events for our oxorhenium catalyst: (1) addition of Si–H across the Re–O bond to form the siloxy hydride **1-c**, (2) coordination of silyl formate (or silyl formal in the last reduction step) and insertion into an Si–H bond of –SiPhH₂ (Scheme 3.4), and (3) product elimination to regenerate the dioxorhenium cationic catalyst. It has been noted previously that primary organosilanes possess more silylene character when they are activated by metals and it is this character that leads to this enhanced activity toward Si–H bond insertion into substrates.³⁰ Recent observations by Ison and co-workers that the rhenium–oxo bond acts as the basic component of a frustrated Lewis pair sheds additional light on this duality;

one can imagine that subtle variations of the -R group within the organosilane yield vastly different reactivities.³¹

Scheme 3.4



4. Conclusion

The reported catalytic system herein marks the first example of a high-valent metal oxo catalyst that is capable of reducing CO₂ to silyl formate, silyl formal, and all the way to silyl methanol, depending on the organosilane employed and time of reaction. Schemes 3.3 and 3.4 illustrate the salient features of the operating mechanisms and the way each product can be obtained selectively. Further studies are aimed at exploring the extent to which these transformations can be generalized to other high-valent metal oxo complexes.

5. References

- (1) Appel, A. M.; et al. *Chem. Rev.* **2013**, *113* (8), 6621–6658.
- (2) Arakawa, H.; et al. *Chem. Rev.* **2001**, *101* (4), 953–996.
- (3) Huff, C. A.; Sanford, M. S. *J. Am. Chem. Soc.* **2011**, *133* (45), 18122–18125.
- (4) Huff, C. A.; Sanford, M. S. *ACS Catal.* **2013**, *3* (10), 2412–2416.
- (5) Rezayee, N. M.; Huff, C. A.; Sanford, M. S. *J. Am. Chem. Soc.* **2015**, *137* (3), 1028–1031.
- (6) Franklin, J.; Serra-Diaz, J. M.; Syphard, A. D.; Regan, H. M. *PNAS* **2016**, *113* (14), 3725.
- (7) Choudhury, J. *ChemCatChem.* **2012**, *4* (5), 609–611.
- (8) Li, Y. N.; Ma, R.; He, L. N.; Diao, Z. F. *Catal. Sci. Technol.* **2014**, *4*, 1498–1512.
- (9) Spencer, M. S. *Top. Catal.* **1999**, *8*, 259–266.

- (10) Jansen, A.; Pitter, S. *J. Mol. Catal. A: Chem.* **2004**, *217* (1–2), 41–45.
- (11) Lalrempuia, R.; Iglesias, M.; Polo, V.; Sanz Miguel, P. J.; Fernández-Alvarez, F. J.; Pérez-Torrente, J. J.; Oro, L. A. *Angew. Chem., Int. Ed.* **2012**, *51* (51), 12824–12827.
- (12) Park, S.; Bežier, D.; Brookhart, M. *J. Am. Chem. Soc.* **2012**, *134* (28), 11404–11407.
- (13) Riduan, S. N.; Zhang, Y.; Ying, J. Y. *Angew. Chem., Int. Ed.* **2009**, *48* (18), 3322–3325.
- (14) Riduan, S. N.; Ying, J. Y.; Zhang, Y. *ChemCatChem.* **2013**, *5* (6), 1490–1496.
- (15) Metsäinen, T. T.; Oestreich, M. *Organometallics.* **2015**, *34* (3), 543–546.
- (16) Schäfer, A.; Saak, W.; Haase, D.; Müller, T. *Angew. Chem., Int. Ed.* **2012**, *51* (12), 2981–2984.
- (17) Deglmann, P.; Ember, E.; Hofmann, P.; Pitter, S.; Walter, O. *Chem. - Eur. J.* **2007**, *13* (10), 2864–2879.
- (18) Mazzotta, M. G.; Pichaandi, K. R.; Fanwick, P. E.; Abu-Omar, M. M. *Angew. Chem., Int. Ed.* **2014**, *53* (32), 8320–8322.
- (19) Nolin, K. A.; Krumper, J. R.; Pluth, M. D.; Bergman, R. G.; Toste, F. D. *J. Am. Chem. Soc.* **2007**, *129* (47), 14684–14696.
- (20) Ison, E. A.; Corbin, R. A.; Abu-Omar, M. M. *J. Am. Chem. Soc.* **2005**, *127* (34), 11938–11939.
- (21) Ison, E. A.; Trivedi, E. R.; Corbin, R. A.; Abu-Omar, M. M. *J. Am. Chem. Soc.* **2005**, *127* (44), 15374–15375.
- (22) Gu, P.; Wang, W.; Wang, Y.; Wei, H. *Organometallics.* **2013**, *32* (1), 47–51.

- (23) Darensbourg, D. J.; Wiegrefte, H. P.; Wiegrefte, P. W. *J. Am. Chem. Soc.* **1990**, *112* (25), 9252–9257.
- (24) Darensbourg, D. J.; Wiegrefte, P.; Riordan, C. G. *J. Am. Chem. Soc.* **1990**, *112* (15), 5759–5762.
- (25) Houghton, A. Y.; Hurmalainen, J.; Mansikkamäki, A.; Piers, W. E.; Tuononen, H. *M. Nat. Chem.* **2014**, *6* (11), 983–988.
- (26) Weicker, S. A.; Stephan, D. W. *Chem. - Eur. J.* **2015**, *21* (37), 13027–13034.
- (27) Zuzek, A. A.; Parkin, G. *J. Am. Chem. Soc.* **2014**, *136* (23), 8177–8180.
- (28) Fernandes, T. A.; Bernardo, J. R.; Fernandes, A. C. *ChemCatChem* **2015**, *7* (7), 1177–1183.
- (29) Zheng, G. Z.; Chan, T. H. *Organometallics* **1995**, *14* (1), 70–79.
- (30) Gigler, P.; Bechlars, B.; Herrmann, W. A.; Kühn, F. E. *J. Am. Chem. Soc.* **2011**, *133* (5), 1589–1596.
- (31) Lambic, N. S.; Sommer, R. D.; Ison, E. A. *ACS Catal.* **2017**, *7* (2), 1170–1180.

Chapter IV. Reactivity of High Valent Pincer Oxo-Rhenium Complexes in Catalytic Reduction with Organosilanes

1. Introduction

Hydrosilylation reaction:

Catalytic hydrosilylation catalysis is an efficient method for making organosilicon compounds and one of the most important reactions in silicon chemistry¹. This method

has been widely used in fine organic synthesis such as cross-coupling reactions², stereocontrolled reduction³, and dehalogenation of organic halides⁴. Hydrosilylation is also commonly applied in industry to produce silane coupling reagents and silicone polymers such as oils, rubbers and resin⁵.

Metal-catalyzed hydrosilylation mechanism:

Metal-catalyzed hydrosilylation of carbonyl compounds is an atom-economical methodology in providing direct access to synthetically useful silyl ethers⁶. The four different types of carbonyl hydrosilylative reduction mechanisms are: catalysis with dihydride complexes, catalysis with monohydride complexes, metal-ligand bifunctional catalysis and catalysis involving ionic mechanism⁷. In most cases, a metal hydride intermediate is generated and assumed to be active catalyst for reduction^{8 9 10 11 12}. Nevertheless, the mechanism for rhenium mediated hydrosilylation still remains unclear because reactive intermediates have not yet been isolated or clearly detected experimentally.

Rhenium (V) catalyzed hydrosilylation:

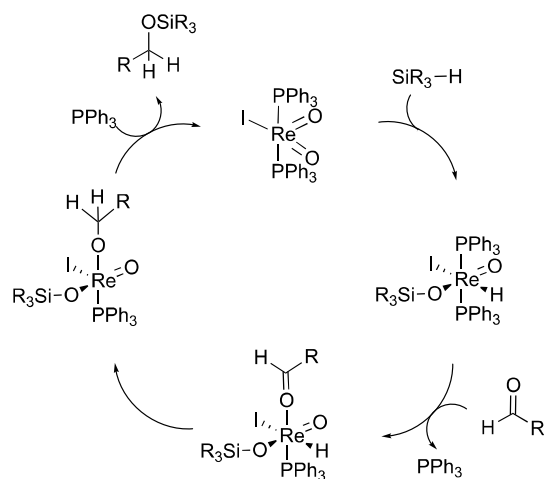
a) Hydride Mechanism:

In the presence of monohydrosilanes, Toste and coworkers proposed hydride mechanism for $\text{ReIO}_2(\text{PPh}_3)_2$ catalyzed hydrosilylation of carbonyl compounds. The cycle proceeds through the formation of a rhenium-hydride intermediate, addition of

substrate, and carbonyl insertion into Re–H bond to produce an alkoxide (Scheme 4.1) ¹³

14

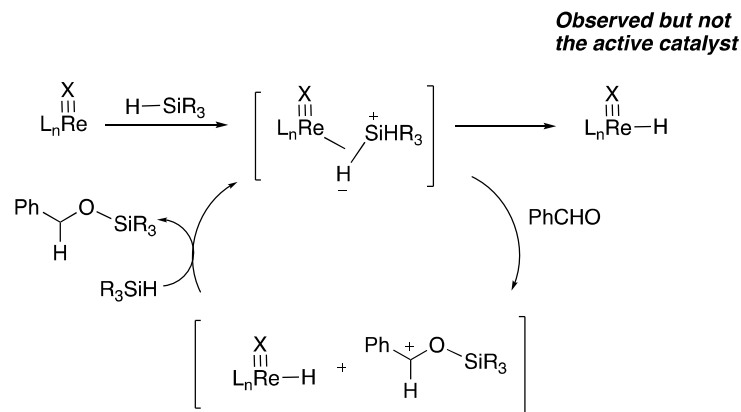
Scheme 4.1 Hydride Mechanism



b) Ionic mechanism:

Our research group has had a long interest in hydrosilylation chemistry of oxorhenium complexes. We established ionic mechanism in mono oxo-rhenium (V) complex $\text{Re}(\text{O})\text{Cl}_2(\text{H})(\text{PPh}_3)_2$ mediated reaction (Scheme 4.2), where heterolytic cleavage of Si–H bond through η^2 -silane Re (V) adduct formation is more favored compare to hydride mechanism¹⁵. Additionally, we probed rhenium hydride formation, but it is not sufficiently reactive towards catalysis. This ionic pathway was later supported by DFT calculations both in $[\text{Re}(\text{O})(\text{hoz})_2]^+$ ¹⁶ and $\text{Re}(\text{O})\text{Cl}_3(\text{PPh}_3)_2$ ¹⁷ catalyzed hydrosilylation. Whereas, there is lack of support on dioxo-rhenium (V) mediated hydrosilylation for an ionic pathway.

Scheme 4.2 Ionic Mechanism



Deoxygenation Reaction:

Direct deoxygenation of aryl ketones can be achieved through hydrosilylation mediated by high-valent oxorhenium complexes¹⁸. Although the mechanistic details for transition-metal catalyzed deoxygenation in the presence of silane are not yet clear in the literature, it was established that the carbonyl is first reduced to alcohol which in turn undergoes hydrogenolysis to form alkylated product^{19,20 21}.

Considering the heightened interest in hydrosilylation and direct deoxygenation catalyzed by high-valent pincer dioxorhenium complexes and the current lack of detailed mechanistic understanding, we decided to investigate the capability of $[(^{\text{tBu}}\text{PNN}^{\text{iPr}})\text{Re}(\text{O})_2][\text{OTf}]$ (**1**) in reduction²². Recently we reported the performance of **1** in reducing CO_2 towards silyl-protected methanol²³. In this chapter, we focus on **1**-mediated carbonyl hydrosilylation. The catalytic performance of different oxo-rhenium complexes, organosilanes and solvents are examined upon optimizing reaction condition. Additionally, we have applied this methodology towards utilization of biomass-derived carbonyl molecules. Direct reductive deoxygenation can be accomplished at moderate

temperature (80 °C). The applicability of our reaction method to imines and amide was also demonstrated.

2. Experimental

a. General Consideration

All reactions were performed in a nitrogen-filled glove box. Solvents were degassed and purified with a solvent purification system (Pure Process Technology INC) prior to use. CD₂Cl₂ was dried with CaH₂, distilled under argon and stored over molecular sieves. Organosilanes and all other chemicals were purchased from commercial sources, degassed and stored over molecular sieves prior to use. Catalyst poisoning experiments were carried out with 275 molar equiv of elemental mercury (Hg) relative to rhenium catalyst.

¹H and ¹³C NMR spectra were recorded on 400 MHz, 500 MHz or 600 MHz spectrometers using residue solvent peaks as reference (CDCl₃, ¹H: 7.26 ppm; ¹³C: 77.00 ppm. CD₂Cl₂, ¹H: 5.32 ppm; ¹³C: 53.84 ppm.). ³¹P NMR spectra were recorded on Agilent 400 MHz spectrometer and referenced versus phosphoric acid external standard (H₃PO₄, ³¹P: 0.00 ppm). ¹⁹F NMR spectra were recorded on Agilent 400 MHz spectrometer and referenced versus trifluoroacetic acid external standard (CF₃COOH, ¹⁹F: -76.55 ppm).

NMR yields were calculated by integration of product versus a known quantity of internal standard. The moles of product are determined by the following equation:

$$\text{mol}_{\text{pdt}} = \text{mol}_{\text{std}} \times (\text{Integral}_{\text{pdt}} / \text{Integral}_{\text{std}}) \times (N_{\text{std}}/N_{\text{pdt}})$$

where N is the number of protons for the relevant signal. The yield is then determined by the following formula:

$$\text{yield}_{\text{pdt}} (\%) = \text{mol}_{\text{pdt}} / \text{mol}_{\text{substrate}} \times 100\%$$

where $\text{mol}_{\text{substrate}}$ is the initial amount of starting material in the reaction mixture.

The crystal of rhenium complexes were mounted on a cryo-loop and transferred to a Bruker Kappa APEX II diffractometer. The APEX2 program was used to determine the unit cell parameters and data collection (10 sec/frame, 0.5 deg. /frame Omega scan). The data was collected at 100K with Oxford cryo-system. The raw frame data was processed using SAINT program. The absorption correction was applied using program SADABS. Subsequent calculations were carried out using SHELXTL program. The structure was solved by direct methods and refined on F^2 by full-matrix least-squares techniques.

ESI mass data was acquired with a Waters Micromass LCT-Premier mass spectrometer. Samples were diluted to an appropriate concentration and infused directly using either a syringe pump or a Waters Alliance 2695 autosampler. Accurate mass data was acquired using poly(ethylene glycol) or poly(ethylene glycol) monomethyl ether as an internal calibrant, as appropriate.

b. Typical Hydrosilylation Conditions for Carbonyl Compounds

1 (1 mol%, 2 μmol) was added to a solution of aldehyde or ketone substrate (0.20 mmol) and PhSiH_3 (0.40 mmol) in C_6D_6 (1.0 mL) with cyclooctane (37 μmol) as internal standard in a J-Young NMR tube (Wilma LabGlass). Conversion and yield were determined based on ^1H peak intensity ratio of the starting material, products and C_8H_{16} .

c. Typical Amide Reduction Conditions

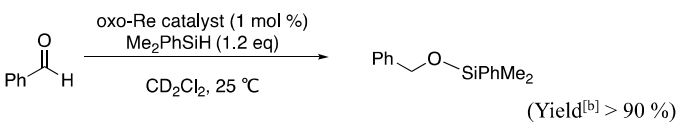
1 (10 mol%, 20 μmol) was added to a solution of N-benzylbenzamide (0.20 mmol) and PhSiH_3 (0.40 mmol) in C_6D_6 (1.0 mL) with cyclooctane (37 μmol) as internal standard in a J-Young NMR tube (Wilma LabGlass). The reaction mixture was heated

in an oil bath gently at 80 °C for 48 hours. Conversion and yield were determined based on ¹H peak intensity ratio of the starting material, products and C₈H₁₆.

3. Results and discussion

a. Hydrosilylation of Benzaldehyde Catalyzed by Various Oxo-Rhenium Catalysts

Table 4.1 Hydrosilylation of benzaldehyde using different oxo-Re catalyst^[a]

			
Entry	Catalyst	Time (h)	Conversion (%) ^[b]
1	[(^t buPNN ⁱ Pr)Re(O) ₂][OTf]	10	100
2	[(^t buPNN ⁱ Pr)Re(O) ₂][BF ₄] / [PF ₆]	10	100
3	ReIO ₂ (PPh ₃) ₂	12	85
4	ReOCl ₃ (PPh ₃) ₂	12	100
5	ReOCl ₃ (dppm)	24	26
6	Bu ₄ NReO ₄	24	32
7	Re ₂ O ₇	48	11
8	Without Catalyst	48	No reaction

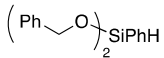
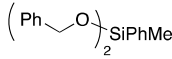
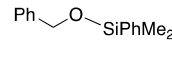
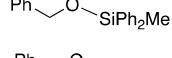
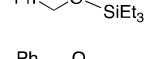
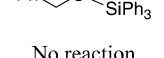
[a] Reaction conditions: benzaldehyde (0.2 mmol), Me₂PhSiH (0.24 mmol), oxo-Re catalyst (1 mol %; 2 μmol), C₈H₁₆ (37 μmol), CD₂Cl₂ (1 ml), 25 °C.
 [b] Conversions and yields were determined by ¹H NMR spectroscopy with C₈H₁₆ (37 μmol) as internal standard.

Unfunctionalized benzaldehyde was chosen as the model substrate along with Me₂PhSiH as the hydrosilane to examine the catalytic competency of different oxorhenium complexes (1 mol %) in CD₂Cl₂ (Table 4.1). Reactions were conducted on NMR scale in a J-Young NMR tube. **1** is very efficient in the series: >90% yield (100% conversion) of the corresponding silyl ether in 10 hours (Table 4.1, entry 1). In contrast,

low conversion of benzaldehyde was obtained in reactions catalyzed by Bu_4NReO_4 and Re_2O_7 (Table 4.1, entries 6 and 7). These results reveal that oxorhenium(V) complexes are more efficient catalysts than oxorhenium(VII) complexes. Among the Re(V) complexes, the low efficiency of $\text{ReOCl}_3(\text{dppm})$ ($\text{dppm} = \text{Ph}_2\text{PCH}_2\text{PPh}_2$) is probably due to the absence of a vacant site that would allow either substrate or organosilane activation (Table 4.1, entry 5). Moreover, ligand dissociation of bidentate phosphine is difficult due to weak thermodynamic driving force at room temperature. The different catalytic performance between $\text{ReOCl}_3(\text{PPh}_3)_2$ and $\text{ReOCl}_3(\text{dppm})$ suggests steric property of chelating ligand such as dppm also inhibits catalytic activity (entry 4). Cationic catalysts bearing a labile ligand such as OTf ($\text{OTf} = \text{CF}_3\text{SO}_3^-$) are significantly more active than neutral rhenium complexes (Table 4.1, entry 1 and 3). Different counter-anions such as BF_4^- and PF_6^- have no effect on efficiency (Table 4.1, entry 2). Finally, it should be noted that no reaction was observed in the absence of a catalyst (Table 4.1, entry 8).

b. Effect of Organosilane on Hydrosilylation

Table 4.2 Hydrosilylation of benzaldehyde with different silanes^[a]

Entry	Silane	Product	Time (h)	Conversion (%) ^[b]	Yield (%) ^[b]
1	PhSiH ₃		1	100	90
2	PhMeSiH ₂		3	100	93
3	PhMe ₂ SiH		10	100	91
4	Ph ₂ MeSiH		16	100	87
5	Et ₃ SiH		12	100	95
6	Ph ₃ SiH		24	12	77
7	Without Silane	No reaction	24	0	0

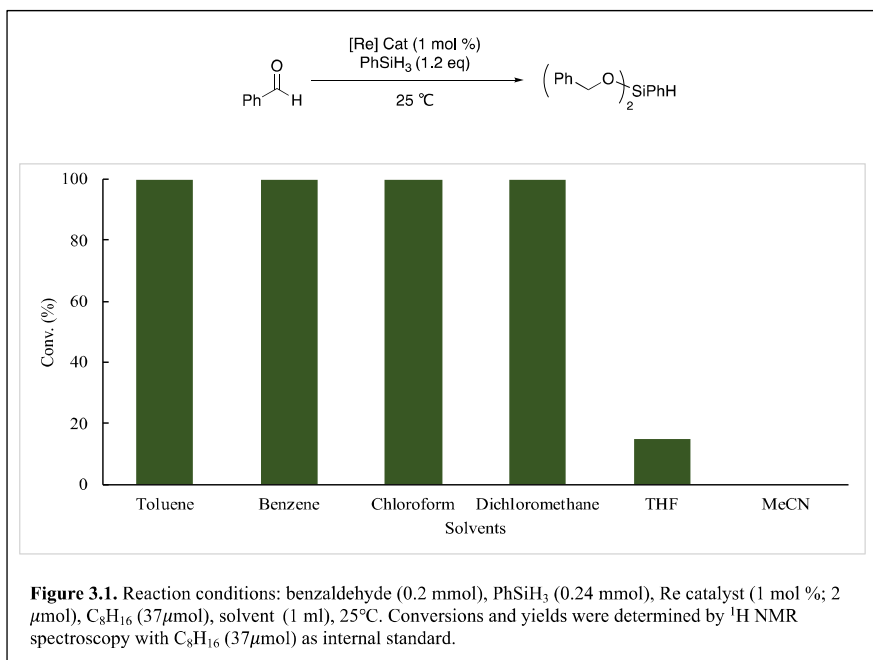
[a] Reaction conditions: benzaldehyde (0.2 mmol), silanes (0.24 mmol), Re catalyst (1 mol %; 2 μmol), C₈H₁₆ (37 μmol), CD₂Cl₂ (1 ml), 25°C.
[b] Conversions and yields were determined by ¹H NMR spectroscopy with C₈H₁₆ (37 μmol) as internal standard.

We next evaluated the scope of organosilanes and observed that a large number of organosilanes were suitable for reduction reactions catalyzed by complex **1** (Table 4.2). PhSiH₃ was the most efficient reducing agent, affording 100% conversion of benzaldehyde (90% yield) in just 1 hour (Table 4.2, entry 1). Similar results were obtained by using higher equivalents (3 equiv.) of PhSiH₃ and demonstrated that the catalysis was not improved by the addition of more organosilane. It was noted that even with 1.0 equiv PhSiH₃ there was still 50 % unreacted PhSiH₃ after complete consumption of benzaldehyde. A 0.5 equiv amount of PhSiH₃ seems to be sufficient. These observations prompted us to investigate the influence of organosilanes upon reduction. Among these silanes, PhMeSiH₂ was also able to achieve full conversion of benzaldehyde within 3 hours (Table 4.2, entry 2). Monohydrosilanes turned out to be less efficient than primary and secondary silanes (Table 4.2, entry 3-5). Full conversion of benzaldehyde was obtained by monohydrosilanes with small and medium-sized aryl and alkyl substituents. The sterically hindered aryl silanes Ph₃SiH severely inhibited the reaction, with conversion of only 12 % after 24 hours (Table 4.2, entry 6). Similar observation of the organosilane steric effects was also noted for molybdenum catalyzed

hydrosilylation²⁴. Finally, no reaction was observed in absence of organosilane (Table 4.2, entry 7).

c. Effect of Reaction Medium

Figure 4.1 Effect of Reaction Medium

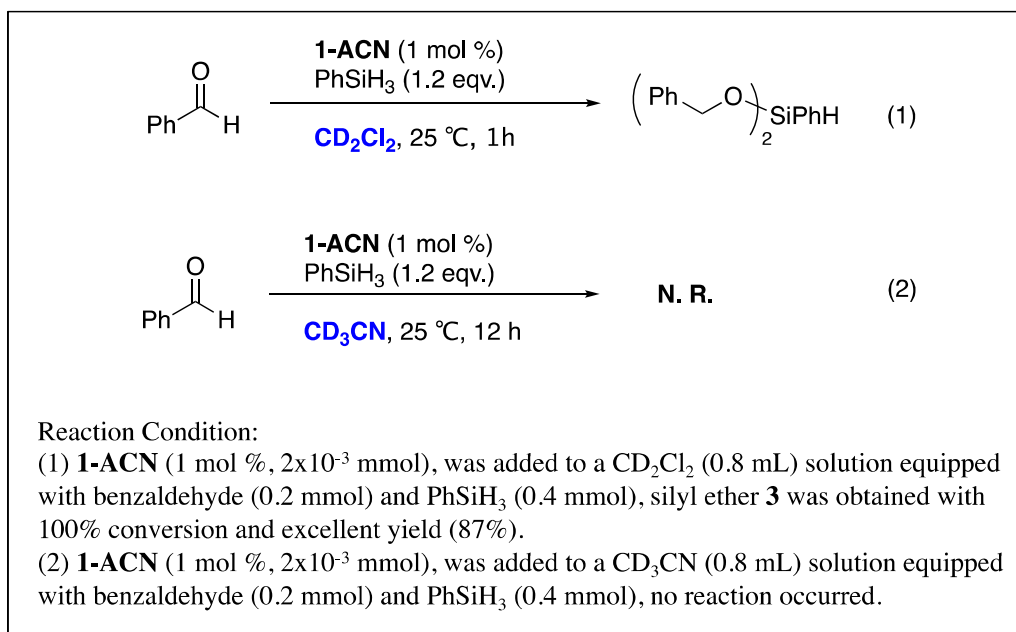


Having identified phenylsilane as being the superior reducing agent, we turned our attention to solvent effect. The data demonstrates that 1-mediated hydrosilylation

does not depend on solvent polarity. Toluene, benzene, chloroform and dichloromethane all achieved 100% conversion with excellent yield (>90%) within 1 hour (Figure 4.1).

In contrast, the reactions showed low to no conversion when performed in THF or ACN. This effect stems from the coordinating ability of these solvents (MeCN > THF > Benzene > Toluene > DCM ~ Chloroform)⁵. [(PNN)Re(O)₂(ACN)][OTf] (**1-ACN**) was successfully crystallized out from acetonitrile solution and supported the strong coordinating ability of ACN to **1**.

Scheme 4.3 Hydrosilylation catalyzed by 1-ACN

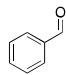
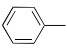
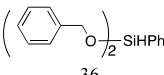
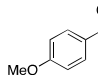
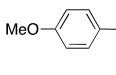
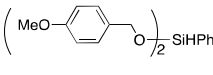
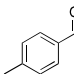
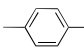
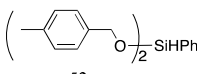
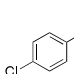
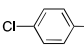
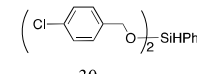
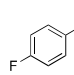
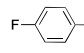
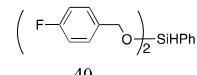
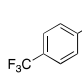
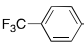
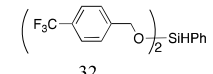
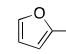
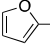
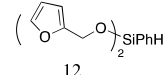
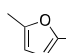
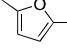
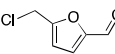
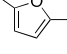
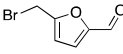
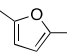
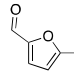
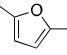


Six ligands coordinated **1-ACN** was then used as catalyst for hydrosilylation reaction in CD_2Cl_2 , and full conversion of benzaldehyde was attained with 87% yield of silyl ether product (Scheme 4.3 (1)). However, **1-ACN** was unreactive in CD_3CN (Scheme 4.3 (2)). The Labile acetonitrile ligand was able to dissociate throughout

catalysis. This solvent effect presumably reflects open coordination site for activating silane or organic carbonyl substrate is essential for catalysis.

d. Substrate Scope

Table 4.3 Hydrosilylation of Various Aldehyde^[a]

Entry	Substrate	Time (h)	Conversion ^[b] (%)	Product Yield ^[b] (%)
1		3	100	 47  36
2		3	100	 48  37
3		3	100	 35  52
4		3	100	 46  30
5		3	100	 33  40
6		3	100	 51  32
7		3	100	 40  12
8		3	100	 52
9		5	100	 67
10		5	100	 60
11 ^[c]		24	56	 53

[a] Unless and otherwise noted, reaction conditions: benzaldehyde (0.2 mmol), PhSiH₃ (0.4 mmol), Re catalyst (1 mol %; 2 μmol), C₈H₁₆ (37 μmol), C₆D₆ (1 ml), 80°C.
[b] Conversions and yields were determined by ¹H NMR spectroscopy with C₈H₁₆ (37 μmol) as internal standard.
[c] Re catalyst (5 mol %, 10 μmol), PhSiH₃ (4 eq. 0.8 mmol).

With these data in hand, we proceeded to expand the scope of the application of **1** catalyzed hydrosilylation towards various other aldehyde substrates, including biomass-derived aldehydes. Under the optimized conditions with excess phenylsilane (2 equiv. relative to substrate), 1 mol % **1** at 80 °C in benzene, hydrosilylation of benzaldehyde resulted a mixture of toluene and silyl ether with 47 % and 36 % yield, respectively

(Table 4.3, entry 1). Whereas higher temperature and longer reaction time did not promote the yield of toluene due to catalyst decomposition. Interestingly, complete deoxygenation of aldehyde was not observed at room temperature.

Further catalytic activity towards functional group tolerance was explored. Hydrosilylation among different benzaldehydes, containing electron-donating and electron-withdrawing groups, afforded 100% conversion to a mixture of corresponding deoxygenation and disilylation products (Table 4.3, entry 2-6).

In order to demonstrate the ability of **1** towards utilization of biomass-derived compounds, furfural and other furan-based aldehydes were investigated (Table 4.3, entry 7-11). Reductive dehalogenation also proceeded during this catalytic process towards 5-chloromethylfurfural and 5-bromomethylfurfural, resulting dimethyl furan as the only product (Table 4.3, entry 9 and 10). This data illustrates the efficiency of **1** in hydrosilylation of heterocyclic aromatic aldehydes. But in the case of 2,5-Furandicarboxaldehyde, conversion to only 56% was observed even with 5 mol % **1** after 24 hours (Table 4.3, entry 11). The yields for furan-based substrates were lower than 70 % overall due to undesired ring opening co-products at high temperature.

Table 4.4 Hydrosilylation of Various Other Substrates^[a]

Entry	Substrate	Catalyst (mol %)	Time (h)	Conversion ^[b] (%)	Product Yield ^[b] (%)
1		5	12	100	 87
2 ^[c]		10	24	57	 75
3 ^[c]		10	24	73	 95
4 ^[c]		10	48	37	 97
5		1	3	100	 96
6		10	48	55	 83
7		10	48	0	0

[a] Reaction conditions: benzaldehyde (0.2 mmol), PhSiH₃ (0.4 mmol), C₈H₁₆ (37 μmol), C₆D₆ (1 ml), 80°C.
[b] Conversions and yields were determined by ¹H NMR spectroscopy with C₈H₁₆ (37 μmol) as internal standard.
[c] Conversions and yields were determined by GC and confirmed by GC/MS.

The catalytic performance of **1** towards various other substrates were screened additionally. However, **1** exhibits poor efficiency in reduction of ketones and esters (Table 4.4, entry 1-4). The reduction of deoxybenzoin resulted in a mixture of trans: cis stilbene in 5:1 ratio with 100% conversion and 5 mol % catalyst loading. (Table 4.4, entry 1). Whereas, unlike the case of aldehyde hydrosilylation, the catalytic performance towards esters was less effective. Reduction on γ -butanolactone only showed 57% conversion over 24 hours with 10 mol % catalyst loading (Table 4.4, entry 2). The catalytic progress was even slower when 6-hexanolactone was tested, affording 37 %

conversion with a loading of 10 mol % catalyst over 48 hours (Table 4.4, entry 4).

Nikonov et al reported similar reactivity for molybdenum hydride catalyzed hydrosilylation and they proposed nonhydride mechanism catalysis²⁵.

Continuing to expand the series of catalysis to imine and amides, it is noteworthy that hydrosilative reduction of imine was very effective. Full conversion of benzylideneaniline to benzylaniline was attained in 1 hour with 1 mol % catalyst loading (Table 4.4, entry 5). On the other hand, only 55% benzanilide was converted to benzylaniline with a catalyst loading of 10 mol % over 48 hours (Table 4.4, entry 6). Further studies on variety of imines and amides are in progress. Finally, hydrosilylation could not be observed when benzoin was used as substrate (Table 4.4, entry 7). Curiously, no reaction was observed when introducing alcohol such as benzyl alcohol or hydroxymethylfurfural into our catalytic system. The mechanistic aspect in complete deoxygenation is still unclear at this point. Catalyst homogeneity was confirmed by conducting benzaldehyde hydrosilylation in the presence of excess Hg^0 , which did not affect conversion.

4. Conclusion

In summary, we report on the use of high valent pincer oxo rhenium complex **1** as an efficient catalyst for reductive hydrosilylation particularly in the presence of the primary organosilane PhSiH₃. This protocol enables cross coupling of an aldehyde and hydrosilane to directly generate the corresponding silyl ether. A variety of commonly used solvents were tested. The data reveals strong coordinating solvents such as THF and ACN inhibit the catalyst capacity by occupying the needed coordination site. Crystallization of **1-ACN** demonstrated the coordination of solvents on to rhenium center.

A great variety of aryl aldehydes including biomass derived substrates were accessed with good activities and excellent yields. Hydrosilative reduction of aldehydes produced silyl ether product at room temperature, and a mixture of deoxygenation and silylation products at higher temperature (80 °C). At optimal reaction conditions using benzaldehyde as a model compound, we were also successful in demonstrating of this system in making value-added chemicals.

5. References

- (1) Morris, R. H. *Chem. Soc. Rev.* **2009**, 38 (8), 2282–2291.
- (2) Denmark, S. E.; Regens, C. S. *Collect. Czech. Chem. Commun.* **2008**, 41 (11), 1486–1499.
- (3) Fleming, I.; Barbero, A.; Walter, D. *Chem. Rev.* **1997**, 97 (6), 2063–2192.
- (4) Miura, K.; Tomita, M.; Yamada, Y.; Hosomi, A. *J. Org. Chem.* **2007**, 72 (3), 787–792.
- (5) Díaz-Torres, R.; Alvarez, S. *Dalton Trans.* **2011**, 40 (40), 10742–10750.
- (6) Carpentier, J. F.; Bette, V. *Curr. Org. Chem.* **2002**, 6 (10), 913–936.
- (7) Chakraborty, S.; Guan, H. *Dalton Trans.* **2010**, 39 (32), 7427–7436.
- (8) Junge, K.; Schröder, K.; Beller, M. *Chem. Commun.* **2011**, 47 (17), 4849–4859.
- (9) Metsänen, T. T.; Hrobárik, P.; Klare, H. F.; Kaupp, M.; Oestreich, M. *J. Am. Chem. Soc.* **2014**, 136 (19), 6912–6915.
- (10) Bolm, C.; Legros, J.; Le Paih, J.; Zani, L. *Chem. Rev.* **2004**, 104 (12), 6217–6254.
- (11) Mock, M. T.; Potter, R. G.; Camaioni, D. M.; Li, J.; Dougherty, W. G.; Kassel, W. S.; Twamley, B.; DuBois, D. L. *J. Am. Chem. Soc.* **2009**, 131 (40), 14454–14465.
- (12) Labinger, J. A.; Komadina, K. H. *J. Organomet. Chem.* **1978**, 155 (2), C25–C28.

- (13) Kennedy-Smith, J. J.; Nolin, K. A.; Gunterman, H. P.; Toste, F. D. *J. Am. Chem. Soc.* **2003**, *125* (14), 4056–4057.
- (14) Nolin, K. A.; Krumper, J. R.; Pluth, M. D.; Bergman, R. G.; Toste, F. D. *J. Am. Chem. Soc.* **2007**, *129* (47), 14684–14696.
- (15) Du, G.; Fanwick, P. E.; Abu-Omar, M. M. *J. Am. Chem. Soc.* **2007**, *129* (16), 5180–5187.
- (16) Gu, P.; Wang, W.; Wang, Y.; Wei, H. *Organometallics*. **2012**, *32* (1), 47–51.
- (17) Huang, L.; Wang, W.; Wei, H. *J. Mol. Catal. A: Chem.* **2015**, *400*, 31–41.
- (18) Fernandes, T. A.; Bernardo, J. R.; Fernandes, A. C. *ChemCatChem*. **2015**, *7* (7), 1177–1183.
- (19) Rahaim, R. J.; Maleczka, R. E. *Org. Lett.* **2011**, *13* (4), 584–587.
- (20) Volkov, A.; Gustafson, K. P.; Tai, C.; Verho, O.; Bäckvall, J.-E.; Murillo, C. *Angew. Chem. Int. Ed.* **2015**, *54* (17), 5122–5126.
- (21) Wang, H.; Li, L.; Bai, X.; Deng, W.; Zheng, Z.; Yang, K.; Xu, L. *Green Chem.* **2013**, *15* (9), 2349–2355.
- (22) Pichaandi, K. R.; Mazzotta, M. G.; Harwood, J. S.; Fanwick, P. E.; Abu-Omar, M. M. *Organometallics*. **2014**, *33* (7), 1672–1677.
- (23) Mazzotta, M. G.; Xiong, M.; Abu-Omar, M. M. *Organometallics*. **2017**, *36* (9), 1688–1691.
- (24) Chakraborty, S.; Blacque, O.; Fox, T.; Berke, H. *ACS Catal.* **2013**, *3* (10), 2208–2217.
- (25) Shirobokov, O. G.; Kuzmina, L. G.; Nikonov, G. I. *J. Am. Chem. Soc.* **2011**, *133* (17), 6487–6489.

Chapter V. Kinetics and Mechanism of Hydrosilylation Catalyzed by Oxo Pincer Rhenium Complex (PNN)Re(O)₂ Cation

1. Introduction

The development of efficient and direct synthetic pathway to silylated alcohols is a fundamental process in organic and organometallic chemistry¹. In the last few decades, the ability of transition metal complexes to induce hydrosilylative catalytic reactions has been studied extensively.

A key feature that makes hydrosilanes stand out as reducing agents over hydrogen is their reactivity can be fine-tuned by the substituents on the silicon atom. The general order of various silanes reactivity is PMHS (polymethylhydrosiloxane) < Et₂(MeO)SiH < (EtO)₃SiH < Ph₃SiH < Ph₂SiH₂ < PhSiH₃². A challenge associate with reduction is that the reaction often requires high-pressure equipment; however, hydrosilanes can be activated under mild conditions and are easy-to-use. The potential for hydrosilylation has clearly been underestimated. Catalytic hydrosilylation will be used more often in challenging synthetic systems because of the straightforward reaction procedure and the ability of fine-tuning reactivity. Although the mechanism for catalytic hydrosilylation has

been investigated intensively, the kinetic investigations especially ones that differ from the traditional hydride mechanism remain relatively unexplored.

Kinetic studies support hydride mechanism:

Hetflejs et al. studied hydrosilylation of tert-butyl phenyl ketone by diphenylsilane using $[\{\text{Rh}((-)\text{diop})\}]^+\text{ClO}_4^-$ and they observed a saturation effect as concentration of ketone increased and the kinetic was found to be first order in catalyst and ketone, fractional order in organosilicon hydride³. Waldman et al. concluded that hydrosilylation of 2,2-dimethylcyclopentanone with $\text{Rh}(\text{diphos})(\text{PPh}_3)_2^+(\text{PF}_6^- \text{ or } \text{BF}_4^-)$ is first order with respect to catalyst and silane; zero order on ketone concentration. Berke et al. reported the same kinetic order upon hydrosilylation of ketone catalyzed by $[\text{Mo}(\text{NO})(\text{P}\cap\text{P})(\text{NCMe})_3]^+[\text{BArF}_4]^-$ ($\text{P}\cap\text{P} = (\text{Ph}_2\text{PC}_6\text{H}_4)_2\text{O}$)⁴.

Kinetic studies support nonhydride ionic mechanism:

In recent years, an ionic hydrosilylation mechanism (Lewis acid catalysis pathway) has been proposed and studied computationally for oxo-rhenium and oxo-molybdenum complexes by Oestreich⁵ and Wei^{6,7}. Our group described this non-hydride hydrosilylation mechanism^{8,9} and this work has been supported by computational studies¹⁰. Brookhart and coworkers also elucidated hydrosilylation of unsaturated compounds catalyzed by iridium complex proceeds through an activated η^1 - σ silane complex¹¹, and this pathway has been supported by detailed mechanism study and DFT calculations^{12,13}. Our group has studied $[\text{Re}(\text{O})(\text{salen})(\text{Solv})][\text{B}(\text{C}_6\text{F}_5)_4]$ catalyzed hydrosilylation and proposed that silane was activated through heterolytic cleavage pathway. Kinetic study on reduction of PhMe_2SiH revealed first order dependence on catalyst and inhibition with increasing substrate concentration. This η^2 activation of Si-H

mechanism is analogous to Ir-catalyzed silane alcoholysis by Crabtree, where $\text{Ir}(\eta^2\text{-HSiR}_3)$ was spectroscopically detected at low temperature. The kinetic study on this silane alcoholysis exhibits first order on the concentration of catalyst and silane, but inverse first order to substrate ¹⁴.

In order to address the lack of mechanistic and kinetic study on transition metal involved Lewis acid catalysis, **1** mediated hydrosilylation was monitored by *in situ* ¹H NMR spectroscopy, and rate constants were reported for benzaldehyde hydrosilylation. Stoichiometric and deuterium scrambling experiments were designed to investigate active catalyst. A Lewis acid mechanism based on Piers FLP system for high-valent oxo-rhenium pincer complex **1** catalyzed hydrosilylation that allows the functionalization of weak nucleophile has been proposed in this chapter.

2. 3 Experimental

Time Profile of Benzaldehyde Hydrosilylation using $\text{PhSiH}_3/\text{Ph}_2\text{SiH}_2$

In a nitrogen filled glove box, a stock solution of **1** in CD_2Cl_2 (0.001 M) was prepared. 10 μL of the stock solution of **1** in CD_2Cl_2 (1×10^{-5} mmol, 1 mol %) was added to a J-Young NMR tube equipped with benzaldehyde (0.1 M, 0.1 mmol), $\text{PhSiH}_3/\text{Ph}_2\text{SiH}_2$ (0.1 M, 0.1 mmol) and internal standard C_8H_{16} (3.7×10^{-5} mmol) in CDCl_3 (0.8 ml) at 25°C. The progress of the reaction was monitored by integrating proton of PhCHO , $\text{PhSiH}_3/\text{Ph}_2\text{SiH}_2$ and $(\text{PhCH}_2\text{O})_2\text{SiPhH}/(\text{PhCH}_2\text{O})_2\text{SiPh}_2$ relative to C_8H_{16} respect to time.

Time Profile of N-benzylideneaniline Hydrosilylation

In a nitrogen filled glove box, a stock solution of **1** in CD₂Cl₂ (0.001 M) was prepared. 5 μL of the stock solution of **1** in CD₂Cl₂ (5×10⁻⁶ mmol, 1 mol %) was added to a J-Young NMR tube equipped with N-benzylideneaniline (0.05 M, 0.05 mmol), PhSiH₃ (0.1 M, 0.1 mmol) and internal standard C₈H₁₆ (3.7×10⁻⁵ mol) in CDCl₃ (0.8 ml) at 25°C. The progress of the reaction was monitored by integrating proton of PhN=CHPh, PhSiH₃ and Ph(H₂PhSi)NCH₂Ph relative to C₈H₁₆ respect to time.

Mercury Poisoning Experiment

Catalytic hydrosilylation of benzaldehyde (0.2 mmol) with **1** (1 mol%, 2×10⁻³ mmol) was carried out in the presence of a 275-fold excess of Hg (0.55 mmol). The catalyst activity was unaffected by the presence of Hg (0). This result rules out heterogeneous Re metal being the active species.

Magnetic Susceptibility Measurement (Evans Method)

The standard Evans method was applied for the measuring magnetic susceptibility of **1** and benzaldehyde (1:1) reaction via 400MHz ¹H NMR spectroscopy at constant temperature 298K.

A J-Young NMR (outer) tube was equipped with benzaldehyde (1.5 ×10⁻⁵ mol) and **1** (1.5 ×10⁻⁵ mol) in CD₂Cl₂ (0.8 ml). The capillary (inner) tube was filled with CH₂Cl₂. From the solvent (CD₂Cl₂ and CH₂Cl₂) shift difference between the inner and outer tubes, the molar paramagnetic susceptibility is obtained using the following equation:

μ_{eff} = Effective magnetic moment in BM (Bohr magnetons) = $(8\chi_M T)^{1/2}$

Diamagnetic Susceptibility χ_M (ml/mol) = $\frac{3\Delta f}{4\pi FC}$ (ml/mol)

Δf (Hz) = Frequency difference between two peaks of the inner and outer tube =
25.78 Hz

F (Hz) = Frequency of NMR instrument = 400×10^6 Hz

C (mol/ml) = Concentration of substance = 1.5×10^{-5} mol/ml

T(K) = 296.3 K

$\chi_M = 1.02 \times 10^{-3}$ (ml/mol)

$\mu_{\text{eff}} = 1.56$ BM

This value is with the range found for paramagnetic (S = 1/2) complexes¹⁵.

NMR Scale Stoichiometric Experiment

Stoichiometric experiment between (PNN)Re(H)(O)(OSiHPh₂) and benzaldehyde/ N-benzylideneaniline

PhCHO/ N-benzylideneaniline (0.1 mmol) was added into a J-Young NMR tube that already contain (PNN)Re(H)(O)(OSiHPh₂) (**1-b**) (0.1 mmol) in CDCl₃ (0.8 ml). The J-Young NMR tube was shaken under room temperature for 12 hours before adding Ph₂SiH₂ (0.1 mmol).

H/D exchange between (PNN)Re(H)(O)(OSiHPh₂) and Ph₂SiD₂

Ph₂SiD₂ (0.1 mmol) was added to (PNN)Re(H)(O)(OSiHPh₂) (**1-b**) (0.1 mmol) in CDCl₃ (0.8 ml). After 24 h the catalyst retained the hydride (Re-H/Re-D = 100:0), no H/D exchange occurred.

Stoichiometric experiment between (PNN)Re(H)(O)(OSiHPh₂), Ph₂SiD₂ and benzaldehyde

PhCHO (0.1 mmol) and Ph₂SiD₂ (0.1 mmol) were added to a solution of (PNN)Re(H)(O)(OSiHPh₂) (**1-b**) (0.1 mmol) in CDCl₃ (0.8 ml). The reaction was complete in 0.5 hour at room temperature giving (PhCHDO)₂SiPh₂ as final product. **1-b** retained in the solution.

Order of Reagents Addition Experiment

PhSiH₃ (0.1 M, 0.1 mmol), **1** (0.001 M, 0.001 mmol), and benzaldehyde (0.1 M, 0.1 mmol) were added in different orders in CD₂Cl₂ (0.8 ml) to examine the reactivity of active rhenium catalyst. Three order of reagent addition scenarios were conducted and reported as following scheme: (A←B)←C, indicating that B was added to a well-mixed solution (CD₂Cl₂ in this experiment) of A, after complete mixing, C was added to solution last.

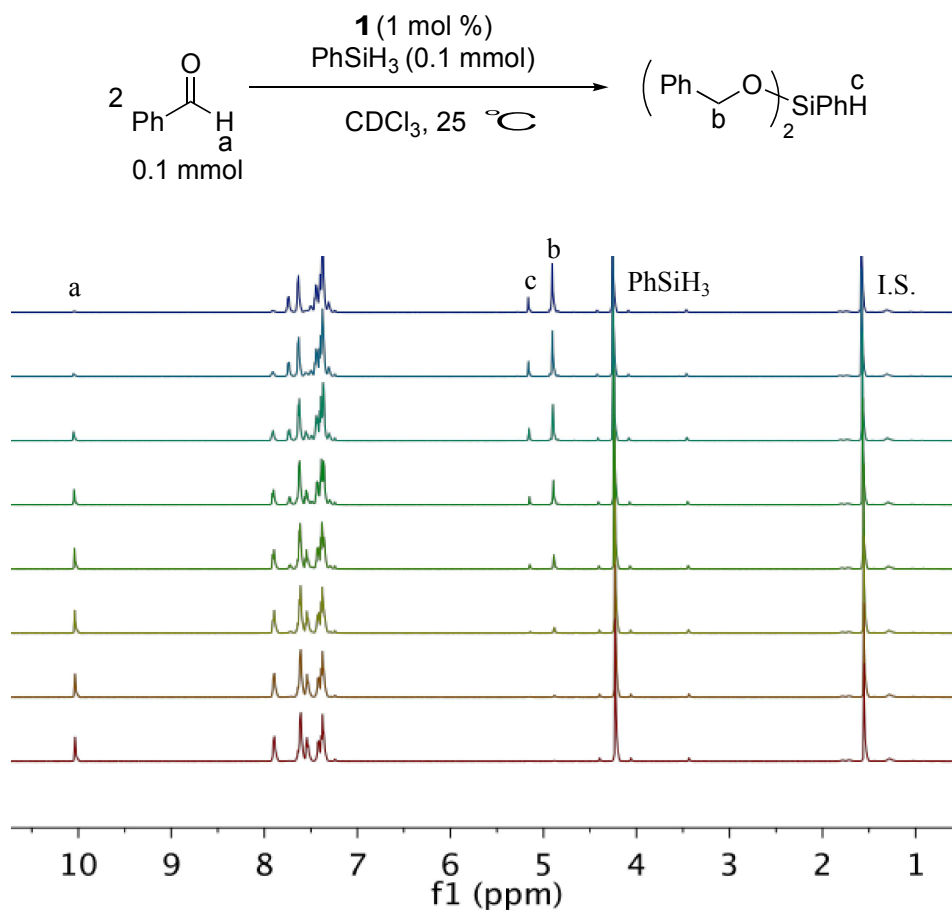
3. Results and Discussion

a. Kinetic Studies of Benzaldehyde Hydrosilylation

Determination of the Rate Law

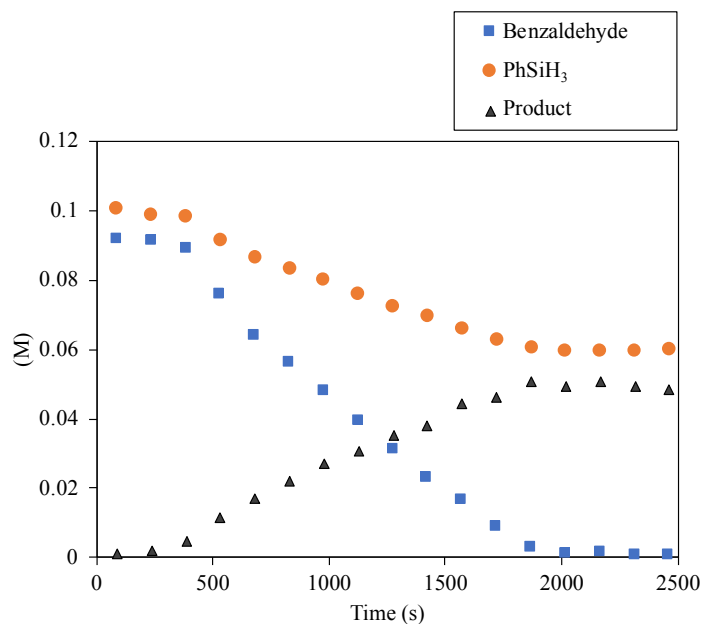
A series of NMR experiments were conducted for kinetic investigation. The ¹H spectra acquired every 5 minutes for **1** catalyzed benzaldehyde hydrosilylation is displayed in Figure 5.1. Aldehyde peak from benzaldehyde (labeled “a”), methylene (labeled “b”), Si–H (labeled “c”) from silylether product, and Si–H from PhSiH₃ were integrated and analyzed to follow the course of reaction.

Figure 5.1 ^1H NMR spectra acquired every 5 minutes for benzaldehyde hydrosilylation using PhSiH_3



Kinetic profile was extracted from NMR spectra. Consumption of benzaldehyde and PhSiH_3 with the formation of silylether product $(\text{PhCH}_2\text{O})_2\text{SiPhH}$ were plotted as a function of time (Figure 5.2). The reduction of benzaldehyde by PhSiH_3 was particularly efficient, achieving full conversion in 0.5 hour at room temperature with 1 mol % loading of catalyst **1**. When benzaldehyde was employed in hydrosilylation reaction, an induction period (~ 10 min) was clearly observed, indicating formation of active species. Monitoring the reaction by NMR reveals that hydrosilylation catalyzed by **1** only produce bis silyl ether product: one equivalent of product requires two equivalent of aldehydes under stoichiometric conditions.

Figure 5.2 Time profile of benzaldehyde hydrosilylation using PhSiH₃



The reaction was carried out with [Benzaldehyde] = 0.1 M, [PhSiH₃] = 0.1 M, and [cat] = 0.001 M in CDCl₃ at 25 °C .

Varying the concentration of all components, we determined rate law of the reaction. The catalyst concentration was first altered in the range of 0.5–3mM (0.5–3 mol %) while aldehyde and PhSiH₃ concentration was constant (0.1 M). The consumption of benzaldehyde was plotted as a function of time with different catalyst loading, and the initial rate was found to be irrelevant towards substrates concentration but first-order dependence on catalyst concentration (Figure 5.3 and 5.5). This is also consistent with linear decrease in benzaldehyde concentration shown in reaction time profile. Variation of PhSiH₃ concentration also displayed a linear dependence which attributes first order dependence (Figure 5.4 and 5.5). Since two equivalent of substrate produce one

equivalent of product under stoichiometric conditions, the initial rate of the reaction was half the rate of benzaldehyde consumption.

Figure 5.3 Left: Benzaldehyde consumption under varying catalytic conditions 0.5–3mM (0.5–3 mol %). Right: Dependence of initial rate on the concentration of catalyst.

Conditions: $[\text{PhSiH}_3] = 0.1 \text{ M}$, $[\text{Benzaldehyde}] = 0.1 \text{ M}$.

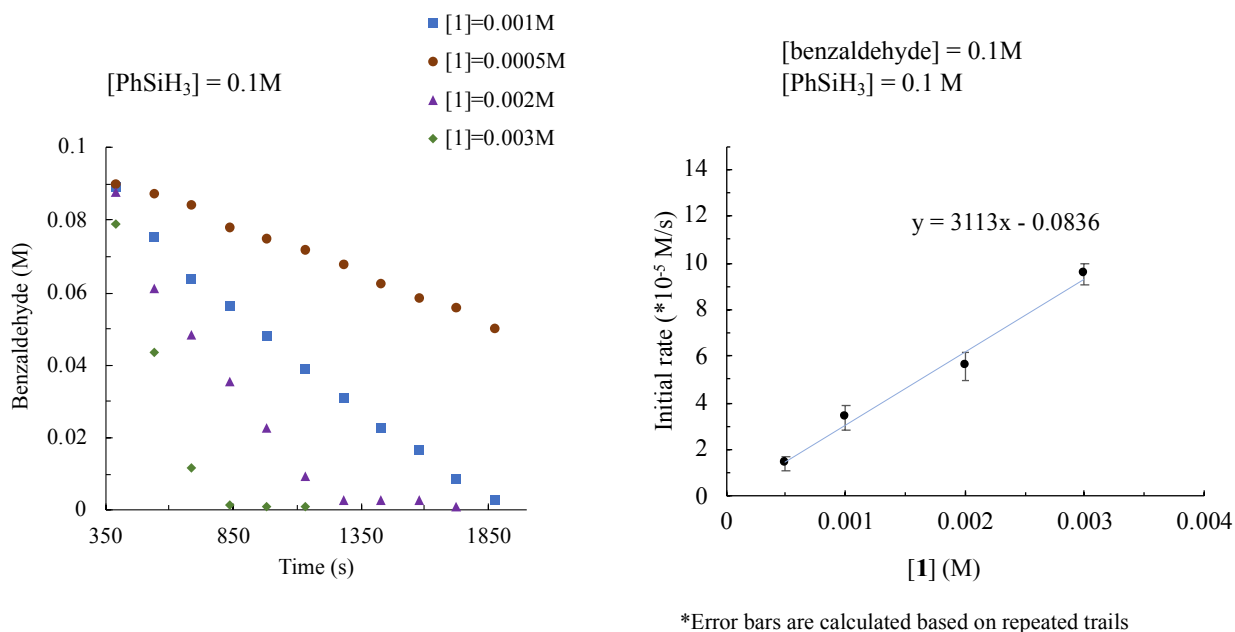


Figure 5.4 Left: Benzaldehyde consumption with varying PhSiH_3 concentration. Right: Dependence of initial rate on the concentration of PhSiH_3 . Conditions: $[\text{benzaldehyde}] = 0.1 \text{ M}$, $[\mathbf{1}] = 0.001 \text{ M}$.

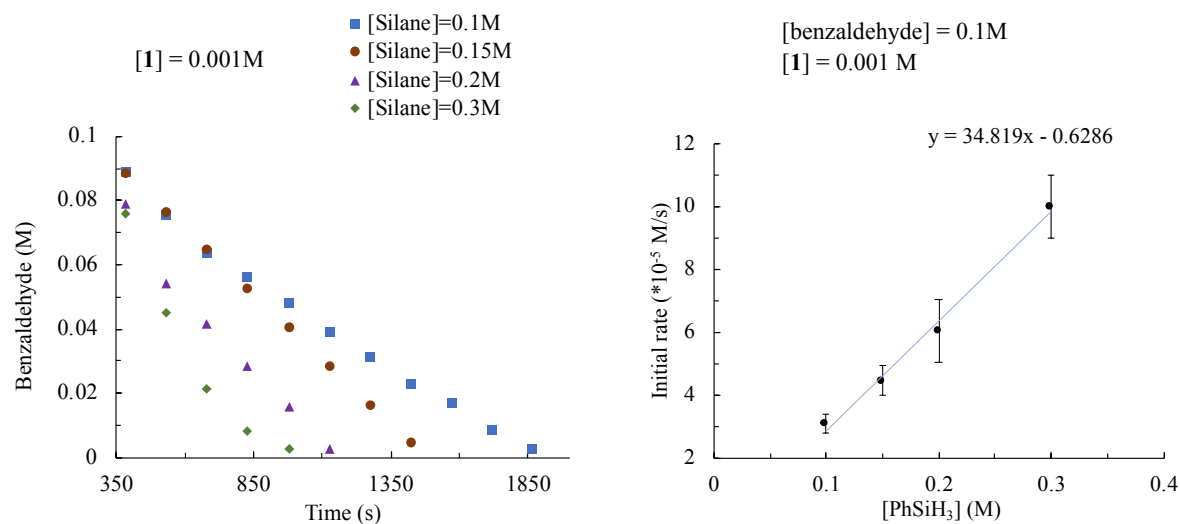
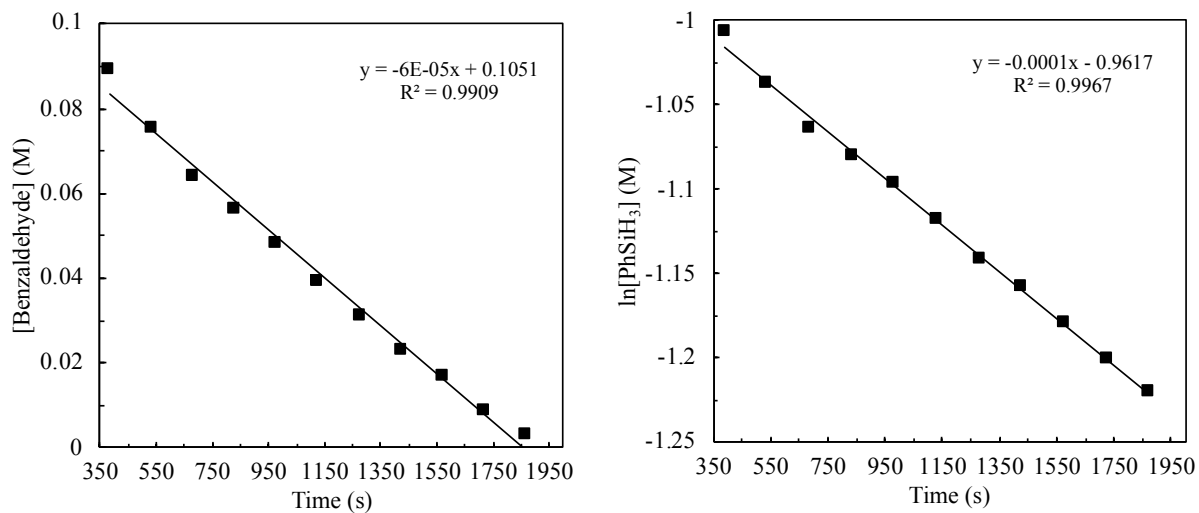


Figure 5.5 Left: Kinetic plot of [Benzaldehyde] vs time. Right: Kinetic plot of $\ln[\text{PhSiH}_3]$ vs time. [Benzaldehyde] = 0.1 M, [PhSiH₃] = 0.1 M, [cat] = 0.001 M in CDCl₃ at 25 °C.



From these kinetic experiments, the following rate law for **1** catalyzed hydrosilylation of aldehydes with PhSiH₃ is derived:

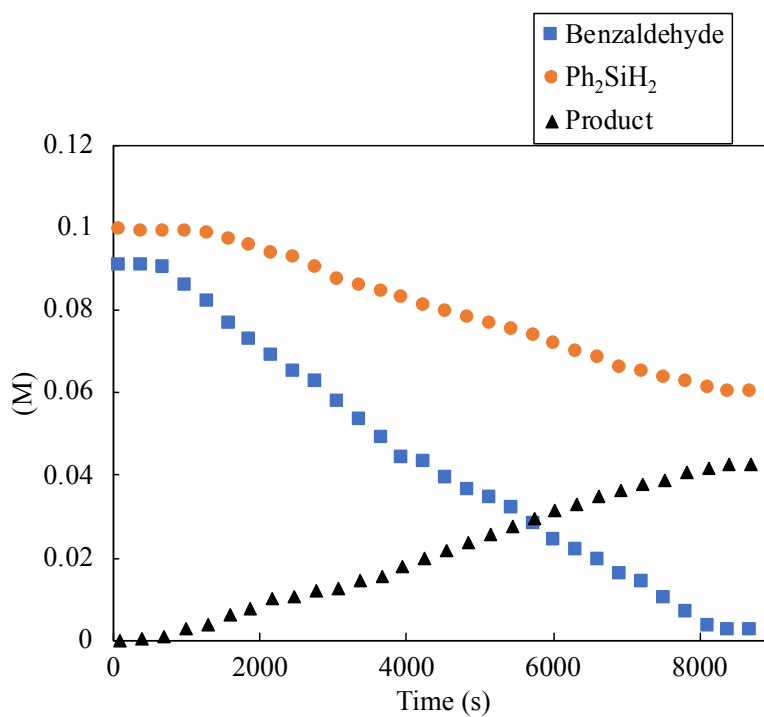
Equation 5.1

$$\frac{d[P]}{dt} = k(\text{PhSiH}_3) \cdot [\text{benzaldehyde}]^0 \cdot [1]^1 \cdot [\text{PhSiH}_3]^1$$

$$k(\text{PhSiH}_3) = (3.3 \pm 0.3) \times 10^{-1} \text{ M}^{-1}\text{S}^{-1}$$

The reaction of benzaldehyde and Ph_2SiH_2 catalyzed by **1** was also monitored by *in situ* NMR spectroscopy and the time profile was reported (Figure 5.6). In comparison to PhSiH_3 reduction, Ph_2SiH_2 was less efficient with an increasing reaction time to 2.5 hours for full conversion. An induction period of first 10 minutes was detected and may exist due to catalyst activation.

Figure 5.6 Time Profile of benzaldehyde hydrosilylation using Ph_2SiH_2



The reaction was carried out with $[\text{Benzaldehyde}] = 0.1 \text{ M}$, $[\text{Ph}_2\text{SiH}_2] = 0.1 \text{ M}$, and $[\text{cat}] = 0.001 \text{ M}$ in CDCl_3 at $25 \text{ }^\circ\text{C}$.

Further kinetic studies were carried out and the reaction exhibited first order on the concentration of catalyst and silane (Figure 5.7), and zero order on the substrate concentration (Figure 5.8).

Figure 5.7 Determining the rate law for reaction of benzaldehyde and Ph₂SiH₂ using **1** as catalyst.

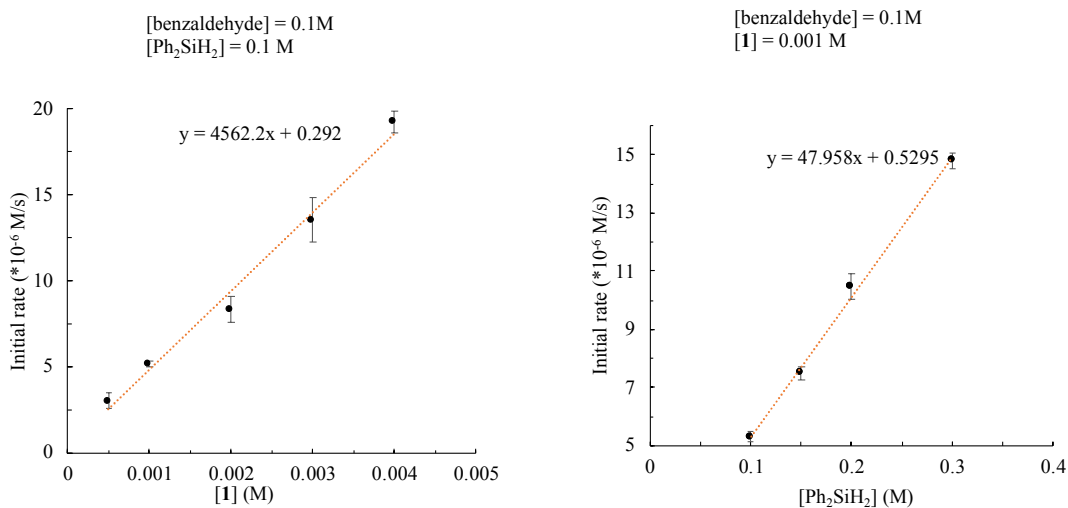
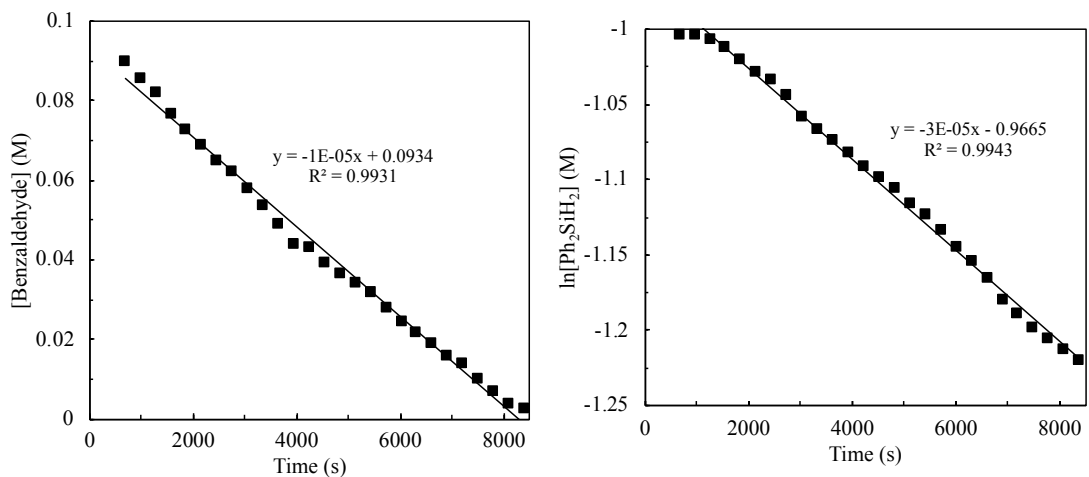


Figure 5.8 Kinetic plots of benzaldehyde hydrosilylation using Ph₂SiH₂



Left: Kinetic plot of [Benzaldehyde] vs time. Right: Kinetic plot of $\ln[\text{Ph}_2\text{SiH}_2]$ vs time. [Benzaldehyde] = 0.1 M, [Ph₂SiH₂] = 0.1 M, [cat] = 0.001 M in CDCl₃ at 25 °C.

This rate law with Ph₂SiH₂ is consistent with PhSiH₃ hydrosilylation reaction and is derived

$$\frac{d[P]}{dt} = k(\text{Ph}_2\text{SiH}_2) \cdot [\mathbf{1}] \cdot [\text{Ph}_2\text{SiH}_2]$$

$$k(\text{Ph}_2\text{SiH}_2) = (4.7 \pm 0.2) \times 10^{-2} \text{ M}^{-1}\text{S}^{-1}$$

b. Influence of the Order of Reagents Addition

Order of reagent addition experiments were conducted in CD_2Cl_2 to examine the reactivity of active rhenium catalyst. PhSiH_3 (0.1 M), **1** (0.001 M), and benzaldehyde (0.1 M) were added in different orders. Three order of reagent addition scenarios were examined, denoted according to the following scheme: $(\text{A} \leftarrow \text{B}) \leftarrow \text{C}$, indicating that B was added to a well-mixed solution (CD_2Cl_2 in this experiment) containing A, and after complete mixing, C was added to the solution. It is noteworthy that the reaction was crucial on order of addition.

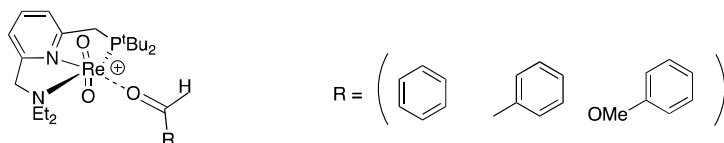
(1) $(\text{PhSiH}_3 \leftarrow \mathbf{1}) \leftarrow$ benzaldehyde: formation of rhenium hydride and active rhenium catalyst, which catalyzed hydrosilylation reaction. The reaction completed in 5 min.

(2) $(\text{PhSiH}_3 \leftarrow$ benzaldehyde) $\leftarrow \mathbf{1}$: no detectable conversion of benzaldehyde without catalyst. After introducing **1** into the solution rhenium hydride, active rhenium catalyst and possible rhenium-aldehyde adduct or Re (VI) complex formed through competition reaction of **1** between PhSiH_3 and benzaldehyde. Induction period was observed within first 10 minutes of the reaction which indicate formation of active catalyst. Full conversion of benzaldehyde was achieved in 30 minutes.

(3) $(\mathbf{1} \leftarrow$ benzaldehyde) $\leftarrow \text{PhSiH}_3$: **1** transformed into possible rhenium-aldehyde adduct (Figure 5.9) or Re (VI) complex and thus slow down catalysis. The coordination between **1** and benzaldehyde could lead the reactivity shut down because no vacant site on metal center is available for silane activation. Benzaldehyde behaves as Lewis base

which is a better nucleophile than silane. Rhenium hydride formed after introducing additional PhSiH_3 into the system. Unfortunately, the rhenium-aldehyde adduct was undetectable by ^1H NMR even under low temperature (-80°C). Attempts to obtain single crystals of adduct or Re(VI) complex were not successful, even with different aldehyde substrates.

Figure 5.9 Proposed Rhenium-Aldehyde Adduct

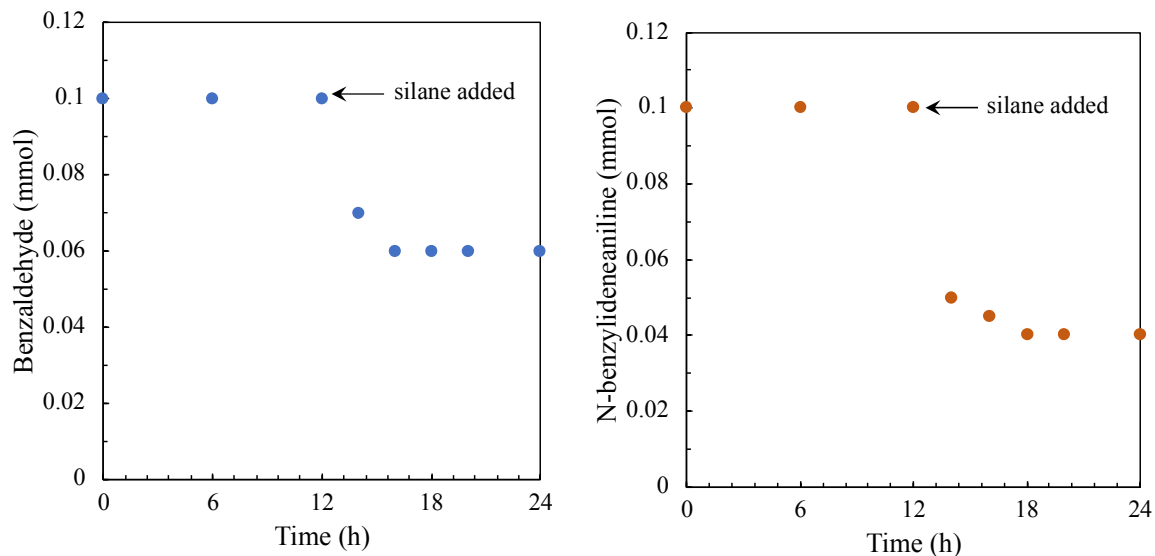


c. Mechanistic Insights into **1** Catalyzed Hydrosilylation

Stoichiometric Reaction between $(\text{PNN})\text{Re(H)(O)(OSiHPh}_2)$ and Benzaldehyde

At first, we speculated a mechanism proceeded through hydride mechanism and rhenium hydride was the active catalyst. Stoichiometric reactions between **1** and various organosilanes generate rhenium hydrides (**1-a**, **1-b**, **1-c**). However, insertion of benzaldehyde into six-coordinate rhenium hydrides was unsuccessful. No carbonyl insertion into Re-H bond was detected between rhenium hydride and benzaldehyde stoichiometrically. Rather, the depletion of benzaldehyde was observed immediately when additional equivalent of silane added into the system (Figure 5.10). This significant observation reveals that rhenium hydride is the resting state of catalyst, and the active catalyst was formed upon additional PhSiH_3 . This information again demonstrated the crucial role of excess silane in product formation step. Similar phenomenon was also detected in the reduction of imine.

Figure 5.10 NMR scale stoichiometric experiment between $(\text{PNN})\text{Re(H)(O)(OSiHPh}_2)$ and benzaldehyde



Left: Time profile of stoichiometric reaction of benzaldehyde (mmol) vs time (s).
 Right: Time profile of stoichiometric reaction of benzaldehyde (mmol) vs time (s). Reaction condition: benzaldehyde = 0.1 mmol, Ph_2SiH_2 = 0.1 mmol, cat = 0.001 mmol in CD_2Cl_2 at 25 °C.

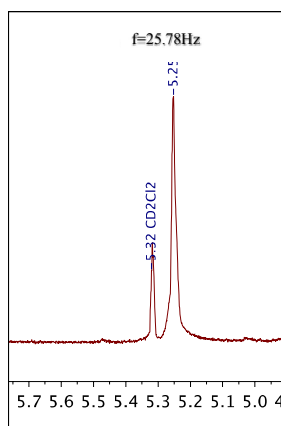
Stoichiometric Reaction between (PNN)ReO₂ and Benzaldehyde: Formation of Proposed Rhenium-Aldehyde Adduct

When a solution of **1** in CD_2Cl_2 mixed with benzaldehyde stoichiometrically at room temperature, ^{31}P NMR spectra exhibits appearance of free PNN ligand signal (δ 49 ppm, 10%) with complete disappearance of complex **1** (δ 53 ppm). ^1H NMR spectra also presents possibility for paramagnetic metal ion with a broadened signal. To probe the reactivity of the proposed rhenium-aldehyde adduct, we treated the existing mixture of **1** (1mM) and aldehyde (0.1M) with silane (0.1M), yet no reaction was observed. This result agrees with order of addition reaction (3).

Analysis of Proposed Rhenium-Aldehyde Adduct by Evans Method and Electron Paramagnetic Resonance (EPR)

Considering the amount of free PNN ligand has been detected spectroscopically as a result of decomposition products, a disproportionation of Re(V) complexes to Re (VI) is proceeding after benzaldehyde was introduced. Hence, we applied the NMR method, known as the Evan's method to the direct measurement of paramagnetic molar susceptibility (χ_M) and effective magnetic susceptibility(μ_{eff})¹⁶. From the measured χ_M value ($1.02 \times 10^{-3} \text{ cm}^3/\text{mol}$), the magnetic moment of new Re complex is $\mu_{\text{eff}} = 1.56$ (Figure 5.11). This value is within the range found for paramagnetic ($S = 1/2$) complexes, which agrees with oxidation state +6 rhenium complexes.

Figure 5.11 ¹H NMR of possible rhenium-aldehyde adduct using Evans method

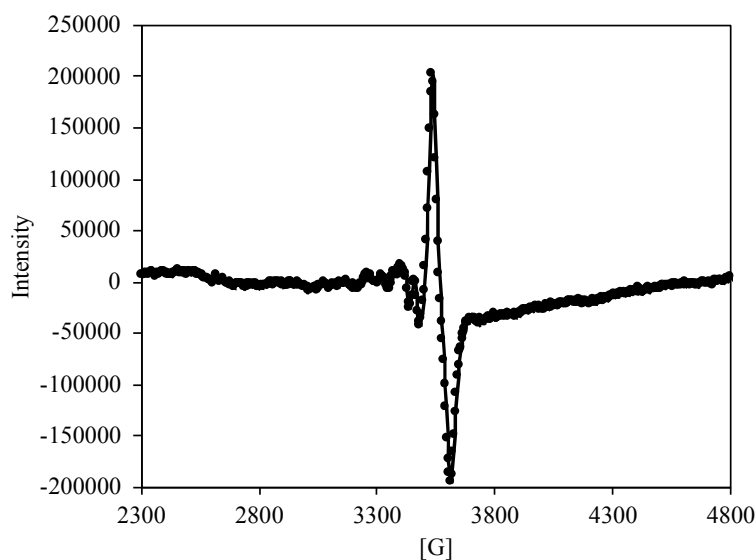


Electron paramagnetic resonance (EPR) spectroscopy allows one to obtain information on the electronic structure of paramagnetic systems¹⁷. The highest temperature for detecting Re (V) is 20 K and 4.2 K for Re (VI). It is known that only EPR of Re (VI) complex (the $5d^1$ configuration) is observed at liquid nitrogen temperature (77 K) and even at room temperature^{18,19}. EPR spectra we obtained for Re (VI) consists six broad lines of parallel orientation of the g-tensor (Figure 5.12) and is

analogous to spectra reported for oxidation state +6 rhenium²⁰. Taken together, both Evans method and EPR spectroscopy feature the presence of rhenium (VI) complexes. ¹⁹F NMR provides evidence that OTf anion (δ -78 ppm) was not coordinate to metal center after salt metathesis reaction with **1**, which leaves one vacant site on rhenium for catalysis. A control hydrosilylation experiment was conducted with (PNN)ReO₂I; no benzaldehyde conversion was detected.

Taken together, these observations demonstrate vacant site plays a significant role in promoting reactivity and it can be occupied by aldehyde coordination. Structure for this new rhenium-aldehyde adduct could not be fully identified.

Figure 5.12 EPR spectra of possible rhenium-aldehyde adduct



Reaction of **1** with Excess PhSiH₃ (20 eq)

Reaction of (PNN)ReO₂ cation (**1**) with excess PhSiH₃ (20 fold) in DCM resulted a maroon color mixture that is both air and moisture sensitive. A sharp color change from

orange (**1**) to purple (**1-a**) to maroon was noted. The solvent and excess PhSiH₃ was removed under vacuum and the maroon colored solid was further washed under pentane. It is noteworthy that this residue acted as an effective catalyst for the hydrosilylation of benzaldehyde with PhSiH₃ without exhibiting an induction period. The ³¹P NMR showed appearance of a new singlet at δ 80.2ppm (43%) along with the signal of **1-a** (δ 61.7ppm, 75%). The absence of an induction period indicated that this mixture contained the active catalyst. Similar results were obtained from hydrosilylation using trioxorhena(VII) carborane [Bu₄N][(η^1 -C₂B₉H₁₁)ReO₃] reported by our group.²¹ Attempts to crystallize active catalyst were unsuccessful. Another plausible interpretation of the induction period is the formation of heterogeneous Re metal (or nanoparticles) that is responsible for catalysis. A common test for heterogeneous catalyst activity is poisoning by metallic Hg²². Catalytic hydrosilylation of benzaldehyde with **1** was carried out in the presence of a 275-fold excess of Hg. The yields of silyl ether and catalyst activity were unaffected by the presence of Hg. This result rules out heterogeneous Re metal being the active catalyst. The exact identity of this species awaits for further elucidation.

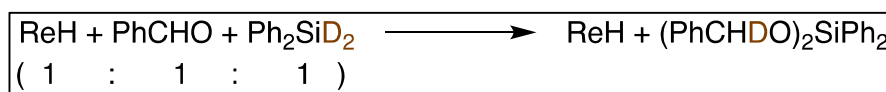
Stoichiometric Reaction of (PNN)Re(H)(O)(OSiHPh₂), Benzaldehyde and Ph₂SiD₂

Nikonov et al. established a stoichiometric (1:1:1) labeling experiment between metal hydride, benzaldehyde substrate and deuterium silane PhSiD₃ which ruled out hydride mechanism²³. They observed consistent results in both (Tp)(ArN=)Mo(H)(PMe₃) and (O=)(PhMe₂SiO)Re(PPh₃)₂(I)(H) catalyzed hydrosilylation, with exclusive formation of PhCHDOSiD₂Ph and metal hydride complex unchanged in the solution. This remarkable evidence supported that substrate insertion into metal hydride bond was not a

catalytical relevant event. Indeed, the catalysis proceeds through a nonhydride mechanism with heterolytic cleavage of silane. They mentioned nonhydride mechanism is not compatible with ketone affording poor reactivity; and this is an analogous result we observed in our substrate scope study (chapter 3).

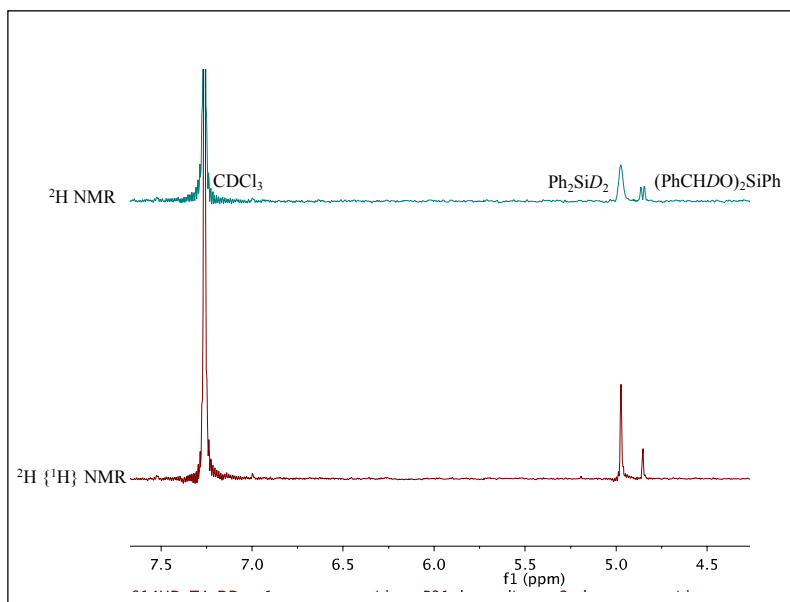
To shed light on mechanism of catalysis, stoichiometric (1:1:1) reaction between (PNN)Re(H)(O)(OSiHPh₂) (**1-b**), benzaldehyde and silane Ph₂SiD₂ was conducted (Scheme 5.2).

Scheme 5.2 Stoichiometric H/D labeling experiment



The formation of (PhCHDO)₂SiPh reflects presumably ReH (**1-b**) and Ph₂SiD₂ generates active catalyst, meanwhile it was confirmed that ReH (**1-b**) does not reduce benzaldehyde. This deuterium labeled silylether (PhCHDO)₂SiPh features a doublet at 4.89 ppm (CDCl₃). In order to confirm the formation of this product, proton-decoupled deuterium NMR (²H {¹H}) was performed and a singlet was detected at 4.89 ppm (Figure 5.13). The presence of **1-b** was also revealed by ¹H (with the retention of Re–H bond) and ³¹P NMR at the end of deuterium labeling experiment.

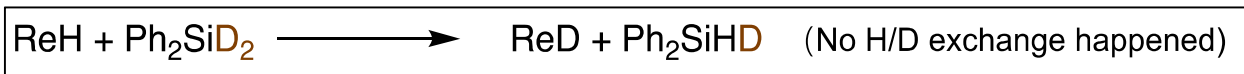
Figure 5.13 ^2H NMR spectrum (CDCl_3) for Stoichiometric H/D labeling experiment



Stoichiometric Reaction between $(\text{PNN})\text{Re}(\text{H})(\text{O})(\text{OSiHPh}_2)$ with Ph_2SiD_2

One limitation for this deuterium scrambling experiment is that rate for H/D exchange on metal hydride equates the rate of substrate addition (Scheme 5.3)²⁴. Then the mechanism would still proceed through hydride pathway. In order to determine whether H/D scrambling product $(\text{PhCHDO})_2\text{SiPh}_2$ could result from ReH/SiD exchange, complex **1-b** (Re–H: 8.27 ppm) was reacted with Ph_2SiD_2 stoichiometrically. No exchange was observed at room temperature even after 24 hours.

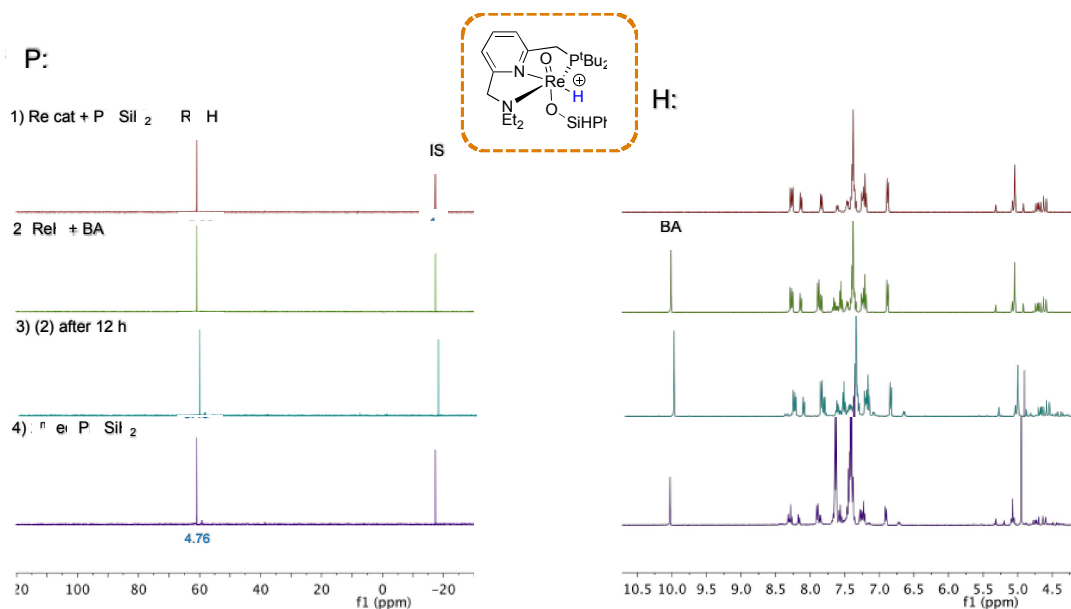
Scheme 5.3 Limitation of H/D scrambling experiment



Stoichiometric Reaction of (PNN)Re(H)(O)(OSiHPh₂) (**1-b**) and Benzaldehyde:

Stoichiometric reaction of **1-b** and benzaldehyde was performed, and no substrate insertion was detected by ¹H NMR as **1-b** remains unchanged throughout the reaction (Figure 5.14, reaction (2) and (3)). Importantly, the depletion of benzaldehyde happened immediately when introducing additional equivalent of silane. In consistent with D-labeling experiment, hydride transfer is driven by excess silane not from rhenium hydride.

Figure 5.14 Stoichiometric reaction of rhenium hydride **1-b** and benzaldehyde. (1) Stoichiometric reaction between **1** and Ph₂SiH₂ generates **1-b**. (2) Benzaldehyde was added to the system stoichiometrically, no carbonyl insertion is observed, benzaldehyde remains unreacted. (3) Reaction (2) after 12 h. (4) 1 more equivalent of silane was added to the system, consumption of benzaldehyde was detected rapidly.



d. Proposed Catalytic Cycle

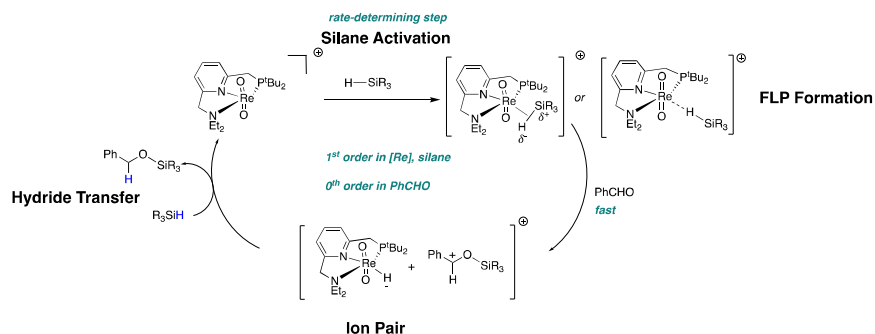
A proposed catalytic cycle based on these arguments is outlined in Figure 5.15. First step is the activation of silane with the formation of frustrated Lewis pair intermediate. In this case, silane acts as a weak Lewis base and is a poor electron donor to metal center; silane lies in the same plane with rhenium d_{xy} orbital to maximize π -backbond donation from d_{xy} to silane Si–H antibonding σ^* orbital. However, this presumed silane rhenium FLP adduct is not detected by ^1H NMR even at low temperature (-80°C). Based on kinetic data, silane activation step is the rate limiting step as a first order dependence on [silane] and [1] was observed and no dependence on [benzaldehyde]. Without further computational study, activation of the silane could occur via η^1 or η^2 coordination.

Next, carbonyl substrate nucleophilic attacks electrophilic silicon center, instead of coordination to metal center, leading to the cleavage of the Si–H bond and the formation of an ion pair analogous to the Piers mechanism. As suggested by kinetic studies rate of reaction is zero-order with respect to aldehyde concentration; aldehyde attacking is a fast step.

Finally, product formation results from hydride transfer from excess silane in the catalytic system, and this is consistent with deuterium labeling experiment of rhenium hydride, D-silane and benzaldehyde (scheme 5.2). Additional silane is the driving force for hydride transfer process. Rhenium hydride complex formed through heterolytic cleavage of silane and is inactive towards catalysis without additional silane. Both stoichiometric experiment between rhenium hydride and benzaldehyde, and

stoichiometric D-labeling experiment support that hydride transfer step is promoted by excess silane, the hydrosilylation proceeds via a nonhydride mechanism.

Figure 5.15 Proposed catalytic cycle



e. Comparison and Discussion of the Rate Constant

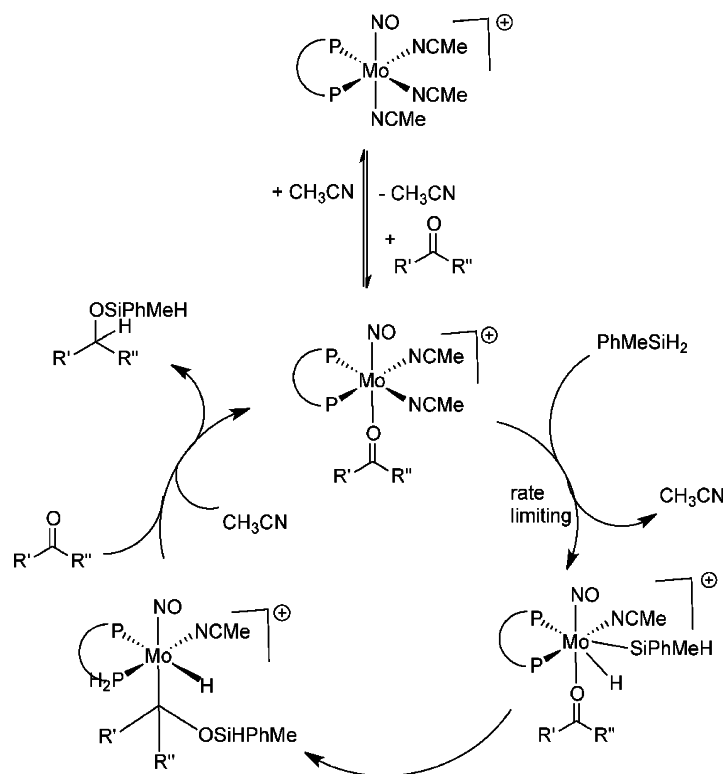
Berke et al. published rate law and rate constant for benzaldehyde hydrosilylation catalyzed by diphosphine molybdenum complex⁴. The kinetic data reveals the reaction rate to be zero order with respect to the substrate concentration and first order with respect to catalyst and PhMeSiH_2 concentration. The initial rate equation was established as

Initial Rate = $1.131 \text{ (M}^{-1}\text{min}^{-1}) [\text{catalyst}] [\text{silane}]$. After converting the unit, rate constant $k_{(\text{Berke})} = 1.9 \times 10^{-2} \text{ M}^{-1}\text{s}^{-1}$. Catalyst **1** is more efficient in hydrosilylation of benzaldehyde with $k(\text{PhSiH}_3) = (3.3 \pm 0.3) \times 10^{-1} \text{ M}^{-1}\text{s}^{-1}$ and $k(\text{Ph}_2\text{SiH}_2) = (4.7 \pm 0.2) \times 10^{-2} \text{ M}^{-1}\text{s}^{-1}$.

However, we cannot exclude the influence of organosilanes since $k_{(\text{Berke})}$ is established by using MePhSiH_2 as reductant. The mechanism was proposed via a hydride pathway (Figure 5.16) (Ojima type mechanism²⁵). They proposed that rate limiting step is the addition of silane to six-coordinate Mo-aldehyde complex, with the formation of a seven-

coordinated MoH-aldehyde complex. This phenomenon is quite unusual in Mo-catalyzed hydrosilylation.

Figure 5.16 Proposed Ojima type mechanism for the hydrosilylation catalyzed by molybdenum complex

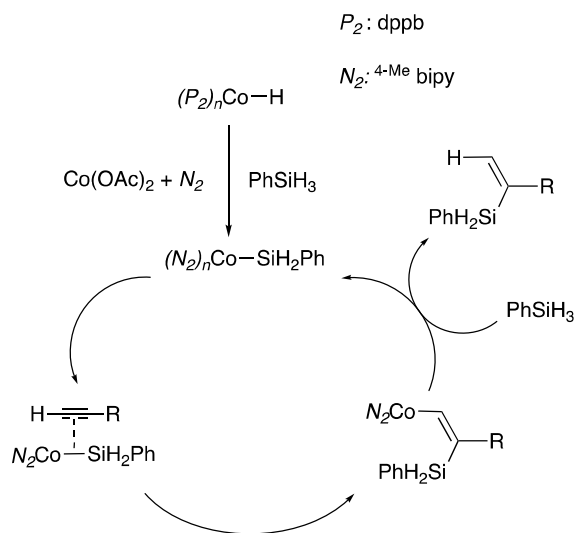


Imido/hydride molybdenum (IV) catalyzed hydrosilylation of unsaturated compounds was reported by Nikonov et al.²⁶ D-labeling experiment of $[Mo]$ with substrate and $PhSiD_3$ in 1:1:1 ratio suggests nonhydride Lewis acid catalysis mechanism. The reaction obeys first order in silane and Mo catalyst concentration and zero order in substrate concentration. Substrate addition is a fast step with the formation of η^2 Mo-aldehyde complex while ligand dissociation is the rate limiting step. Rate constant was derived from supporting information for $PhSiH_3$: $k_{Nikonov} = 1.9 \times 10^{-2} M^{-1}s^{-1}$. By

comparison our catalyst is more reactive with a rate constant $k(\text{PhSiH}_3) = (3.3 \pm 0.3) \times 10^{-1} \text{ M}^{-1}\text{S}^{-1}$.

Cobalt-catalyzed hydrosilylation of alkyne was studied and nonhydride Lewis acid mechanism was established by Wu and coworkers.²⁷ Frustrated Lewis pair between cobalt complex and silane was proposed upon silane activation (Figure 5.17). Kinetic study reveals hydrosilylation is first order in [Co] and [silane] and zero order in [phenylacetylene]. This rate law indicates rate limiting step is the releasing of alkenylsilane product. Rate constant was derived from initial rate values provided in supporting information: $k_{Wu} = 7 \times 10^{-1} \text{ M}^{-1}\text{s}^{-1}$. By comparison with $k(\text{PhSiH}_3) = (3.3 \pm 0.3) \times 10^{-1} \text{ M}^{-1}\text{S}^{-1}$, this (bipy) cobalt complex exhibits superior activity over alkynes hydrosilylation with the formation of alkenylsilanes. Considering the fact this methodology is based on inexpensive and environmentally benign 3d base Co complex.

Figure 5.17 Proposed mechanism of hydrosilylation catalyzed by (bipy)cobalt complex

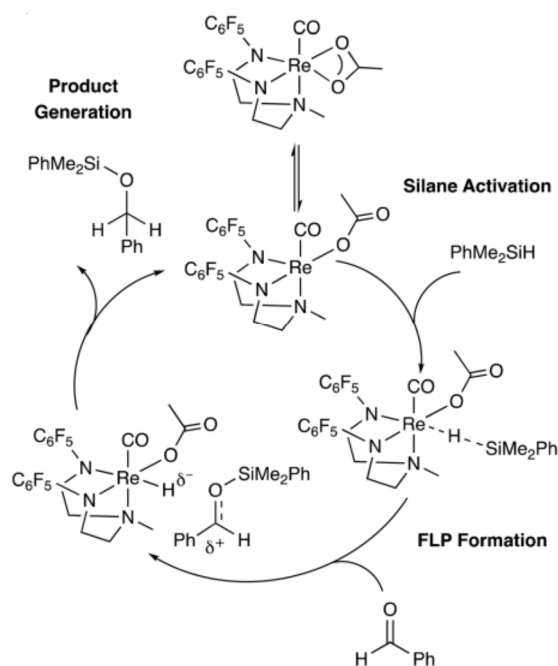


Ison and coworkers determined hydrosilylation of benzaldehyde catalyzed by cationic rhenium (III) complex proceeds via a nonhydride ionic hydrosilylation pathway.

²⁸ The kinetic data suggest hydrosilylation to be zeroth order dependence on

[benzaldehyde], first order dependence on [catalyst] and [PhMe₂SiH] with $k_{\text{Isom}_1} = 3.8 \times 10^{-2} \text{ (M}^{-1}\text{S}^{-1}\text{)}$. Recently in 2020, the same group reported the discover of Re–Silane complex as frustrated Lewis pair for catalytic hydrosilylation ²⁹(Figure 5.18). Both experimental and computational study reveal Lewis acid catalysis. The reaction rate was found to be first order with respect to substrate, catalyst and PhMe₂SiH concentrations: $k_{\text{Isom}_2} = 2.4 \times 10^{-2} \text{ (M}^{-1}\text{S}^{-1}\text{)}$. KIE of 1.4 was reported for catalytic reactions employing PhMe₂SiH and PhMe₂SiD. This KIE is consistent with the activation of silane happens prior to rate limiting step: nucleophilic attack by carbonyl substrate at silicon atom (FLP formation). The energy decomposition analysis study suggest FLP reactivity between metal complex and silane arises from the change in ratio electronic and steric energy between Lewis acid and base. The Lewis acidity of the metal complex is critical for catalytic reactivity. And this strategy allows for future catalyst design.

Figure 5.18 Mechanism for catalytic hydrosilylation reaction with Re(III) complex



4. Conclusion

Possible catalytic cycle for carbonyl compounds hydrosilylation was proposed on the basis of studying conceivable stoichiometric reactions, deuterium labeling experiments, and kinetic measurements. With these evidence in hand, we elucidated a nonhydride Lewis acid mechanism for **1** catalyzed hydrosilylation system and proved rhenium hydride is inactive towards catalysis which is in contrast to general hydride mechanism in dioxorhenium (V) system ³⁰.

Kinetic study reveals the rate of reaction show a first order dependence on the concentration of the catalyst and the silane and is independent of the substrate concentration, which is in agreement mechanistic proposal that activation of silane is the rate determining step, aldehyde attacking is a fast step and excess silane is essential for catalyst activation. The lack of reactivity on stoichiometric reaction between benzaldehyde and rhenium hydride reveals excess silane is essential for generating the active catalyst, rhenium hydride is the resting state of the catalyst. A 1:1:1 deuterium labeling experiment between ReH, benzaldehyde and deuterium silane further supported the proposal that active catalyst was generated by additional silane, intuitively between rhenium hydride and silane. Further computational study is needed for understanding coordination of silane and rhenium complex.

5. References

- (1) Hegedus, L. S. *Transition Metals in the Synthesis of Complex Organic Molecules*; 1999; pp 39–53.
- (2) Bochmann, M.; Das, S.; Junge, K.; Beller, M. *Angew. Chem. Int. Ed.* **2011**, *50* (27), 6004–6011.
- (3) Kolb, I.; Hetflejs, J. *Collect. Czech. Chem. Commun.* **1980**, *45*, 2808.
- (4) Chakraborty, S.; Blacque, O.; Fox, T.; Berke, H. *ACS Catal.* **2013**, *3* (10), 2208–2217.
- (5) Rendler, S.; Oestreich, M. *Modern Reduction Methods*; WILEY-VCH Verlag GmbH & Co. KGaA, Weinheim, 2008; pp 183–207.
- (6) Wang, J.; Wang, W.; Huang, L.; Yang, X.; Wei, H. *ChemPhysChem.* **2015**, *16* (5), 1052–1060.
- (7) Wang, J.; Huang, L.; Yang, X.; Wei, H. *Organometallics.* **2014**, *34* (1), 212–220.
- (8) Du, G.; Fanwick, P. E.; Abu-Omar, M. M. *J. Am. Chem. Soc.* **2007**, *129* (16), 5180–5187.
- (9) Du, G.; Abu-Omar, M. M. *Organometallics.* **2006**, *25* (20), 4920–4923.
- (10) Gu, P.; Wang, W.; Wang, Y.; Wei, H. *Organometallics.* **2012**, *32* (1), 47–51.

- (11) Park, S.; Brookhart, M. *Organometallics*. **2010**, *29* (22), 6057–6064.
- (12) Metsänen, T. T.; Hrobárik, P.; Klare, H. F.; Kaupp, M.; Oestreich, M. *J. Am. Chem. Soc.* **2014**, *136* (19), 6912–6915.
- (13) Robert, T.; Oestreich, M. *Angew. Chem. Int. Ed.* **2013**, *52* (20), 5216–5218.
- (14) Luo, X. L.; Crabtree, R. H. *J. Am. Chem. Soc.* **1989**, *111* (7), 2527–2535.
- (15) Cotton, F. A.; Wilkinson, G.; Murillo, C. A.; Bochmann, M. *Advanced Inorganic Chemistry*; Wiley Interscience: New York, 1999; Vol. 6.
- (16) Piguet, C. *J. Chem. Educ.* **1997**, *74* (7), 815.
- (17) Roessler, M. M.; Salvadori, E. *Chem. Soc. Rev.* **2018**, *47* (8), 2534–2553.
- (18) Rahn, R. O.; Dorain, P. B. *The Journal of Chemical Physics* **1964**, *41* (10), 3249–3254.
- (19) Borisova, L. V.; Borodkov, A. S.; Grechnikov, A. A.; Ugolkova, E. A.; Minin, V. V. *Russ. J. Inorg. Chem.* **2013**, *58* (8), 940–944.
- (20) Lancaster, K. M.; Hu, Y.; Bergmann, U.; Ribbe, M. W.; DeBeer, S. *J. Am. Chem. Soc.* **2012**, *135* (2), 610–612.
- (21) Pichaandi, K. R.; Fanwick, P. E.; Abu-Omar, M. M. *Organometallics*. **2012**, *31* (5), 1888–1896.
- (22) Widegren, J. A.; Finke, R. G. *J. Mol. Catal. A: Chem.* **2003**, *198* (1-2), 317–341.
- (23) Shirobokov, O. G.; Kuzmina, L. G.; Nikonov, G. I. *J. Am. Chem. Soc.* **2011**, *133* (17), 6487–6489.
- (24) Issenhuth, J. T.; Notter, F. P.; Dagorne, S.; Dedieu, A.; Bellemin-Laponnaz, S. *Eur J Inorg Chem* **2010**, *2010* (4), 529–541.

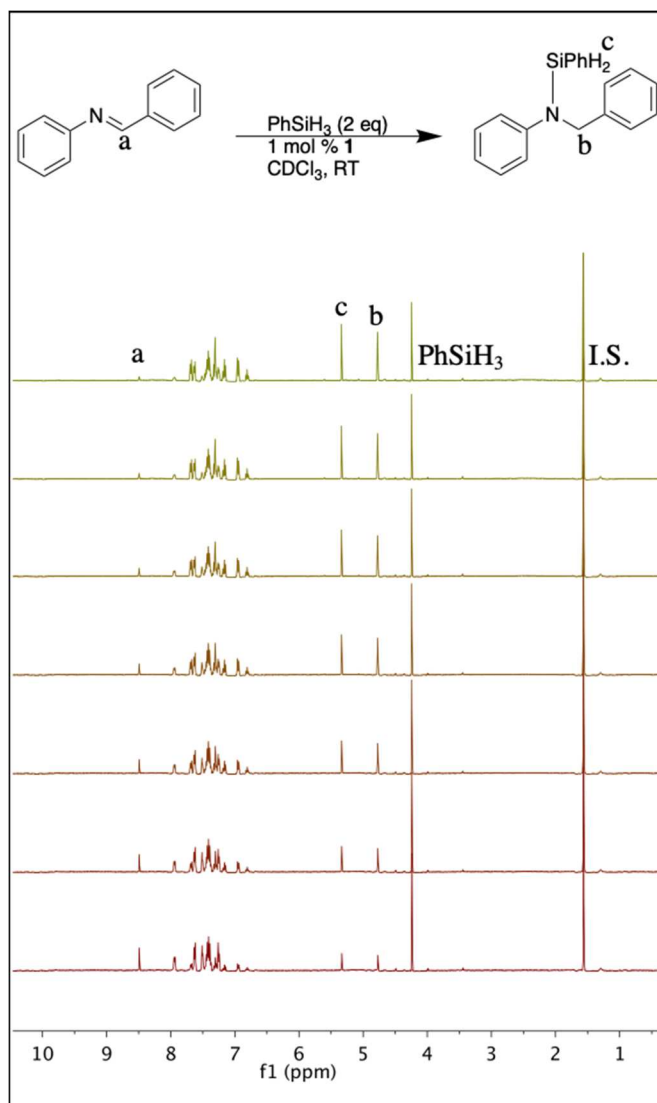
- (25) Ojima, I.; Kogure, T.; Kumagai, M.; Horiuchi, S.; Sato, T. *J. Organomet. Chem.* **1976**, *122* (1), 83–97.
- (26) Khalimon, A. Y.; Shirobokov, O. G.; Peterson, E.; Simionescu, R.; Kuzmina, L. G.; Howard, J. A. K.; Nikonov, G. I. *Inorg. Chem.* **2012**, *51* (7), 4300–4313.
- (27) Wu, G.; Chakraborty, U.; Jacobi von Wangelin, A. *Chem. Commun.* **2018**, *54* (87), 12322–12325.
- (28) Pérez, D. E.; Smeltz, J. L.; Sommer, R. D.; Boyle, P. D.; Ison, E. A. *Dalton Trans.* **2017**, *46* (14), 4609–4616.
- (29) Ison, E. A.; Brown, C. A.; Abrahamse, M. *Dalton Trans.* **2020**, *49*, 11403–11411.
- (30) Kennedy-Smith, J. J.; Nolin, K. A.; Gunterman, H. P.; Toste, D. *J. Am. Chem. Soc.* **2003**, *125* (14), 4056–4057.

Chapter VI. Additional Reactions and Studies of Rhenium Pincer Complexes

1. Kinetic Studies of Imine Hydrosilylation Catalyzed by **1**

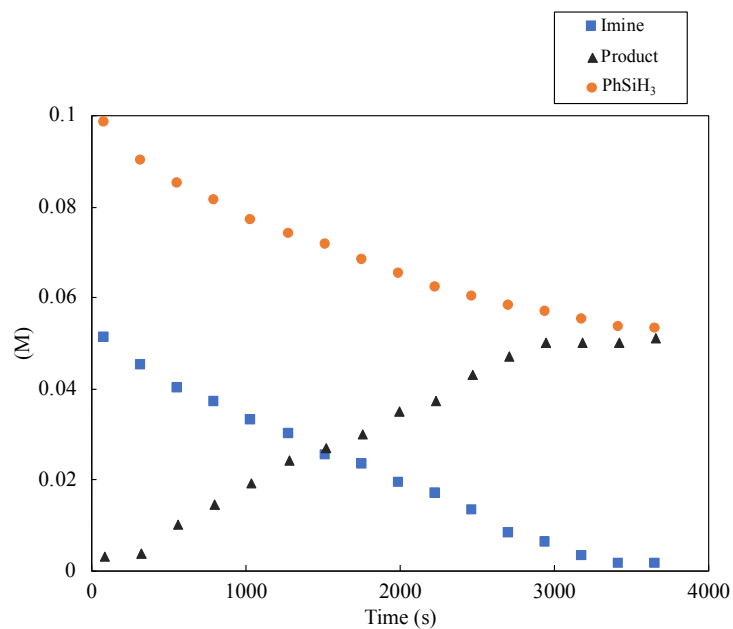
To further expand kinetic studies on different substrates, imine hydrosilylation was investigated at catalyst loading 1 mol % using NMR spectroscopy. The selected ^1H spectra during the course of reaction represents consumption of N-benzylideneaniline and PhSiH_3 , while formation of product (Figure 6.1). The methine peak from N-benzylideneaniline (labeled “a”), methylene (labeled “b”) and Si–H peak (labeled “c”) from silyl product, and Si–H peak from PhSiH_3 were integrated and analyzed. The reaction stoichiometry is 1:1 in imine hydrosilylation.

Figure 6.1 ^1H NMR spectra acquired every 10 minutes for imine hydrosilylation using PhSiH_3



Time profile for N-benzylideneaniline hydrosilylation was extracted from NMR spectra and plotted as a function of time (Figure 6.2). No apparent induction period was observed during the course of imine hydrosilylation compare to benzaldehyde reaction. Further mechanistic investigations are necessary to shed light on imine hydrosilylation.

Figure 6.2 Time profile of imine hydrosilylation using PhSiH₃

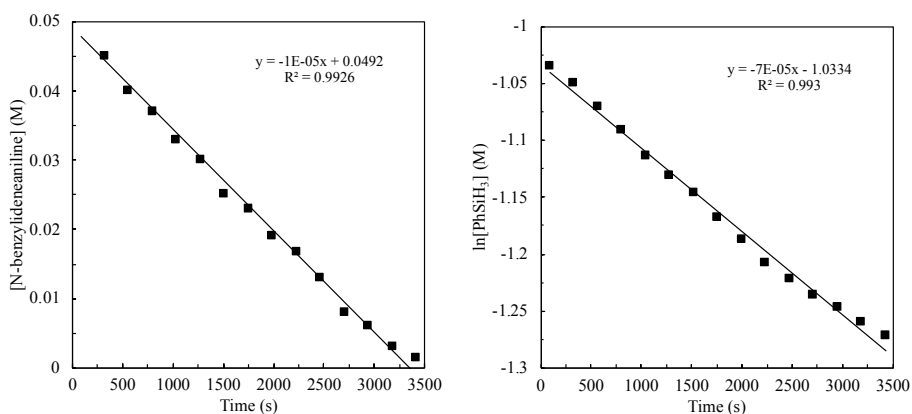


The reaction was carried out with [N-benzylideneaniline] = 0.05 M, [PhSiH₃] = 0.1 M, and [cat] = 0.0005 M in CDCl₃ at 25 °C .

Kinetic study on imine hydrosilylation reveals first order on concentration of catalyst and silane, zero order on concentration of imine (Figure 6.3). This rate law is consistent with benzaldehyde hydrosilylation. The initial rate equation was derived as

$$\text{rate} = 0.34 \text{ (M}^{-1} \text{ s}^{-1}\text{) [catalyst][silane]}$$

Figure 6.3 Kinetic plots of imine hydrosilylation using PhSiH₃



Left: Kinetic plot of [N-benzylideneaniline] vs time. Right: Kinetic plot of $\ln[\text{PhSiH}_3]$ vs time.
 [N-benzylideneaniline] = 0.05 M, [PhSiH₃] = 0.1 M, [cat] = 0.0005 M in CDCl₃ at 25 °C.

In order to derive the complete rate law, more kinetic experiments with various concentration of catalyst, imine and silane need to be performed. This imine hydrosilylation rate law was determined from [substrate] = 0.05 M, [PhSiH₃] = 0.1 M and [1] = 0.0005 M.

General procedure for the N-benzylideneaniline hydrosilylation:

In a nitrogen filled glove box, a stock solution of **1** in CD₂Cl₂ (0.001 M) was prepared. 5 μL of the stock solution of **1** in CD₂Cl₂ (5×10^{-6} mmol, 1 mol %) was added to a J-Young NMR tube equipped with N-benzylideneaniline (0.05 M, 0.05 mmol), PhSiH₃ (0.1 M, 0.1 mmol) and internal standard C₈H₁₆ (3.7×10^{-5} mol) in CDCl₃ (0.8 ml) at 25°C. The progress of the reaction was monitored by integrating proton of PhN=CHPh, PhSiH₃ and Ph(H₂PhSi)NCH₂Ph relative to C₈H₁₆ respect to time.

2. Hammett Correlation Study

To understand the influence of various para-substituted benzaldehyde derivatives, Hammett correlations¹ were established applying catalyst **1** in hydrosilylation of para-methoxy, -methyl, -H, -chloro, and -trifluoromethyl substituted benzaldehyde at room temperature. There is no correlation of $\ln(\text{rate})$ vs substituent constant (σ) (Figure 6.4). Electron-withdrawing/donating groups on substrate did not alter the reaction rate. Investigation on Hammett correlation supports proposed Lewis acid catalysis mechanism, in which aldehyde addition is the fast step and aldehyde is not part of the active complex in the transition state of the rate-determining step.

General procedure for the Hammett studies:

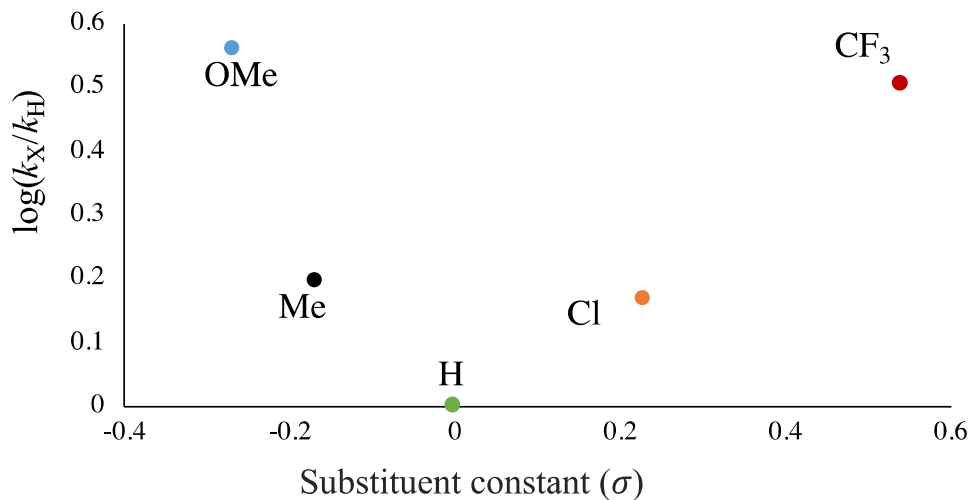
In a nitrogen filled glove box, a stock solution of **1** in CD_2Cl_2 (0.001 M) was prepared. 10 μL of the stock solution of **1** in CD_2Cl_2 (1×10^{-5} mmol, 1 mol %) was added to a J-Young NMR tube equipped with PhSiH_3 (0.1 M, 0.1 mmol) and

internal standard C_8H_{16} (3.7×10^{-5} mmol) in $CDCl_3$ (0.8 ml) at $25^\circ C$. Benzaldehyde (0.1 M, 0.1 mmol) and indicated para-substituted benzaldehyde (0.1 M, 0.1 mmol) were added to the J-Young NMR tube. 1H NMR was taken after 15 min of reaction. The NMR integration of PhCHO and aldehyde proton of para-substituted benzaldehyde derivatives were used to determine k_X/k_H value (Table 6.1).² Overlapping signals from silyl ether products were hard to integrate.

Table 6.1 Calculation for Hammett correlation

	σ	k_X/k_H	$\log(k_X/k_H)$
OMe	-	2.43	0.385
	0.268		
Me	-0.17	0.982	-0.00765
Cl	0.227	1.46	0.166
CF ₃	0.54	3.19	0.504
H	0	1	0

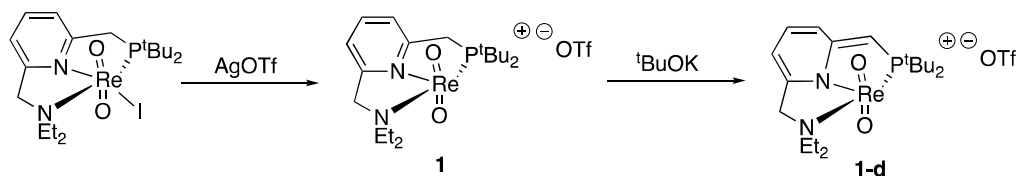
Figure 6.4 Hammett correlation for **1** catalyzed hydrosilylation of various para substituted benzaldehyde derivatives.



3. Dearomatized rhenium complexes catalyzed hydrosilylation

The concept of aromaticity in pincer ligand design was discussed in detail in chapter 2. Dearomatized rhenium complexes were synthesized in order to provide insights into their metal-ligand cooperative activities. Dearomatized cationic rhenium complex $[(\text{PNN}^*)\text{Re}(\text{O})_2(\text{ACN})][\text{OTf}]$ (**1-d**) was generated according to our previous work (scheme 6.1)³ or through salt metathesis with $\text{Re}(\text{O})_2(\text{PNN}^*)\text{I}$ (**2**).

Scheme 6.1

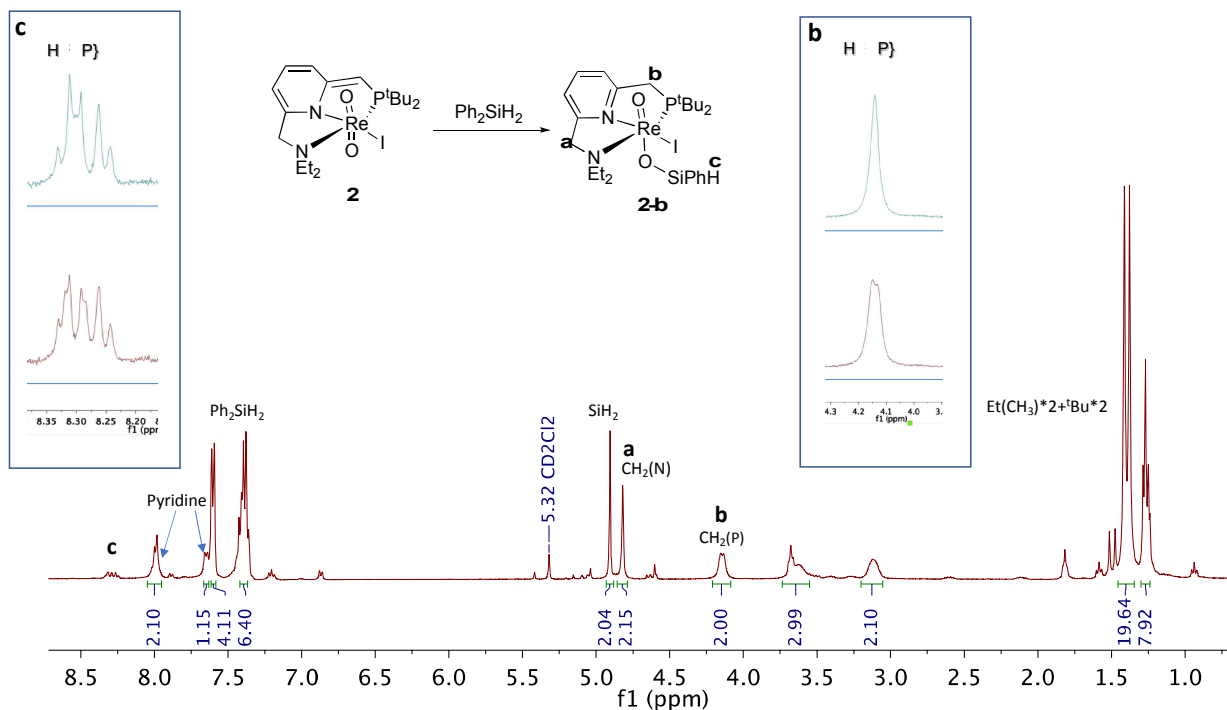


Activation of Si–H bond by dearomatized six-coordinate rhenium complex **2**

We started our investigation on simple Si–H bond activation on $\text{Re}(\text{O})_2(\text{PNN}^*)\text{I}$ (**2**). The stoichiometric reaction of Ph_2SiH_2 results in the formation of **2-b** which was clearly detected by ^1H and ^{31}P NMR. The ^{31}P NMR spectrum of **2-b** has a singlet centered at 61 ppm, with a shift of 10 ppm downfield comparing to **2**. The ^1H NMR spectrum has a characteristic doublet methylene CH_2 peak b, integrating to two protons, as a result of aromatized pincer complex **2-b**. $^{31}\text{P}\{^1\text{H}\}$ NMR was presented to confirm the CH_2 attached to di-*tert*-butylphosphine ligand.

The activation of Si–H bond triggered by six-coordinate dearomatized rhenium complex **2-b** was successful comparing to six-coordinate aromatized rhenium complex $\text{Re}(\text{O})_2(\text{PNN})\text{I}$. This evidence suggests that dearomatized rhenium pincer complex **2-b** is capable of bond activation through metal ligand corporation without the assist of metal center. Stoichiometric reaction between organosilane and **1-d** is under investigation.

Figure 6.5 ^1H NMR spectrum of **2-b**.



General procedure for synthesis **2-b**

To a solution of **2** (21 mg, 0.03 mmol) in CD_2Cl_2 (1.0 mL), Ph_2SiH_2 (4 μL , 0.03 mmol) was added at ambient conditions.

Hydrosilylation reaction catalyzed by cationic dearomatized rhenium pincer complex **1-d**

Hydrosilylation reaction catalyzed by six-coordinate rhenium complex **2-b** was unsuccessful. In agreement with Lewis acid catalysis proposed in chapter 5, **2-b** has no vacant site for either $^1\eta$ or $^2\eta$ silane activation, which is considered as rate-limiting step by kinetic studies. Hydrosilylation mediated by **1-d** revealed comparable reaction rate and product distribution in both aldehyde and imine reactions. This result suggests that metal-ligand corporation in **1-d** did not

facilitate catalyst efficiency and activation of silane only involves metal center not the dearomatized pincer arm. Further mechanistic and kinetic study is needed to shed the light.

General procedure for hydrosilylation catalyzed by **1-d**

In a nitrogen filled glove box, a stock solution of **1-d**³ in CD₂Cl₂ (0.001 M) was prepared. 5 μL of the stock solution of **1-d** in CD₂Cl₂ (5×10⁻⁶ mmol, 1 mol %) was added to a J-Young NMR tube equipped with substrate (0.1 M, 0.1 mmol), PhSiH₃ (0.1 M, 0.1 mmol) and internal standard C₈H₁₆ (3.7×10⁻⁵ mol) in CDCl₃ (0.8 ml) at 25°C. The progress of the reaction was monitored by integrating proton of PhN=CHPh, PhSiH₃ and Ph(H₂PhSi)NCH₂Ph relative to C₈H₁₆ respect to time for N-benzylideneaniline, or PhCHO and (PhCH₂O)₂SiPhH relative to C₈H₁₆ respect to time for benzaldehyde.

Activation of H–H bond by **1-d**

Milstein and coworkers reported deoxygenative hydrogenation of amides catalyzed by manganese pincer complex via metal-ligand cooperation with Lewis acid additive.⁴ Hydrogenation of benzanilide mediated by dearomatized complex **1-d** was unsuccessful, even with a strong Lewis acid B(C₆F₅)₃ as additive. Due to the fact that imine is probably the intermediate in the hydrogenation of amide, hydrogenation of N-benzylideneaniline was examined and no catalytic reactivity was observed. These hydrogenation reactions were performed at 150 °C under 50 bar H₂ pressure. ³¹P NMR analysis indicates the presence of free pincer ligand at 41 ppm at the end of the reaction under this harsh condition. The dissociation of pincer ligand from rhenium may lead to this catalyst reactivity shutdown.

Determination of equilibrium constant between 1-d and 3

Since the vacant site availability plays an essential role in potential catalysis, the dissociation/association of solvent molecules coordinated on metal center was examined and equilibrium constant between 1-ACN and 1 was determined (chapter 2). In order to understand whether aromaticity of a ligand has any effect on solvent coordination, dearomatized rhenium pincer complex of [(PNN*)Re(O)₂(ACN)][OTf] (**3**) was synthesized, and equilibrium constant determination between **3** and **1-d** is underway.

Discussion on acridine-based rhenium pincer complex 4 and 5

Acridine-based rhenium pincer complex (ⁱPrPNPⁱPr)Re(O)₂I (**4**) was synthesized by fine tuning the steric property of pincer ligand. This distorted trigonal bipyramidal bidentate pincer complex has one coordination site available for bond activation. By salt metathesis with silver triflate, cationic complex [(ⁱPrPNPⁱPr)Re(O)₂][OTf] (**5**) was afforded with two vacant sites after the removal of iodide ligand. These two complexes can further go through dearomatization for bond activation and catalysis. Acridine based ruthenium pincer complex [RuHCl(A-*i*Pr-PNP)(CO)] has been reported by Milstein and coworkers for catalyzing the synthesis of primary amine from alcohol and ammonia.⁵ The proposed mechanism involve dissociation of one hemilabile phosphine arm with the generation of a dihydride ruthenium (transfer hydrogenations). Later in 2009, the same group described conversion of alcohol to acetal catalyzed by same

acridine ruthenium complex, or to ester in the presence of a base. This pathway involves a challenging step of selective oxidation of primary alcohols to aldehydes. Importantly, no reaction was observed under the same condition with pyridine-based ruthenium complexes. These results indicate a much longer Ru–N bond and distorted middle acridine ring could probably result in “hemilability” of the acridine moiety, providing a coordination site and a localized internal base. It is important to obtain a detailed comparison between tridentate and bidentate pincer complexes for new catalyst design. The reactivity of acridine-based bidentate pincer complexes **4** and **5** is now under investigation in our lab.

4. References

- (1) Hansch, C.; Leo, A.; reviews, R. T. C.; 1991. *Chem. Rev.* **1991**, *91*, 165.
- (2) Yau, H. M.; Croft, A. K.; Harper, J. *Chem. Commun.* **2012**, *48* (71), 8937.
- (3) Mazzotta, M. G.; Pichaandi, K. R.; Fanwick, P. E.; Abu-Omar, M. M. *Angew. Chem. Int. Ed.* **2014**, *53* (32), 8320.
- (4) Zou, Y.-Q.; Chakraborty, S.; Nerush, A.; Oren, D.; Diskin-Posner, Y.; Ben-David, Y.; Milstein, D. *ACS Catal.* **2018**, *8* (9), 8014.
- (5) Gunanathan, C.; Milstein, D. *Angew. Chem. Int. Ed.* **2008**, *47* (45), 8661.

